0920

PB 206 487

Final Report to the Air Pollution Control Office of the U.S. Environmental Protection Agency under Contract Number CPA 22-69-65 July 15, 1971

# Petrographic and Mineralogical Characteristics of Carbonate Rocks Related to Sulfur Dioxide Sorption in Flue Gases

*Richard D. Harvey*

**ILLINOIS STATE GEOLOGICAL SURVEY, Urbana, Illinois**

Reproduced by
NATIONAL TECHNICAL
INFORMATION SERVICE
Springfield, Va. 22151

100

296

| | | | |
|---|---|---|---|
| **BIBLIOGRAPHIC DATA SHEET** | 1. Report No.<br>APTD-0920 | 2. | 3. Recipient's Accession No. |

4. Title and Subtitle

Petrographic and Mineralogical Characteristics of Carbonate Rocks Related to Sulfur Dioxide Sorption in Flue Gases

5. Report Date
July 15, 1971

6.

7. Author(s)
Richard D. Harvey

8. Performing Organization Rept. No.

9. Performing Organization Name and Address

Illinois State Geological Survey
Natural Resources Building
Urbana, Illinois 61801

10. Project/Task/Work Unit No.

11. Contract/Grant No.
CPA 22-69-65

12. Sponsoring Organization Name and Address
Environmental Protection Agency
Air Pollution Control Office
Division of Process Control Engineering
Cincinnati, Ohio 45227

13. Type of Report & Period Covered
Final

14.

15. Supplementary Notes

16. Abstracts

Detailed petrographic, mineralogical, and chemical analyses of 26 carbonate rocks were made and compared with the capacity (3 1/2 hr. reaction period) and differential reactivity (120 sec. reaction period) of calcined specimens for sorption of sulfur dioxide ($SO_2$). The study also included petrographic and chemical examination of limestone-modified fly ashes and boiler deposits obtained from the Tennessee Valley Authority's limestone injection tests at their Shawnee Plant, Paducah, Kentucky. Image analysis and scanning electron microscope methods were employed to examine limestones, dolomites, and a variety of other types of carbonates and their calcines. A wide range of petrographic and $SO_2$ sorptive properties were revealed. The relatively high $SO_2$ reactivity observed for chalks, calcareous marls, and oolitic aragonite sand samples is believed due mainly to the high pore volume and fine grain size of these carbonate rocks. Geologically, high pore volume is indicated by the relatively unconsolidated nature of these rock materials.

17. Key Words and Document Analysis. 17a. Descriptors

Air pollution
Sulfur dioxide
Flue gases
Carbonates
Rocks
Fly ash
Limestone
Chemical reactions
Sodium inorganic compounds
Oxides

17b. Identifiers/Open-Ended Terms

17c. COSATI Field/Group 13B

| | | |
|---|---|---|
| 18. Availability Statement<br>Unlimited | 19. Security Class (This Report)<br>UNCLASSIFIED | 21. No. of Pages<br>100 |
| | 20. Security Class (This Page<br>UNCLASSIFIED | 22. Price<br>3.00 - 0.95 |

STATE OF ILLINOIS
DEPARTMENT OF REGISTRATION AND EDUCATION
WILLIAM H. ROBINSON, DIRECTOR, SPRINGFIELD
BOARD OF NATURAL RESOURCES AND CONSERVATION
CHAIRMAN · · WILLIAM H. ROBINSON
GEOLOGY · · · · LAURENCE L. SLOSS
CHEMISTRY · · · · ROGER ADAMS
ENGINEERING · ROBERT H. ANDERSON
BIOLOGY · · · · · THOMAS PARK
FORESTRY · · · CHARLES E. OLMSTED
UNIVERSITY OF ILLINOIS
DEAN WILLIAM L. EVERITT
SOUTHERN ILLINOIS UNIVERSITY
DEAN ROGER E. BEYLER

**ILLINOIS STATE GEOLOGICAL SURVEY**
NATURAL RESOURCES BUILDING, URBANA, ILLINOIS 61801 TELEPHONE 217 344-1481
JOHN C. FRYE, CHIEF

July 15, 1971

Dr. Dennis C. Drehmel
Division of Process Control Engineering
Air Pollution Control Office
Environmental Protection Agency
3914 Virginia Avenue
Cincinnati, OH 45227

Dear Dr. Drehmel:

Contract No. CPA 22-69-65

Enclosed are 50 copies and one reproducible copy of our final report on the subject "Petrographic and Mineralogical Characteristics of Carbonate Rocks Related to Sulfur Dioxide Sorption in Flue Gases." This report covers work done on this project since it was initiated April 22, 1969.

I shall welcome your comments on the report and on the research.

Sincerely yours,

Richard D. Harvey
Richard D. Harvey
Geologist
Industrial Minerals Section

Enclosures

# Petrographic and Mineralogical Characteristics of Carbonate Rocks Related to Sulfur Dioxide Sorption in Flue Gases

*Richard D. Harvey*

*Final report to the Air Pollution Control Office of the U.S. Environmental*
*Protection Agency under Contract Number CPA 22-69-65*
*July 15, 1971*

**ILLINOIS STATE GEOLOGICAL SURVEY,** Urbana, Illinois

BLANK PAGE

# CONTENTS

Page

- Abstract 1
  - Conclusion and recommendation 2
- Introduction 2
- Petrographic studies of selected types of carbonate rocks (phase I) 3
  - Mineral and chemical analyses 3
    - Petrographic classification and source of samples 3
    - Mineralogy 5
    - Chemical analyses 6
  - Petrographic characterization of carbonate rocks 7
    - Description of type samples 9
      - Type 1 - Iceland spar calcite 9
      - Type 2 - Calcite spar 9
      - Type 3 - Coarse-grained calcitic limestone 9
      - Type 4 - Fine-grained calcitic limestone 11
      - Type 5 - Reef dolomite 11
      - Type 6 - Nonreef dolomite 11
      - Type 7 - Magnesite 11
      - Type 8 - Oolitic aragonite 13
      - Type 9 - Calcitic-limonitic dolomite 13
    - Petrographic characterization of pore structure 14
      - The Quantimet and its operation 14
      - Measurements 15
      - Results of pore studies with the Quantimet 15
    - Petrographic grain-size distribution 17
  - Characterization of the calcined samples 17
    - Description of the calcined samples 19
    - Discussion of the calcines 25
- Petrographic studies of samples of certain commercial carbonate rocks (phase II) 28
  - Samples and methods 28
  - Petrographic characterization of samples 28
  - Marls and chalks 39
  - Grain and pore size distributions 39
  - Mineralogy 41
  - Chemical analyses 43
- Discussion of results related to sulfur dioxide sorption tests 43
  - Petrography related to $SO_2$ sorption 47
  - Grain size and pore structure related to sorption 47
  - Chemical analyses and sorption 51
- Reaction products 51

Page

Petrographic studies of limestone-modified fly ash and boiler deposits . . . 55
  Mineral analyses . . . 57
  Chemical analyses . . . 62
  Grain size distribution . . . 65
  Electron microscopy of limestone-modified fly ash . . . 65
  Studies of boiler deposits . . . 71
    Deposits collected September 1970 . . . 71
      Inner layer material . . . 77
      Outer layer material . . . 79
    Deposits collected June 1970 . . . 79
    Concluding remarks on boiler deposits . . . 84

Summary and conclusions . . . 85
  Petrography and reactivity . . . 85
  Fly ash and boiler deposits . . . 86
  Acknowledgments . . . 87

References . . . 89

Glossary . . . 91

## ILLUSTRATIONS

Figure Page

1. Type 1; Iceland spar calcite . . . 8
2. Type 2; calcite spar . . . 8
3. Type 3; coarse-grained limestone . . . 8
4. Type 3; coarse-grained limestone . . . 8
5. Type 4; fine-grained limestone . . . 8
6. Type 4; fine-grained limestone . . . 8
7. Type 5; dolomite . . . 10
8. Type 5; dolomite . . . 10
9. Type 6; impure dolomite . . . 10
10. Type 6; impure dolomite . . . 10
11. Type 7; magnesite . . . 10
12. Type 7; magnesite . . . 10
13. Type 8; oolitic aragonite . . . 12
14. Type 8; oolitic aragonite . . . 12
15. Type 8; oolitic aragonite . . . 12
16. Type 9; limonitic dolomite . . . 12
17. Type 9; limonitic dolomite . . . 12
18. Type 9; limonitic dolomite . . . 12
19. Type 1 calcine . . . 20
20. Type 1 calcine . . . 20
21. Type 1 calcine . . . 20
22. Type 1 calcine . . . 20
23. Type 1 calcine . . . 20
24. Type 1 calcine . . . 20
25. Type 2 calcine . . . 22

Figure Page

26. Type 2 calcine . . . . . 22
27. Type 2 calcine . . . . . 22
28. Type 2 calcine . . . . . 22
29. Type 2 calcine . . . . . 22
30. Type 2 calcine . . . . . 22
31. Type 3 calcine . . . . . 23
32. Type 3 calcine . . . . . 23
33. Type 3 calcine . . . . . 23
34. Type 3 calcine . . . . . 23
35. Type 4 calcine . . . . . 24
36. Type 4 calcine . . . . . 24
37. Type 4 calcine . . . . . 24
38. Type 4 calcine . . . . . 24
39. Type 5 calcine . . . . . 26
40. Type 5 calcine . . . . . 26
41. Type 5 calcine . . . . . 26
42. Type 5 calcine . . . . . 26
43. Type 6 calcine . . . . . 27
44. Type 7 calcine . . . . . 27
45. Type 8 calcine . . . . . 27
46. Type 8 calcine . . . . . 27
47. Type 9 calcine . . . . . 27
48. Type 9 calcine . . . . . 27
49. Photomicrographs of limestone and marble (phase II) . . . 33
50. Photomicrographs of dolomites (phase II) . . . . . 35
51. Photomicrographs of marls and chalks (phase II) . . . . . 37
52. $SO_2$ capacity versus mean grain size . . . . . 48
53. $SO_2$ capacity versus volume of pores larger than 0.9 μ . . 49
54. $SO_2$ capacity versus volume of pores 2 to 16 μ . . . . . 49
55. $SO_2$ differential reactivity versus volume of pores larger than 0.9 μ . . . . . 50
56. $SO_2$ differential reactivity versus pore projection . . . 50
57. $SO_2$ capacity versus $Na_2O$ . . . . . 50
58. Distribution of S in $SO_2$-reacted calcines . . . . . 52
59. Exterior surface of $SO_2$-reacted calcine of dolomite . . . 53
60. Exterior surface of $SO_2$- reacted calcine of limestone . . 54
61. Cross section of the quarry of Fredonia Valley Quarries . 56
62. X-ray diffraction patterns of limestone-modified fly ash . . . . . 59
63. Particle size of limestone-modified fly ash from planes AA and CC . . . . . 67
64. Normal fly ash particles . . . . . 68
65. Limestone-modified fly ash, mechanical hopper . . . . . 69
66. Limestone-modified fly ash, mechanical hopper . . . . . 70
67. Limestone-modified fly ash, plane AA . . . . . 72
68. Limestone-modified fly ash, plane CC and electrostatic hopper . . . . . 73
69. Reheat section of boiler and cross section of boiler deposit . . . . . 74
70. Specimens of boiler deposit . . . . . 76
71. Specimen of boiler deposit showing inner layer material . 78

Figure Page

72. Photomicrographs of boiler deposits collected September 1970 . . . . . . . . . . . . . . . . . . . . . . 81
73. Photomicrographs of boiler deposits collected June 1970 . 83

## TABLES

Table Page

Type Carbonate Rocks (phase I)

1. Petrographic description and source of samples . . . . . . 4
2. Mineralogy of type samples . . . . . . . . . . . . . . . . . 5
3. Chemical analyses . . . . . . . . . . . . . . . . . . . . . 6
4. Trace element analyses . . . . . . . . . . . . . . . . . . . 7
5. Quantimet analyses of pore structure of phase I samples . 16
6. Grain size distribution . . . . . . . . . . . . . . . . . . 18
7. Description of the calcines . . . . . . . . . . . . . . . . 19

Commercial Carbonate Rocks (phase II)

8. Petrographic description and source of samples . . . . . . 29
9. Grain size analyses . . . . . . . . . . . . . . . . . . . . 40
10. Quantimet analyses of pore structure . . . . . . . . . . . 42
11. Void inclusions in dolomite grains . . . . . . . . . . . . 43
12. Mineral analyses . . . . . . . . . . . . . . . . . . . . . . 44
13. Chemical analyses . . . . . . . . . . . . . . . . . . . . . 45
14. $SO_2$ reactivities . . . . . . . . . . . . . . . . . . . . . 46

Fly Ash and Boiler Deposits (phase III)

15. Fly ash samples studied . . . . . . . . . . . . . . . . . . 57
16. Mineralogy of fly ash samples . . . . . . . . . . . . . . . 58
17. Chemical analyses of fly ash materials . . . . . . . . . . . 61
18. Chemical analyses of normal fly ashes . . . . . . . . . . . 63
19. Chemical analyses of limestone-modified fly ash samples from planes AA and CC . . . . . . . . . . . . . 64
20. Particle size analyses of fly ash samples from planes AA and CC . . . . . . . . . . . . . . . . . . . . . 66
21. Chemical and mineral analyses of fire-side boiler deposits . . . . . . . . . . . . . . . . . . . . . . . . . 75

# PETROGRAPHIC AND MINERALOGICAL CHARACTERISTICS OF CARBONATE ROCKS RELATED TO SULFUR DIOXIDE SORPTION IN FLUE GASES

Richard D. Harvey

## ABSTRACT

Detailed petrographic, mineralogical, and chemical analyses of 26 carbonate rocks were made and compared with the capacity (3½ hr. reaction period) and differential reactivity (120 sec. reaction period) of calcined specimens for sorption of sulfur dioxide ($SO_2$). The study also included petrographic and chemical examination of limestone-modified fly ashes and boiler deposits obtained from the Tennessee Valley Authority's limestone injection tests at their Shawnee Plant, Paducah, Kentucky. Image analysis and scanning electron microscope methods were employed to examine limestones, dolomites, and a variety of other types of carbonates and their calcines. A wide range of petrographic and $SO_2$ sorptive properties were revealed.

Three petrographic and chemical properties appear to be useful indexes of the $SO_2$ sorption capacity: the pore volume, the grain size, and the sodium oxide content of the rocks. The larger the pore volume (determined by image analysis of polished sections of limestones and dolomites), the greater was the sorption capacity of the rock. Pores with a maximum chord length between 2 and 16 μ appear to have the most influence on this behavior. In general, the finer the grain size of the rock, the higher was the sorption capacity, although certain limestone samples showed the opposite correlation owing to the positive effect of the intracrystalline pores in the crinoidal fossil fragments abundant in some of these samples. Of the chemical elements analyzed, only sodium showed a correlation trend with the $SO_2$ test data. The sodium present in the samples increased with increasing sorption capacity.

Unlike the sorption capacity tests, the differential reactivity tests showed little or no correlation with petrographic and chemical properties.

The reaction products of the samples calcined at 980° C for 2 hours and exposed to sulfur oxides in laboratory tests are solid grains of anhydrite ($CaSO_4$). Electron microscopy shows two types of behavior. The calcines of the Iceland spar calcite absorbed sulfur on the outer surface of its particles, whereas in calcines of a porous limestone absorption took place throughout the particles. Sulfation occurred on the outer surfaces of particles by multiple nucleation of anhydrite crystallites, which enlarged until they abutted each other to produce a tightly interlocking texture of subrounded grains.

Anhydrite was the only sulfur-bearing compound positively detected in $SO_2$-reacted calcines and limestone-modified fly ashes. Limited X-ray diffraction data suggest also the presence of trace amounts of $CaSO_3$ in the coarse fraction of dust from the 650° F position behind the reheat section in the TVA boiler. Anhydrite crystallites in the fly ashes are subrounded in shape and submicron to about 2 μ in diameter. The growth of anhydrite on surfaces of large lime particles results in notable percentages of anhydrite in the coarse fractions of the ash. A nonporous and interlocking grain texture similar to that of laboratory-reacted specimens was observed on a few lime-rich particles in the ash, although many such particles appeared to retain a porous structure.

### Conclusion and Recommendation

The relatively high $SO_2$ reactivity observed for chalks, calcareous marls, and oolitic aragonite sand samples is believed due mainly to the high pore volume and fine grain size of these carbonate rocks. Geologically, high pore volume is indicated by the relatively unconsolidated nature of these rock materials. It is recommended that further studies be made of these rock types. Detailed geologic and petrographic investigations should be made of widely distributed deposits of chalk, calcareous marl, and calcareous shell (similar to the oolitic sand discussed in this paper). A representative number of deposits should be examined in the field and samples taken to determine the natural variability of pore volume and grain size within the deposits. Further, relations between the pore structure of the samples and that of their calcined products should be examined for possible aids to prospecting for highly reactive limestones.

## INTRODUCTION

Air pollution due to emission of sulfur dioxide ($SO_2$) from power plants is a major environmental concern, especially in highly industrialized areas. One of the current areas of research on this problem is concerned with the limestone injection process for control of $SO_2$ that is formed during combustion of fuels containing sulfur. This process, if it can be shown to be technically feasible, is of considerable importance because it involves the minimum capital and operating costs of any prospective process for $SO_2$ control.

The basic procedure for this method of $SO_2$ control is injection of pulverized carbonate rock, composed chiefly of calcite ($CaCO_3$) or dolomite ($CaMg(CO_3)_2$), into a high-temperature zone of a coal-fired boiler, where it is converted to lime ($CaO$) and carbon dioxide ($CO_2$). The lime then combines with $SO_2$ from the flue gas to form anhydrite ($CaSO_4$), which is removed as solid particles from the flue gases.

This investigation was jointly supported by the Illinois State Geological Survey and the Air Pollution Control Office (APCO), U. S. Environmental Protection Agency, under Contract No. CPA 22-69-65. The study was made to determine the basic mineralogic and petrographic reasons for the wide variation in $SO_2$ sorption by various types of carbonate rocks that had been observed in laboratory and pilot-plant tests. Phase I of the project involved the study and testing of a number of samples representative of a wide diversity of naturally occurring carbonate rock types. The samples were analyzed for their mineral and chemical components, including certain trace elements, and subjected to detailed petrographic examinations. Correlations were observed between the grain size, pore structure, and sodium oxide content of the samples and their capacity to absorb $SO_2$.

In phase II, samples of commercially available crushed carbonate rocks were examined and tested to evaluate the above-mentioned criteria developed in phase I. Phase III involved the study of fly ash from the Tennessee Valley Authority's full-scale limestone injection project at their Shawnee Steam Plant, Paducah, Kentucky.

## PETROGRAPHIC STUDIES OF SELECTED TYPES OF CARBONATE ROCKS (PHASE I)

### Mineral and Chemical Analyses

### Petrographic Classification and Source of Samples

Nine types of carbonate rocks and minerals were selected for detailed study and testing of their capacity to react with $SO_2$. Specific petrographic, mineralogic, and chemical analyses of several provisional samples were made so that samples could be selected that would represent a wide diversity of naturally occurring carbonate rocks and minerals that possibly could be used for controlling $SO_2$ emission. The samples selected for study included two limestones (one coarse grained and one fine grained), two calcite spars (one Iceland spar and the other bearing numerous crystal imperfections), an oolitic aragonite sand, three dolomites (a reef, a nonreef, and one rich in limonite), and a magnesite. The petrographic rock types and sources of the samples are listed in table 1, as are the distinguishing characteristics for which the samples were selected.

TABLE 1—PETROGRAPHIC DESCRIPTION AND SOURCE OF SAMPLES

| Sample type no. | Rock or mineral classification | Distinguishing characteristics | Color | Grain shape | Degree of grain interlocking | Other textural features | Source of samples | |
|---|---|---|---|---|---|---|---|---|
| | | | | | | | Location | Geologic formation |
| 1 | Calcite (Iceland spar) | Nearly perfect crystals | Clear | Cleavage rhombs | None | | Ecjungo, Durango, Mexico | — |
| 2 | Calcite spar | Abundant crystal defects | Milky | Cleavage rhombs | None | Abundant intracrystalline voids, solid inclusions, twin lamellae; subgrains present in some specimens. | Hillside mine dump, Rosiclare, Ill. | — |
| 3 | Limestone | Coarse-grained, high purity | Gray | Anhedral | High | Inequigranular; crinoid and bryozoan fossil fragments; intragranular voids abundant. | Columbia Quarry Co. mine, Valmeyer, Ill. | Kimmswick Subgroup |
| 4 | Limestone | Fine-grained, high purity | Gray | Anhedral | High | Equigranular; dense; a few veinlets occur with medium-sized grains of clear calcite. | Allied Stone Co. Quarry, Milan, Ill. | Davenport Member of Wapsipinicon |
| 5 | Dolomite | Reef type, high purity | Gray | Anhedral | High | Recrystallized granular; porous; abundant intragranular voids. | Midway Stone Quarry, Osborne, Ill. | Racine |
| 6 | Dolomite | Nonreef type, clayey and silty | Buff | Anhedral & rhombic | Low | Equigranular; microporous; grains adjacent to pores are rhombic. Clay along bedding planes; iron oxide along dolomite grain boundaries. | Abandoned quarry near Bourbonnais, Ill. | Waukesha |
| 7 | Magnesite | Fine-grained, high purity | Milky | Anhedral & rhombic | Low | Equigranular and microporous. | Red Mountain Dist., Santa Clara Co., Cal. | — |
| 8 | Aragonite | Oolitic and strontium-bearing | Light buff to milky | Fibrous & bladed | High | Elliptical and cylindrical remains of marine organisms abundant; very smooth exterior surfaces; most microporous. | North Cat Cay, Bahama Islands | Recent marine deposit |
| 9 | Dolomite | Limonite- and calcite-bearing | Brown & gray | Anhedral & rhombic | Low | Equigranular and microporous; rhombic grains along pores; fibrous limonite (?) occurs along dolomite grain boundaries; abundant intragranular voids. | Jeffrey Limestone Co. Quarry, Parma, Mich. | — |

TABLE 2—MINERALOGY OF TYPE SAMPLES IN WEIGHT PERCENTAGE

| Sample | Major component (%) | Minor and trace components | Insoluble residue (%) |
|---|---|---|---|
| Type 1 | 100 calcite | None detected | 0.0 |
| Type 2 | 100 calcite | Traces of soluble salts of Cl and $SO_3$ | 0.1 |
| Type 3 | 91 calcite | 8% dolomite and < 1% limonite | 0.2 |
| Type 4 | 98 calcite | < 2% quartz | 0.9 |
| Type 5 | 99 dolomite | < 1% calcite; approximately 0.3 mole % $FeCO_3$ is present in the dolomite | 0.1 |
| Type 6 | 81 dolomite | 9% quartz; 4% calcite; 5% clay; approximately 0.8 mole % $FeCO_3$ is present in the dolomite | 14.4 |
| Type 7 | 99 magnesite | < 0.5% quartz and clay; approximately 0.26 mole % $FeCO_3$ and 4.51 mole % $CaCO_3$ are present in the magnesite | 0.1 |
| Type 8 | 96+ aragonite | Approximately 3% Mg-calcite and < 1% clay; approximately 1.38 mole % $SrCO_3$ is present in the aragonite | 0.4 |
| Type 9 | 70 dolomite | 18% calcite; 4% quartz; $\leq$ 2% clay; 5% limonite | 4.2 |

## Mineralogy

The samples were subjected to X-ray analysis with a diffractometer equipped with a recording potentiometer output, to acid treatment, and to study under an optical microscope for quantitative identification of their mineralogy. The results are listed in table 2. The mole fractions of the various carbonates present in some of the samples were calculated from chemical analyses. X-ray data verified the presence of magnesium carbonate in solid solution in calcite impurities in the oolitic aragonite (sample type 8).

TABLE 3—CHEMICAL ANALYSES IN WEIGHT PERCENTAGE
(Analyses by Analytical Chemistry Section of the Illinois State Geological Survey)

| Oxides | Sample type number 1 | 2 | 3 | 4 | 5 | 6 | 7 | 8 | 9 |
|---|---|---|---|---|---|---|---|---|---|
| $SiO_2$ | ND[a] | ND | ND | 1.53 | 0.03 | 11.8 | 0.47 | 0.19 | 5.88 |
| $TiO_2$ | ND | ND | ND | ND | ND | 0.02 | ND | ND | 0.15 |
| $Al_2O_3$ | ND | 0.01 | ND | 0.01 | 0.02 | 1.77 | 0.08 | 0.27 | 0.69 |
| $Fe_2O_3$ | ND | 0.19[c] | 0.20[c] | 0.31[c] | 0.34[c] | 0.13 | ND | ND | 2.82 |
| FeO | 0.13 | — | — | — | — | 0.41 | 0.07 | 0.01 | 1.75 |
| MnO | ND | 0.06 | 0.10 | 0.09 | 0.02 | 0.02 | ND | ND | 0.21 |
| MgO | ND | ND | 1.86 | ND | 21.40 | 17.4 | 44.2 | ND | 15.33 |
| CaO | 55.3 | 55.5 | 53.4 | 54.8 | 30.30 | 26.5 | 2.93 | 55.2 | 30.82 |
| $Na_2O$ | 0.003 | 0.015 | 0.015 | 0.047 | 0.008 | 0.040 | 0.026 | 0.53 | 0.16 |
| $K_2O$ | 0.02 | 0.02 | 0.02 | 0.04 | 0.03 | 0.90 | 0.03 | 0.03 | 0.22 |
| $P_2O_5$ | trace[b] | — | — | — | — | 0.02 | trace | 0.01 | 0.10 |
| $CO_2$ | 43.95 | 43.35 | 43.75 | 43.35 | 47.30 | 40.27 | 50.96 | 42.10 | 40.68 |
| $SO_3$ | 0.01 | 0.17 | 0.20 | 0.15 | 0.13 | 0.03 | 0.01 | 0.37 | 0.42 |
| SrO | 0.014 | 0.002 | 0.009 | 0.019 | 0.019 | 0.04 | 0.01 | 0.10 | 0.04 |
| Cl | ND | 0.04 | 0.03 | ND | 0.09 | trace | ND | 0.24 | ND |
| Ign. loss | 43.49 | 43.15 | 43.67 | 43.15 | 47.24 | 40.46[d] | 51.56[e] | 43.33 | 41.85 |

[a] ND - not detected: Limits of detection for $SiO_2$, 0.03; $TiO_2$ and MnO, 0.01; $Al_2O_3$, 0.05; $Fe_2O_3$, 0.01; MgO, 0.10; Cl, 0.02.

[b] Trace of $P_2O_5$, approximately 0.005%.

[c] Percentage of total iron expressed as $Fe_2O_3$.

[d] Includes 0.3% $H_2O$+.

[e] Includes 0.61% $H_2O$+.

## Chemical Analyses

The results of chemical analyses of the major and minor elements present in the samples are listed in table 3. Flame photometry was used to determine the $K_2O$ and some of the SrO results; gravimetric methods were used to determine the FeO, $CO_2$, $P_2O_5$, and $SO_3$ results; and neutron activation methods were used to determine the Cl, $Na_2O$, and the remaining SrO results. All other oxides were determined by X-ray fluorescence. Neutron activation methods were used to detect the trace element content of the samples. The results are shown in table 4.

TABLE 4—TRACE ELEMENT ANALYSES OF CARBONATE ROCKS DETERMINED BY NEUTRON ACTIVATION METHODS

(Analyses by Dr. R. R. Ruch of the Analytical Chemistry Section of the Illinois State Geological Survey)

| Sample type | Element (ppm) | | | | | | | | |
|---|---|---|---|---|---|---|---|---|---|
| | Cu | Br | La | Sc | Eu | As | Ga | Cr | Hg |
| 1 | 15 | ≤ 2 | < 0.3 | 0.03 | < 0.03 | 2 | < 1 | < 2 | 0.06 |
| 2 | 44 | < 2 | 3.3 | 0.35 | 5.2 | ≤ 2 | < 7 | < 11 | 0.06 |
| 3 | ≤ 7 | ≤ 3 | 1.6 | 0.16 | < 0.07 | 2 | < 2 | ≤ 5 | 0.06 |
| 4 | < 3 | 17 | < 1 | 0.10 | < 0.2 | —[a] | < 6 | < 2 | 0.04 |
| 5 | 11 | ≤ 1 | 1.2 | 0.23 | < 0.05 | ≤ 0.8 | < 2 | < 4 | 0.03 |
| 6 | ≤ 25 | ≤ 5 | 9.6 | 1.4 | < 0.3 | ≤ 4 | < 6 | 35 | 0.07 |
| 7 | ≤ 8 | < 0.9 | < 0.2 | 0.06 | < 0.1 | < 0.7 | < 3 | 127 | 0.03 |
| 8 | —[b] | 17 | < 1 | 0.05 | —[b] | —[a] | —[b] | ≤ 12 | 0.02 |
| 9 | 25 | ≤ 1 | 3.4 | 1.0 | < 0.7 | ≤ 2 | < 14 | ≤ 31 | 0.23 |

[a] Not determined, excessive interference from Br.

[b] Not determined, excessive interference from Na.

## Petrographic Characterization of Carbonate Rocks

The petrographic studies were focused primarily on the textural relations between the grains, the grain shape and size distribution, and the pore structure of the samples. Many of the geologic terms used in this paper are defined in a glossary at the end of the report. The petrographic descriptions that follow are based on studies made with a scanning electron microscope and a Quantimet, an image-analyzing computer with a polarizing microscope. The scanning electron microscope (SEM) permits direct examination of the surface of a solid specimen about 1 x 1 x ½ cm at magnifications from 20 to over 20,000 times.

Two to four specimens of each sample were selected as representative, and polished and etched surfaces were prepared for petrographic analyses. Fractured surfaces also were examined to determine the nature of the surface exposed to the $SO_2$. The specimens were studied at both low and high magnifications to determine their most typical and representative textural features. From a total of 158 scanning electron micrographs of the specimens, two or three of each type were selected that showed the most typical textural characteristic, and these pictures are reproduced in figures 1 through 18.

## TYPICAL SURFACE TEXTURES, TYPES 1 THROUGH 4

NOT REPRODUCIBLE

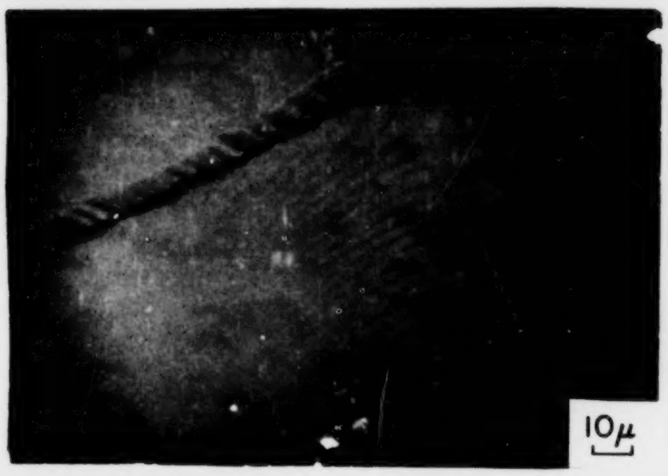

Fig. 1. Type 1; Iceland spar calcite; cleaved and etched.

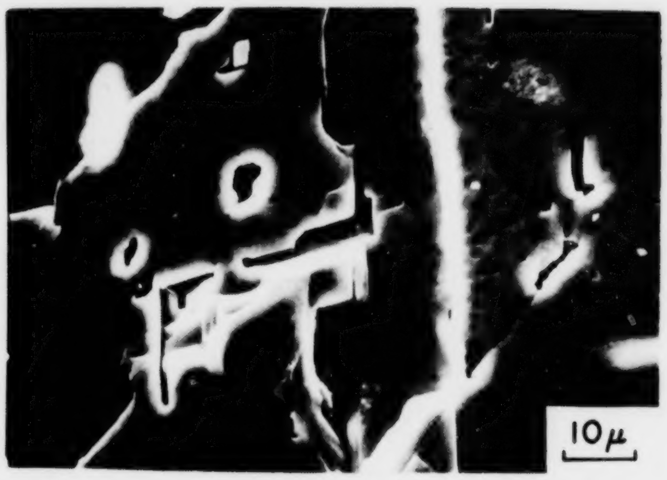

Fig. 2. Type 2; calcite (spar); cleaved and etched.

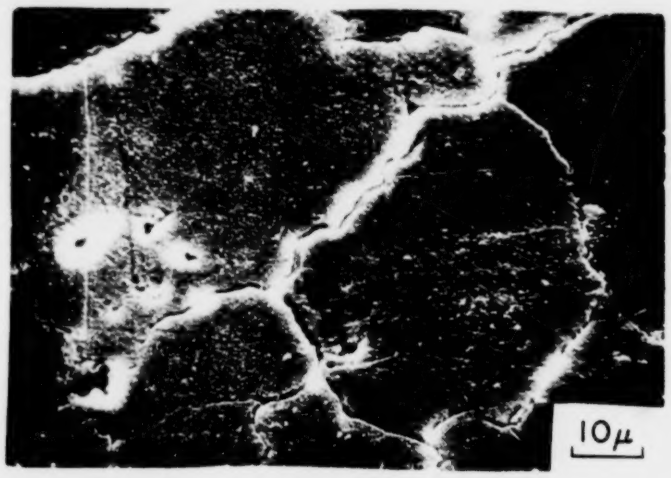

Fig. 3. Type 3; coarse-grained limestone; polished and etched.

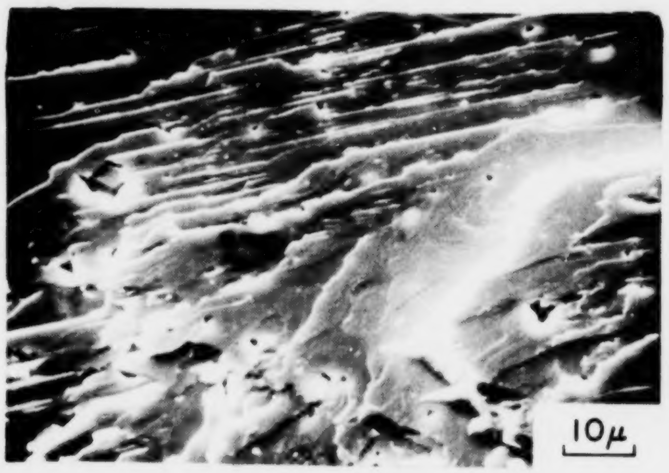

Fig. 4. Type 3; coarse-grained limestone; extension fracture.

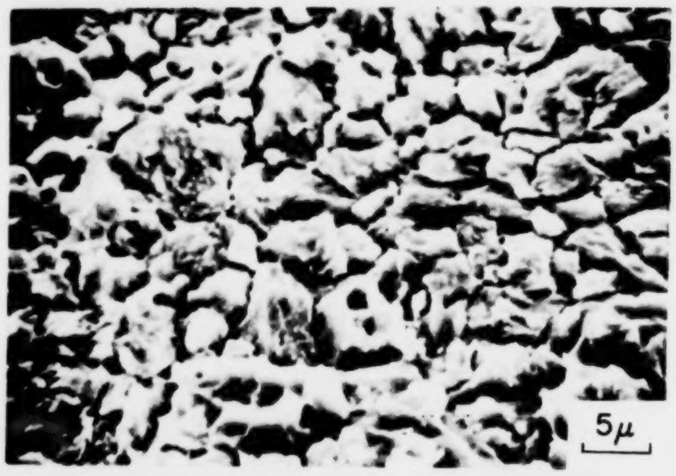

Fig. 5. Type 4; fine-grained limestone; polished and etched.

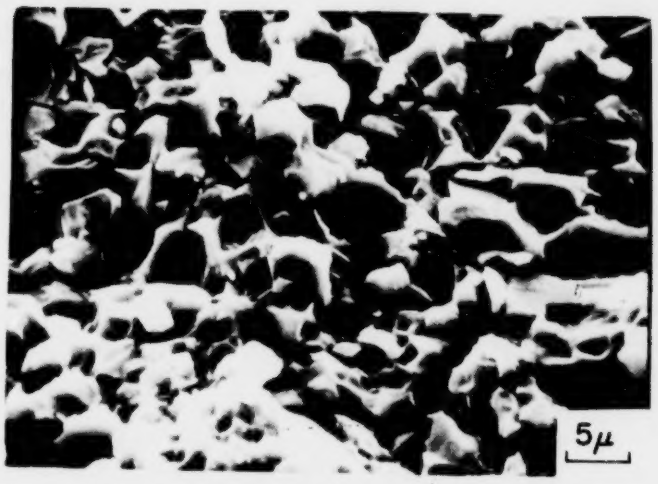

Fig. 6. Type 4; fine-grained limestone; extension fracture.

Interpretation of the electron micrographs is direct; that is, knolls on the specimen appear as knolls on the photographs. Edges of grains are highlighted in such a way that they appear as though the "lighting" is directed at a high angle from the top of the photographs. Intragranular voids and cleavage steps, thought to be sites of high chemical activity during calcination, were noted. The descriptions of the samples that follow are summarized in table 1.

## Description of Type Samples

### *Type 1 - Iceland Spar Calcite*

The Iceland spar sample consists of clear, transparent cleavage rhombs as much as 1 inch across (very coarse-grained). Few cleavage steps occur on the surfaces of the rhombs (fig. 1), which the electron microscope revealed as essentially free of crystal imperfections or dislocations. Fresh cleavage surfaces, lightly etched in 0.02 N HCl for 5 seconds and thoroughly rinsed, up to magnifications of X5000, show no intracrystalline voids or dislocation etch pits. Several polygonal and flat-bottomed pits vaguely detected in figure 1 are interpreted as the result of random dissolution of a perfect crystal rather than as sites of dislocations.

### *Type 2 - Calcite Spar*

The calcite spar sample consists of colorless or milky white, translucent, and irregular cleavage rhombs as much as 1 inch across. Some of the specimens contain numerous twin lamellae and several subgrains, each of which has a crystal orientation slightly different from those of neighboring subgrains. The sample is characterized by the abundance of intracrystalline voids and cleavage steps (fig. 2). Many solid inclusions also are present, such as the one at the top of figure 2. These crystal inclusions are possibly Ca and Na precipitated as chlorides and sulfates that were previously trapped in the calcite crystal as fluids under high temperatures. The chemical composition of the inclusions cannot be determined with the scanning electron microscope, although they probably contain the trace amounts of Na, Cl, and S present in the sample (table 3). The nature of the cleavage surfaces of certain crystal inclusions suggests they may be calcite.

### *Type 3 - Coarse-Grained Calcitic Limestone*

The coarse-grained calcitic limestone is gray with a few dark gray, very thin seams of carbonaceous stylolites. It consists of fragments of crinoid and bryozoan fossils with minor amounts of fine-grained calcite and a few rhombic grains of dolomite scattered between them. The crinoids are very coarsely crystalline broken plates and stems (frequently single crystalline grains). The bryozoans are finely crystalline and polygranular particles that have a matted and/or net structure. The limestone has an inequigranular texture characterized by tightly interlocking anhedral grains of calcite. The grains vary in size from approximately 2 μ to over 5,000 μ. The grain boundaries are predominantly curvilinear (fig. 3). The crinoid grains contain numerous intragranular voids (fig. 4). Fractured surfaces, especially on the large grains, show numerous cleavage steps, as shown in the linear features in figure 4. Fracture surfaces of the fine-grained particles, which form a minor fraction of the sample, are

# TYPICAL SURFACE TEXTURES, TYPES 5 THROUGH 7

NOT REPRODUCIBLE

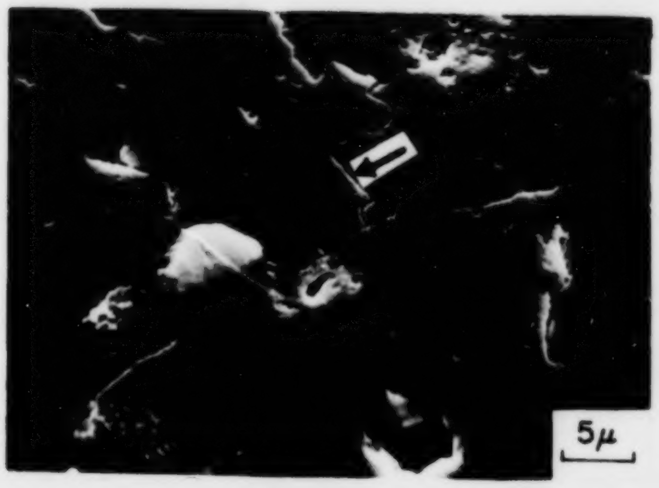

Fig. 7. Type 5; dolomite; polished and etched.

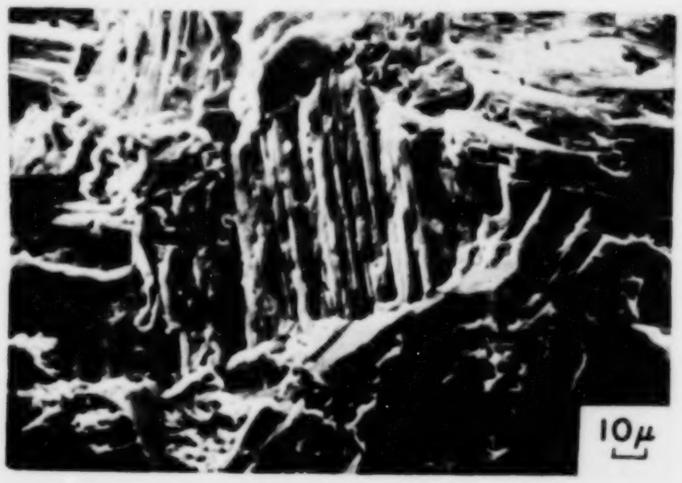

Fig. 8. Type 5; dolomite; extension fracture.

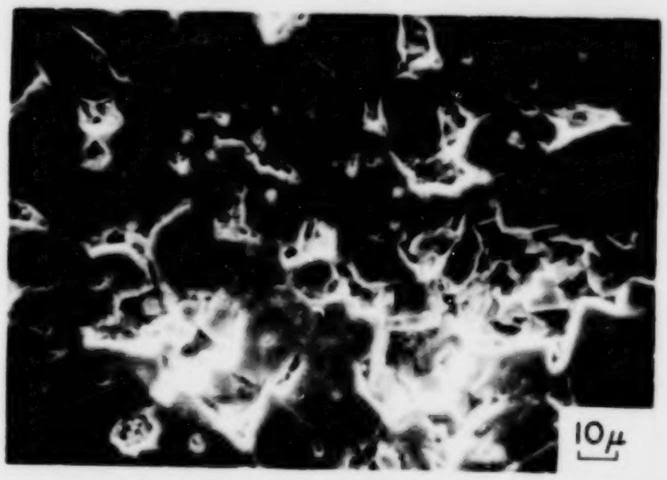

Fig. 9. Type 6; impure dolomite; polished and etched.

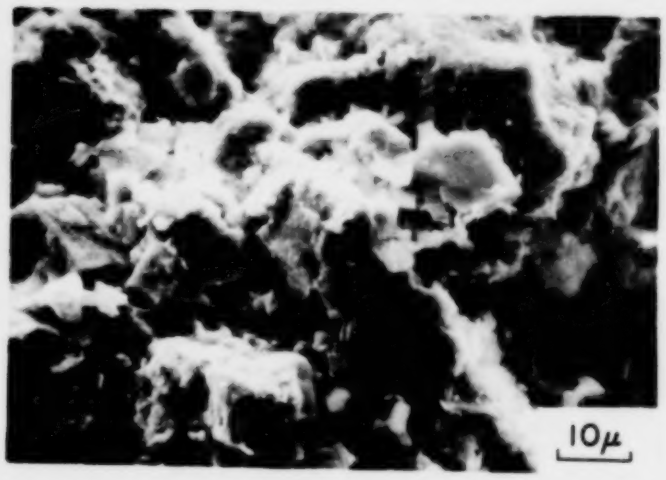

Fig. 10. Type 6; impure dolomite; extension fracture.

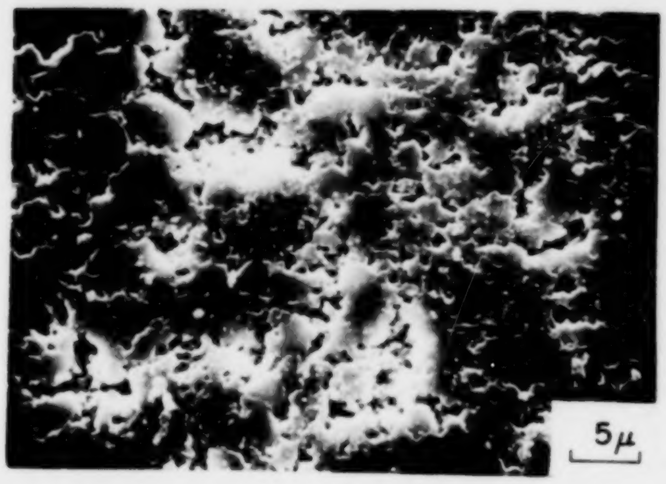

Fig. 11. Type 7; magnesite; polished and etched.

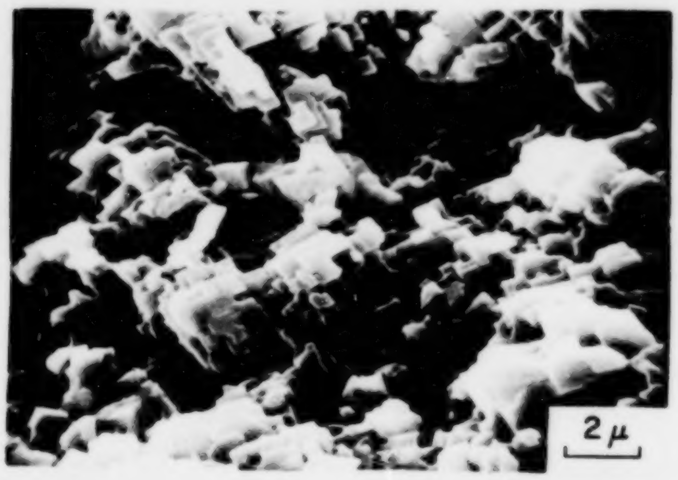

Fig. 12. Type 7; magnesite; extension fracture.

generally free of cleavage steps and appear to have propagated along grain boundaries. The sample is typical of the Kimmswick Limestone Subgroup in southwestern Illinois.

### *Type 4 - Fine-Grained Calcitic Limestone*

The fine-grained calcitic limestone is uniformly gray and equigranular. A few small veinlets of clear, sparry calcite occur in some specimens. Studies indicate the anhedral grains are tightly interlocked, and grain boundaries are distinctly curvilinear (fig. 5). The fractured surfaces show the equigranular nature of the sample, abundant sharp edges on the broken grains, cleavage steps on a few grains, and highly irregular surfaces with abundant tiny nooks and crevices (fig. 6). The mode of the fracture is transgranular. The sample is typical of the Davenport Member of the Wapsipinicon Limestone Formation in the vicinity of Davenport, Iowa.

### *Type 5 - Reef Dolomite*

The sample of reef dolomite was obtained from the core area of a large recrystallized reef. It is gray, hard, and porous, has abundant fossil fragments, and is of high purity. The grains are generally medium in size. The shape of the grains is anhedral and highly irregular, as shown by the grain boundary indicated by the arrow in figure 7. As a rule, the grains have curvilinear boundaries and are tightly interlocking. Intragranular voids are abundant throughout the sample (figs. 7 and 8). The light-colored grain on the left in figure 7 is harder and less soluble in acid than the surrounding dolomite, and it is probably chert. Fracture surfaces show transgranular mode (fig. 8), except when the fracture passes through a pore space. The sample is typical of the reef dolomite in the R[illegible]ne Formation in northern Illinois.

### *Type 6 - Nonreef Dolomite*

The nonreef dolomite is uniformly buff and is fine grained, equigranular, and microporous. It is clayey and silty. Polished and etched surfaces of the sample show small pore spaces adjacent to nearly every grain. The grains are frequently rhombic along the pore surfaces and anhedral elsewhere (fig. 9). A high percentage of grains contain intragranular voids.

Clay particles are concentrated along bedding planes and can be seen on a few surfaces broken normal to the bedding, as shown by the tiny, light-colored flakes near the edge of the rhombic dolomite grain in the center of figure 10. X-ray data indicate the clay mineral is predominantly illite. Iron oxide occurs along boundaries of the dolomite grains. The fracture surfaces of the rock are highly irregular and show more particles of less than 5 μ than are seen on polished surfaces of the sample, suggesting that the fracture tends to follow the boundaries of the smaller particles. The sample is typical of much of the Waukesha Formation of northeastern Illinois.

### *Type 7 - Magnesite*

The magnesite sample is of high purity and is colorless or milky and has a very fine-grained and microporous texture (figs. 11 and 12). The grain size of the sample is uniform, ranging from 1 to 10 μ, and the grains are both

## TYPICAL SURFACE TEXTURES, TYPES 8 THROUGH 9

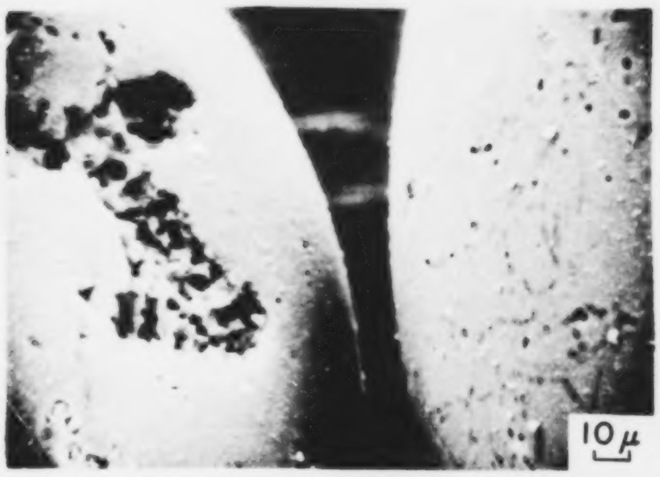

Fig. 13. Type 8; oolitic aragonite; surfaces of two oolites.

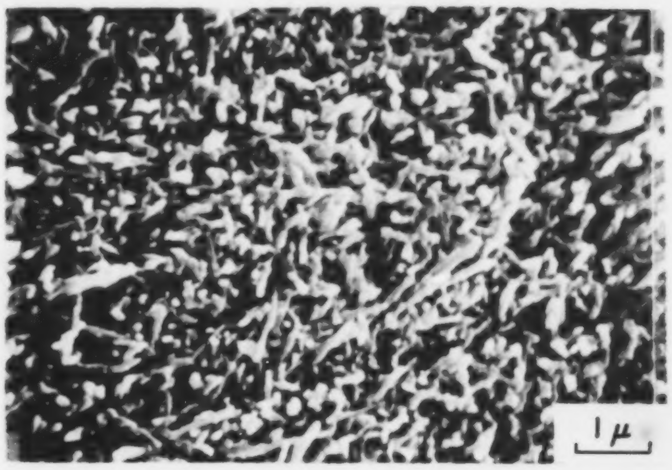

Fig. 14. Type 8; oolitic aragonite; polished and etched.

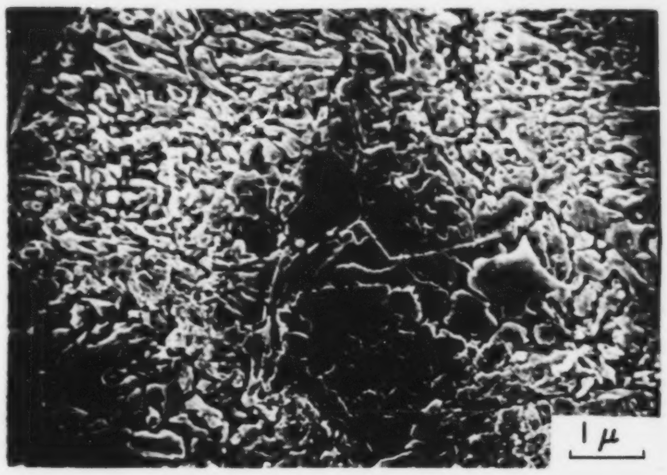

Fig. 15. Type 8; oolitic aragonite; polished and etched.

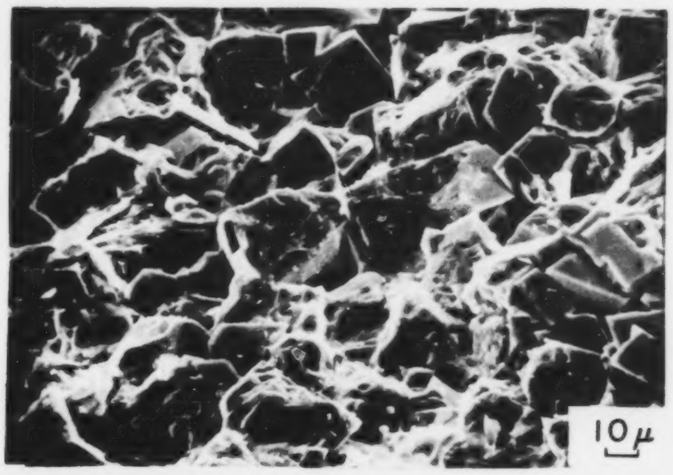

Fig. 16. Type 9; limonitic dolomite; extension fracture.

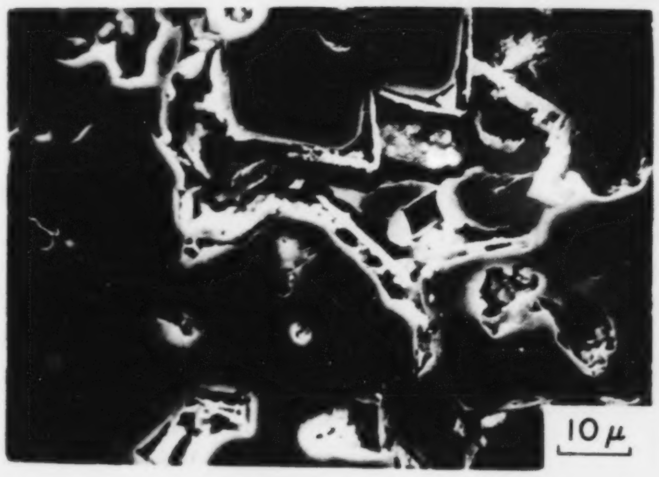

Fig. 17. Type 9; limonitic dolomite; polished and etched.

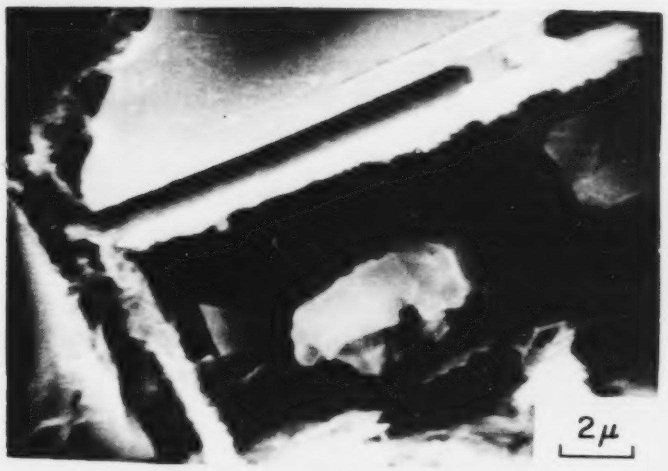

Fig. 18. Type 9; limonitic dolomite; polished and etched.

anhedral and rhombic. The polished surfaces show pore spaces around parts of nearly every grain. A few small areas in the sample have unusually large pores that contain traces of brown iron oxide stains and magnesite grains up to 40 μ. The fractured surfaces of the magnesite (fig. 12) show that a very high percentage of the grains have a distinct rhombic shape.

### *Type 8 - Oolitic Aragonite*

The aragonite sample is an oolitic sand composed of light buff to milky elliptical oolites and remains of marine organisms, many of which are cylindrical. The oolites and other particles have a median size of 400 μ and are predominantly aragonite. The exterior surfaces of the oolites and fossils are very smooth. Many of the oolites contain pore spaces just underneath the outermost layer of aragonite, as is shown by the oolite on the left in figure 13. Some of these porous areas are now exposed because of attrition between the particles.

The oolites consist mainly of fibrous aragonite, as shown in figure 14. Aragonite (orthorhombic structure) is an unstable form of $CaCO_3$ and it inverts to calcite (rhombohedral structure) with time and heat. The strontium present in the sample (0.10%) is thought to occur by substitution for calcium in the aragonite structure. The fibers are approximately 0.1 μ in diameter, range from approximately 0.5 to 2 μ long, and show a slight tendency for preferred orientation in the southwest to northeast direction (fig. 14). This orientation is about 45 degrees from the direction of the radius vector of the oolite. The fibrous habit of the aragonite is the most common form of aragonite in nature.

Very small gray patches that contain a bladed form of aragonite (fig. 15) occur on the surface of the oolite, as can be seen on the right side of figure 13. They possibly also contain the minor amounts of magnesium-calcite grains detected in the sample by X-ray diffraction. In some cases, the aragonite blades show preferred orientation normal to the outer boundary surface of the gray areas. The size of the bladed aragonite particles averages about 2½ μ long and one-half μ wide.

### *Type 9 - Calcitic-Limonitic Dolomite*

Sample 9 consists of limonite-coated gray and brown particles of crushed dolomite. The texture of the dolomite is fine, equigranular, and microporous (figs. 16 and 17). As is true of type 6, the dolomite grains that occur next to the pores have rhombic crystal surfaces; others are anhedral. Some specimens show numerous intragranular voids in the dolomite grains.

Certain brown weathered particles (as distinguished from the buff-gray unweathered particles) contain equigranular dolomite grains rimmed along the pores by platy minerals (light colored in fig. 17). Close examination reveals that the structure of this material is fibrous (fig. 18). Chemical and mineralogical analyses suggest that these fibrous bands are limonite and/or clay. The clay that is present in the sample is mainly illite, with lesser amounts of kaolinite. Observations of thin sections with the petrographic microscope indicate both limonite and clay occur along the carbonate grain boundaries. The effect of the fibrous layer on the $SO_2$ reaction of the calcine of the dolomite is not known.

If the layer is clay, it may have an adverse effect; if it is limonite, such a close association with the carbonates should enhance the catalytic effect of the iron oxide on the reaction with $SO_2$.

Calcite occurs in patches within the dolomite and consists of tightly interlocking anhedral grains with curvilinear grain boundaries.

## Petrographic Characterization of Pore Structure

The pore volume and pore-size distribution are fundamental properties of carbonate rocks and are basic to the physical and chemical behavior of rock materials. The porosity and pore-size distribution can be measured on cross-section surfaces on the basis of the principle that the volume fraction and the area fraction of a phase occupied on a random cross-section surface are equal (Sorby, 1856). This principle has been verified in a number of studies, including those of Rosiwal (1898), Thomason (1930), and Chayes (1956).

### *The Quantimet and Its Operation*

The instrument used in this work is an image analyzing computer, called a Model B Quantimet by the manufacturer.* It was described in detail by Fisher and Nazareth (1968). The instrument has several components—a polarizing microscope, a television camera and monitor, a detector, a computer, and an output meter. The microscope accommodates vertically reflected illumination, as well as transmitted polarized and ordinary light. A large specimen holder and associated illumination system (epidiascope) can be substituted for the microscope for analyzing photographs.

An image of the specimen is produced on the vidicon tube of the television camera through the microscope or epidiascope. This electronic image is scanned by a detector that responds to changes in voltage as the scanner passes over contrasting features. A discriminator (threshold control) sets the lower level of the voltage detected. Signals thus accumulated in the detector are fed to the computer, which counts and makes area summations. The output from the detector is fed into the television monitor for visual check by the operator that the desired features are being detected. Quantitative data are read out of the computer by means of a multiscale meter.

Briefly, three basic measurements, or modes, may be made: area, projection, and count. An additional mechanism is provided that permits the determination of the cumulative sizing of the projection and count measurements. Basic to the operation is the detection of the desired features, such as pores. Relatively good and uniform contrast must exist between the features to be measured and the other components in the specimen image. The image of the specimen and a rectangular area, called the blank frame, over which features are detected and measured, are displayed on the monitor. The highest intensity areas of the image are detected first by use of the threshold control. As the control is increased, more and more of the image is detected. The specific areas detected are clearly indicated on the monitor by extra-high intensity flooding. Adjustments of the level of flooding are made with the threshold control until the flooded (detected) areas and the features to be measured exactly match on the television monitor. The polarity of the detection can be reversed, i.e., the lowest intensity areas, or black areas, are detected first and progressively higher intensity areas are detected by increasing the threshold control setting.

---

* Metals Research Limited, Melbourn, England.

### *Measurements*

With the mode selector switch in the area position, the area of the detected features within the entire image in the blank frame is read from the meter as a fraction of the total blank frame area. When the projection is measured, the edges or boundaries of the detected features are indicated on the monitor by white dots at the intercepts of each television scan line and the features. The meter gives the projected length in terms proportional to the height of the blank frame. With the minimum chord control set at zero, the total projection, $P_t$, of the image features is

$$P_t = P\ H/M$$

where P is the meter reading, H the blank frame height, and M the image magnification. The units of the total projection value are those that are used to measure the height of the blank frame on the television screen.

The size distribution of the projected chord intercept lengths of the features detected is obtained from meter readings with the minimum chord control set at various minimum chord values. As the setting of the minimum chord control is increased to various positive values, progressively longer intercept chords of the features are disregarded by the detector. In this way the cumulative frequency of the chords greater than selected chord lengths is determined.

The number of features in the image of the specimen is obtained by the count mode. The total number of features detected is indicated on the meter when the minimum chord control is set on zero. As the setting is increased, the number of features detected (counted) decreases, depending on the size distribution. The cumulative size distribution of features is found by noting the count on the meter at increasing settings of the minimum chord control.

### *Results of Pore Studies With the Quantimet*

Quantimet (QTM) measurements of the pore structure of the type samples were made on specimens polished with 0.05 µ alumina on an open, silk-covered lap. The surfaces were coated with a film of chromium 200 to 400 Angstroms thick under high vacuum. Examined under vertical illumination, the surfaces show good contrast between the highly reflective solid areas and the nonreflective areas, or pores.

One to three carefully selected specimens considered to be representative of each sample were analyzed within 30 to 90 different rectangular areas. The area analyzed in each field of view by the Quantimet with the 20-mm objective lens used in this analysis is 0.195 by 0.136 mm. The lens provided a specimen-to-monitor magnification of X1300 and a resolution of approximately 0.9 µ. The volume of pores larger than 0.9 µ (QTM pore volume), the pore boundary projection lengths, and the pore volume distribution are listed in table 5 for all type samples except magnesite (type 7). The values listed in table 5 are averages of the output obtained from 30 or more areas (fields of view) chosen at random on each

TABLE 5—QUANTIMET ANALYSES OF PORE STRUCTURE OF PHASE I SAMPLES[*]

| Sample type | Mean pore volume ($mm^3/g$) | Pore projection (mm) | Pore volume distribution[†] ($mm^3$/gram) | | | | | | | | | Predominant occurrence of pores[‡] |
|---|---|---|---|---|---|---|---|---|---|---|---|---|
| | | | 0.9-2 | 2-2.8 | 2.8-3.9 | 3.9-5.5 | 5.5-7.8 | 7.8-11 | 11-16 | 16-22 | 22-32 (μ) | |
| 1 | 1.4 | 0.03 | 0.7 | 0.1 | 0.1 | 0.2 | 0.1 | 0.0 | 0.1 | 0.0 | 0.0 | Within crystals |
| 2 | 8 | 0.18 | 4.1 | 1.6 | 0.6 | 0.6 | 0.4 | 0.3 | 0.1 | 0.0 | 0.0 | Within crystals |
| 3 | 30 | 0.38 | 13.7 | 4.7 | 2.8 | 2.5 | 2.1 | 1.4 | 1.2 | 0.8 | 0.5 | Within and between grains |
| 4 | 13 | 0.45 | 8.2 | 3.2 | 1.0 | 0.4 | 0.2 | 0.0 | 0.0 | 0.0 | 0.0 | Between grains |
| 5 | 24 | 0.72 | 13.5 | 5.3 | 2.4 | 1.6 | 0.7 | 0.3 | 0.1 | 0.1 | 0.1 | Within and between grains |
| 6 | 54 | 0.99 | 21.6 | 9.4 | 6.0 | 7.0 | 4.4 | 2.8 | 1.7 | 0.7 | 0.1 | Between grains |
| 8 | 18 | 0.22 | 6.2 | 3.0 | 1.7 | 2.2 | 1.8 | 0.9 | 0.9 | 0.7 | 0.2 | Between grains |
| 9 | 63 | 0.79 | 18.8 | 8.1 | 5.9 | 8.5 | 7.5 | 5.4 | 4.5 | 2.8 | 1.3 | Between grains |

[*] Image analyses of pores larger than 0.9 μ (Quantimet magnification 1300X) exclusive of type 7.

[†] The intervals, in microns, corresponds to a constant interval of 1/2 phi units.

[‡] Determined by scanning electron microscopy.

sample. The predominant occurrence (within or between the grains) of pores also is indicated in table 5.

### Petrographic Grain-Size Distribution

The grain sizes of the type samples were individually determined in thin sections with only the polarized light microscope on the Quantimet. Specimen preparation methods attempted to date have failed to produce sufficient contrast between the grains and the grain boundaries to enable the automatic sizing feature of the Quantimet to be used. One to four thin sections of each of the type samples were examined, and 300 to 700 grains were measured in each sample. Standard point-counting methods were used to select the grains for measurement. The measurements were grouped into eight to ten logarithmic size intervals (phi units, where $phi = -\log_2 D$ and D is the apparent diameter in millimeters). Mathematical analyses of the observed size frequency were made, with minor modifications, according to the method presented by Rose (1968). This analysis makes a statistical correction on the bias that occurs in the observed frequency data.

The bias results from two factors — large grains have a greater chance of being counted than do small grains; and grain diameters observed in cross section rarely are as large as the true diameter of the grain. The analysis assumes the grains are spherical, which is a reasonable first approximation of the shape of calcite and dolomite grains. Cumulative curves and histograms of the corrected data were drawn. The graphic mean size, equal to one third of the sum of the 16th, 50th, and 84th cumulative percentiles of the distribution (Folk and Ward, 1957), were computed. The arithmetic mean of the distribution (Krumbein and Pettijohn, 1938) also was computed for the samples. The percentiles were computed by linear interpolation between the cumulative data points. The distribution and means of the samples are shown in table 6.

## Characterization of the Calcined Samples

As part of the petrographic characterization of the carbonate rocks, a study was made of the calcined products of the samples. These observations are pertinent to the over-all project because these products are the main material that reacts with $SO_2$ in the test.

Approximately 180 grams of rock sample was calcined while being rotated in a laboratory furnace, at a preset temperature, for 2 hours by personnel in the Process Research Section of APCO. The temperature of calcination for all samples was 1800° F, except for a few specific test runs on the samples of calcite (types 1 and 2). Each calcine was subdivided into three size grades for tests and microscope studies: 12 by 16, 42 by 65, and 150 by 170 Tyler mesh grades. A portion of each sample was placed in a glass vial immediately after its removal from the furnace, was sealed with an air-tight cap and melted paraffin to prevent absorption of moisture, and was shipped to the Illinois Geological Survey for microscope study. The samples were stored in a dessicator until just prior to examination.

Because the grain size of the calcined samples is mainly in the range of 0.1 to 10 microns, a scanning electron microscope was used for the study. In

TABLE 6—GRAIN SIZE DISTRIBUTION

| Size interval (μ) | Frequency of grains (%) (Number of grains X midpoint of interval) | | | | | | |
|---|---|---|---|---|---|---|---|
| | Sample: Type 3 | Type 4 | Type 5 | Type 6 | Type 7 | Type 8 | Type 9 |
| 1000-4000 | 5.8 | 0 | 3.2 | 0 | 0 | 0 | 0 |
| 500-1000 | 26.7 | 0.3 | 5.7 | 0 | 0 | 0 | 0 |
| 250-500 | 19.4 | 2.0 | 6.7 | 0 | 0 | 0 | 2.3 |
| 125-250 | 9.2 | 0.9 | 32.4 | 0 | 0 | 0.4 | 0.5 |
| 63-125 | 9.8 | 1.2 | 13.8 | 11.9 | 0 | 1.7 | 2.2 |
| 32-63 | 4.8 | 0.2 | 30.0 | 7.4 | 0 | 2.4 | 6.7 |
| 16-32 | 6.6 | 0.7 | 7.5 | 49.6 | 0.6 | 4.5 | 44.7 |
| 8-16 | 9.2 | 11.9 | 0.5 | 21.2 | 13.2 | 4.2 | 29.6 |
| 4-8 | 7.1 | 46.1 | 0.3 | 9.5 | 44.2 | 3.3 | 11.4 |
| 1-4 | 1.3 | 36.7 | 0.1 | 0.4 | 42.0 | 83.5 | 2.6 |
| Mean (arith.*) μ | 31.6 | 4.2 | 69.0 | 16.7 | 4.0 | 2.8 | 13.1 |
| Mean (graphic†) μ | 138.0 | 4.1 | 101.0 | 20.0 | 4.0 | 2.3 | 16.0 |
| Graphic standard deviation* (log units) | 2.6 | 1.2 | 1.4 | 1.2 | 1.1 | 1.2 | 1.0 |

* Krumbein and Pettijohn (1938, p. 240).

† Folk and Ward, 1957.

addition, each sample was subjected to X-ray diffraction analysis to determine the mineral phases present. Each was also examined with the Quantimet under polarized light while immersed in oils of various indices of refraction. The descriptions of the calcined samples that follow are briefly summarized in table 7.

## Description of the Calcined Samples

Type 1, calcined at 1700° F, was found by X-ray and optical analyses to be entirely lime (CaO). The lime retains the rhombic shape and size of the original 1-mm Iceland spar calcite rhombs. At high magnification, the exterior and broken surfaces of the rhombs are covered with angular granules, or subgrains, averaging about 0.25 μ in diameter (figs. 19 and 20). The subgrains are closely packed, and little or no porosity is observed in SEM photographs.

TABLE 7—DESCRIPTION OF THE CALCINES

| Sample type | Temperature (°F) | Minerals present | Particle size[†] (μ) | Texture | Relative porosity |
|---|---|---|---|---|---|
| 1 | 1700 | Lime | 0.1 to 0.5[*] | Granular | Very low |
| | 1800 | Lime | 1 to 2 | Rounded | Moderate |
| 2 | 1700 | Lime and minor calcite | 2 to 4 | Partly spongy | Low to moderate |
| | 1800 | Lime | 2 to 5 | Spongy | Low |
| | 1900 | Lime | 2 to 10 | Blocky | Low |
| 3 | 1800 | Lime, minor periclase | 1 to 2 | Spongy, partly rounded | Moderate to high |
| 4 | 1800 | Lime | 0.5 to 1 | Granular, partly spongy | Low to moderate |
| 5 | 1800 | Lime and periclase | 0.2 to 1 | Granular-agglomeratic | Moderate |
| 6 | 1800 | Lime, periclase, and quartz | 0.2 to 1 | Granular-agglomeratic | High |
| 7 | 1800 | Periclase | 0.1 to 0.5 | Granular | Very low |
| 8 | 1800 | Lime | 2 to 10 | Spongy, partly blocky | Low to moderate |
| 9 | 1800 | Lime and periclase | 0.5 to 2 | Granular-agglomeratic | Moderate |

[†] Determined from scanning electron micrographs.

[*] These particles are subgrains of 1 mm grains that are anisotropic and laminated. All other samples are isotropic limes.

## LIMES FROM ICELAND SPAR CALCITE, TYPE 1, CALCINED AT 1700 AND 1800° F

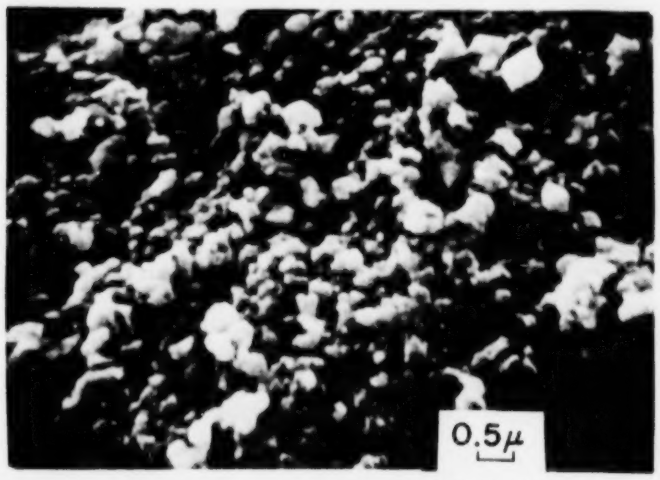

Fig. 19. Type 1 calcine; 1700° F, 42/65-mesh particles; angular grains of lime; SEM, X10,000.

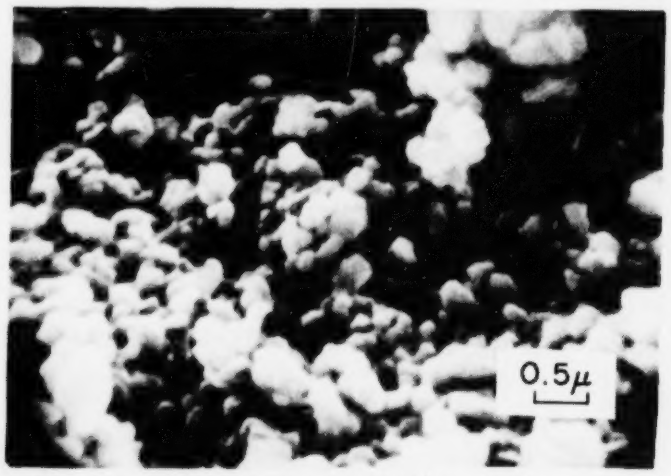

Fig. 20. Type 1 calcine; 1700° F, 150/170-mesh particles; angular grains of lime; SEM, X15,000.

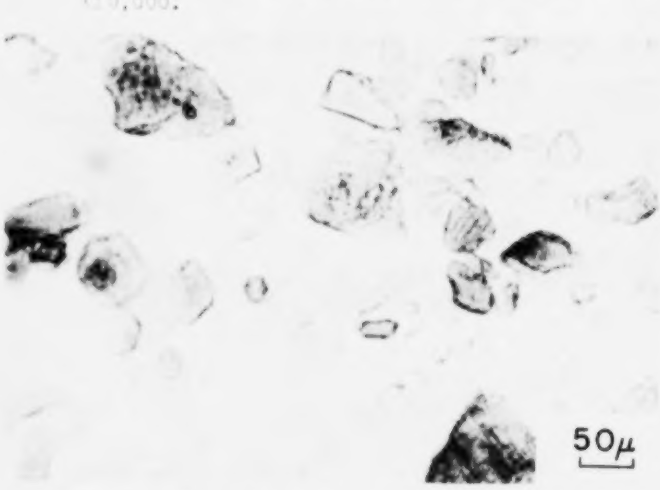

Fig. 21. Type 1 calcine; 1700° F, crushed 12/16 mesh; each lime particle has a polygranular surface, as in Fig. 19; in transmitted light, X124.

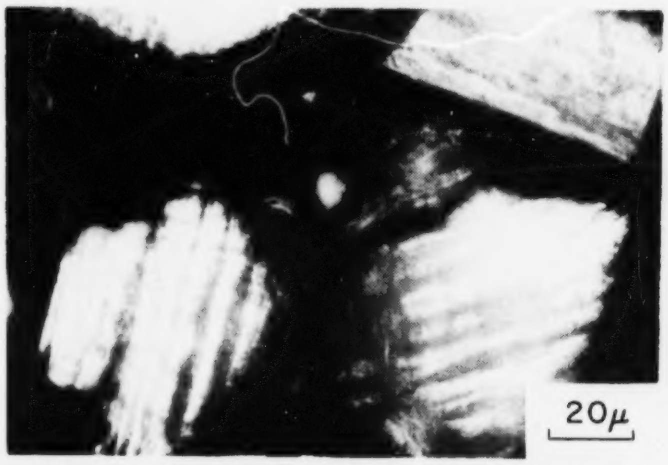

Fig. 22. Same as fig. 21; laminated structure probably due to internal strain; in crossed polarized transmitted light, X575.

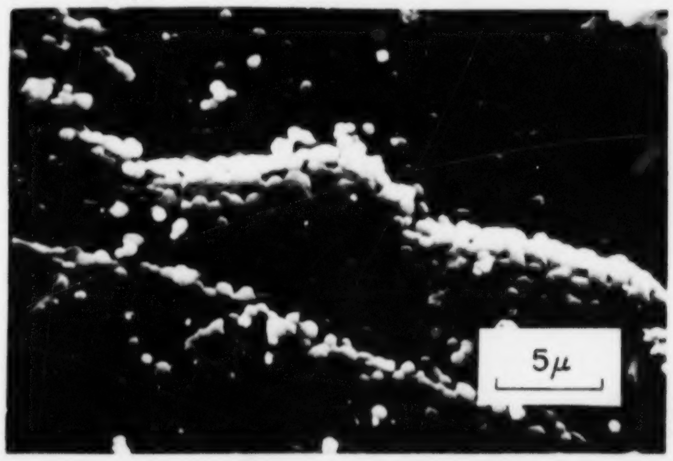

Fig. 23. Type 1 calcine; 1800° F, 10/28 mesh; rounded granules of lime; SEM, X2240.

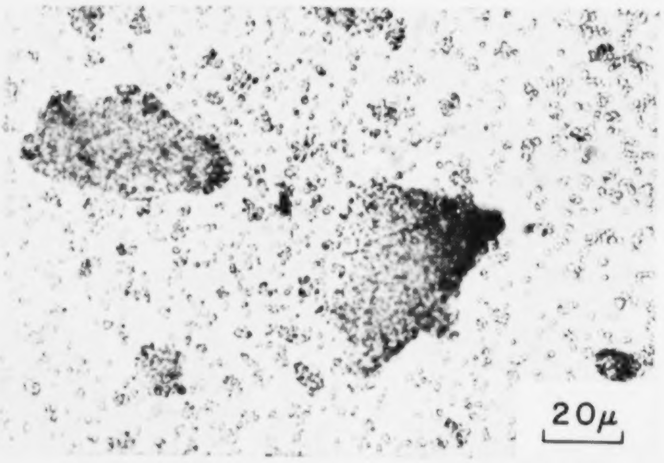

Fig. 24. Same as fig. 23; partly dispersed granules of lime; in transmitted light, X550.

In reflected light the particles are colorless, but in transmitted light most are brown to tan (fig. 21). Nearly all grains are distinctly anisotropic and are revealed in crossed polarized light to be laminated (fig. 22), which results in an anomalous wavy exinction as the grains are rotated. Anisotropism is not a normal characteristic of lime. All other samples of calcines described below are more than 95 percent isotropic particles of lime and periclase (MgO). Also, the 1700° calcine of type 1 is the hardest to crush in a mortar and pestle of all the samples studied.

Type 1 calcined at 1800° F consists of isotropic and rounded grains of lime (figs. 23 and 24). The grains average about 1 µ in size. The 1800° F calcine is essentially the same color as the 1700° F material, but it is not as hard.

Calcination of type 2 at 1700° F yields lime and approximately 5 percent unburned calcite. The material is slightly porous and granular in texture as observed with the SEM (fig. 25); it breaks up easily into angular particles about 2 to 4 µ in diameter (fig. 26). Samples calcined at 1800° F are typified by their spongy texture (fig. 27) and show a three-dimensional configuration of lime particles that are very irregular in shape. The calcine has a complex maze of void spaces throughout. Patches of blocky lime of low porosity and consisting of interlocking grains also occur in the sample (fig. 28). Samples calcined at a still higher temperature, 1900° F, have more areas of blocky, interlocking texture (fig. 29). In figure 29 the presence of joints or cracks in certain raised material that occurs mainly along edges of several lime grains can be seen. This material is thought to be portlandite ($Ca(OH)_2$) formed by reaction of the calcine with moisture sometime after its removal from the furnace. The joints were probably formed by desiccation during high-vacuum processing of the specimen for SEM study. Incipient cubic (010) crystal surfaces on a few lime grains are indicated by arrows in figure 29. The 2040° F calcine (fig. 30) appears to have a dense interlocking texture of equant grains of lime, although much of the surface is coated with jointed material, probably portlandite.

Type 3 calcines (1800° F) are mainly spongy textured lime (figs. 31 to 34). Figure 31 is a typical view of the sample at low magnification. Many areas of the specimens are highly porous and have elongated lime particles (fig. 32), while in other areas the particles are rounded and granular (fig. 33). Figure 34 shows the lime and periclase (MgO) that were derived from a single dolomite rhomb. The obtuse angle of the rhomb is shown in the upper part of the figure. The larger highlighted particles in the lower left and upper part of the figure are dust particles.

Type 4 calcines are illustrated in figures 35 to 38. The stone is a high-purity limestone composed of equant calcite grains that average about 4 µ in diameter. The texture of the limestone is faintly preserved in the calcine by the distribution of the lime particles (fig. 35). The texture of the lime is typically granular (figs. 35 and 36), although certain parts of the sample are spongy (fig. 37) and others are mixtures of the two types (fig. 38). The grain size of the lime is mainly between 0.5 and 1 µ. Type 4 calcined at 1800° F is relatively hard compared with other samples.

## LIMES FROM CALCITE SPAR, TYPE 2, CALCINED AT VARIOUS TEMPERATURES

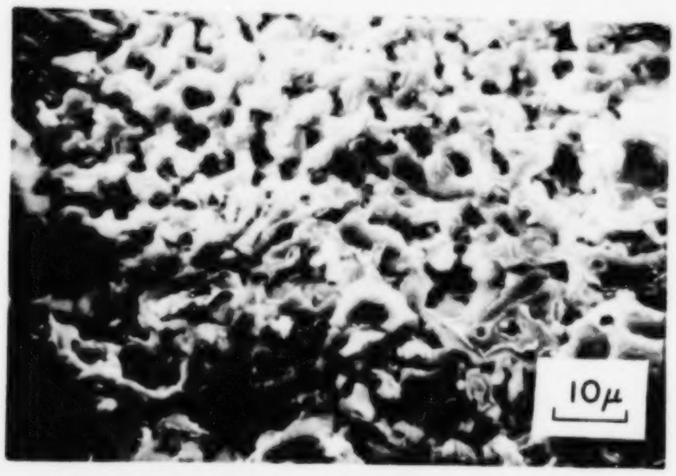

Fig. 25. Type 2 calcine; 1700° F, 42/65 mesh; partly calcined to lime; low pore volume; SEM, X1000.

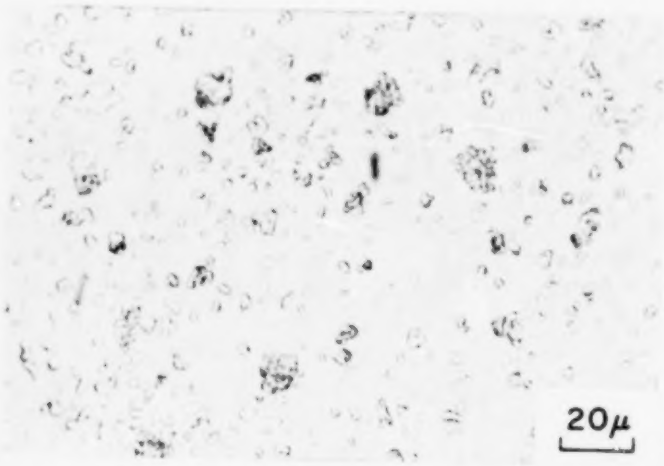

Fig. 26. Same as fig. 25; dispersed granules of lime and calcite; in transmitted light, X550.

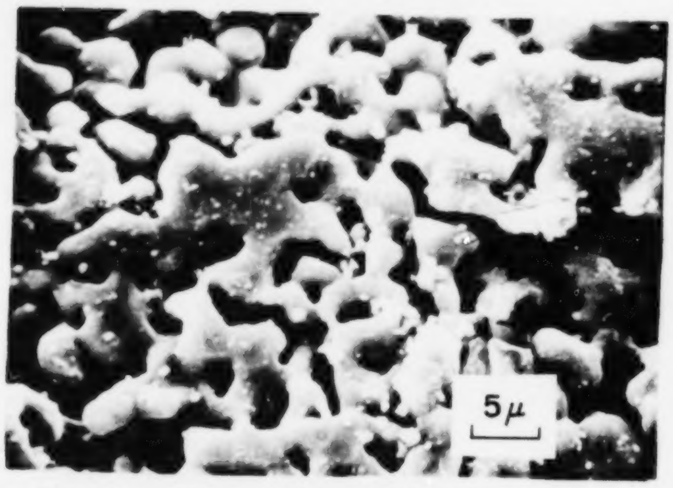

Fig. 27. Type 2 calcine; 1800° F, 42/65 mesh; typical view, showing spongy texture and high porosity; SEM, X2000.

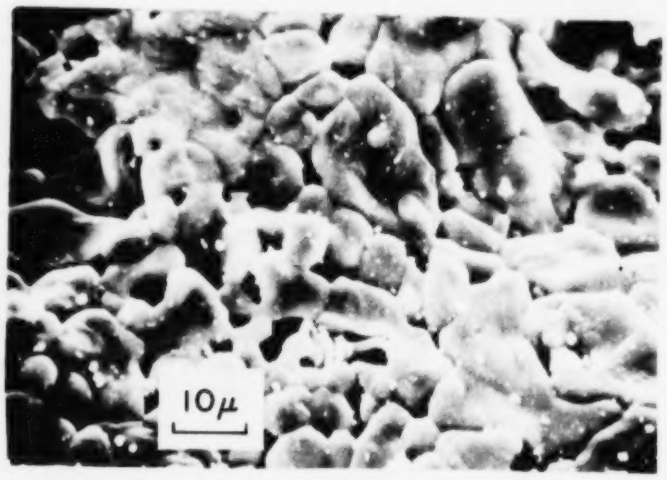

Fig. 28. Same as fig. 27; an area of low porosity and partly sintered lime; SEM, X1000.

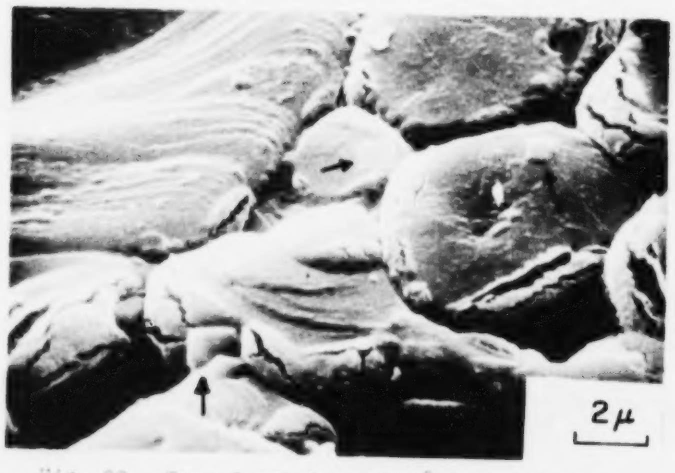

Fig. 29. Type 2 calcine; 1900° F, 12/16 mesh; interlocking grains of lime with incipient crystal faces (arrows); note cracks in surficial material, possibly portlandite, $Ca(OH)_2$; SEM, X5000.

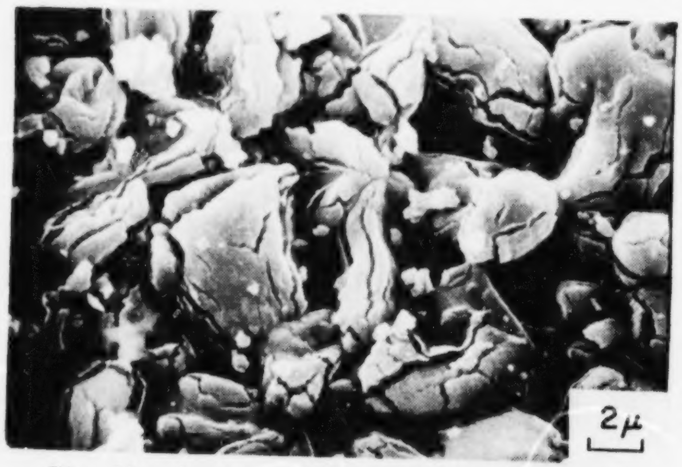

Fig. 30. Type 2 calcine; 2040° F, 42/65 mesh; sintered lime, low-pore-volume lime with interlocking grains; pronounced surface cracking; SEM, X4330.

## LIME FROM COARSE-GRAINED LIMESTONE, TYPE 3. CALCINED AT 1800° F

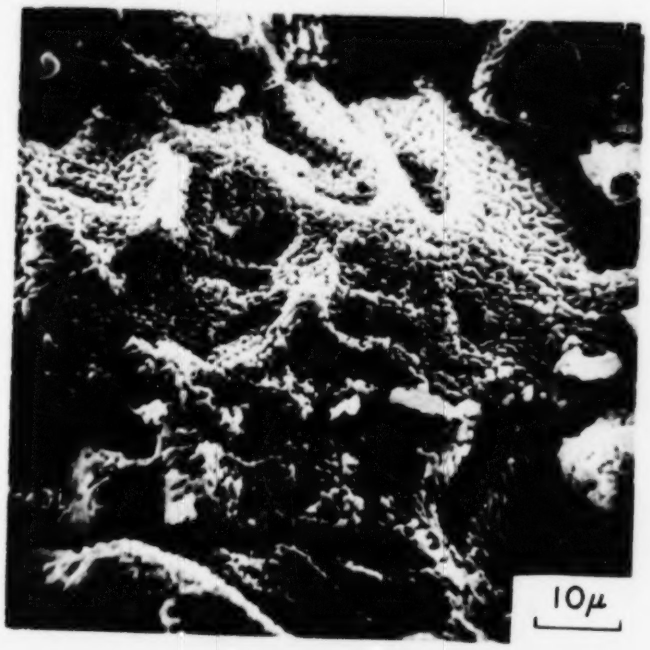

Fig. 31. Type 3 calcine; 12/16 mesh; typical view of specimen, showing spongy texture; SEM, X1100.

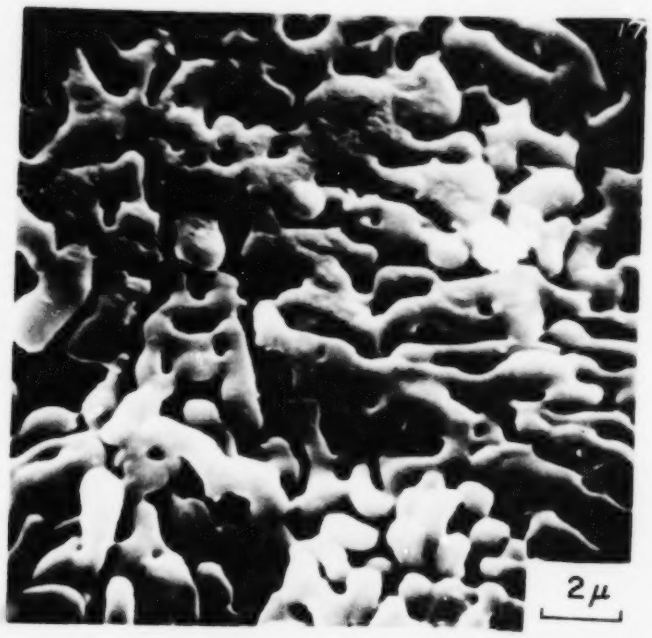

Fig. 32. Close-up of specimen in fig. 31, showing detail of spongy textured lime; SEM, X5440.

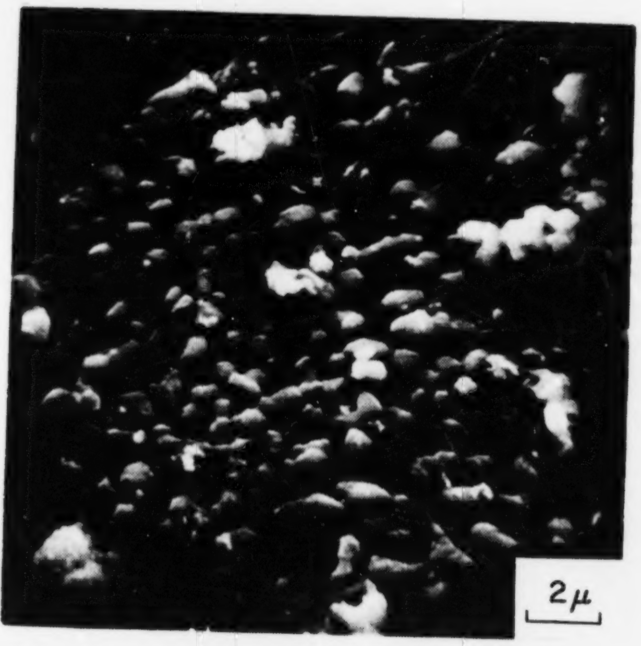

Fig. 33. Type 3 calcine; 42/65 mesh; rounded-granular texture; SEM, X5000.

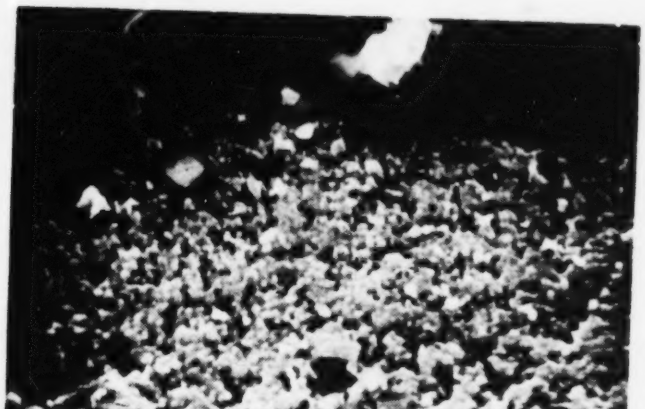

Fig. 34. Type 3 calcine; 150/170 mesh; mixture of lime and periclase (medium gray) derived from a dolomite grain in the limestone; SEM, X5000.

## LIME FROM FINE-GRAINED LIMESTONE, TYPE 4, CALCINED AT 1800° F

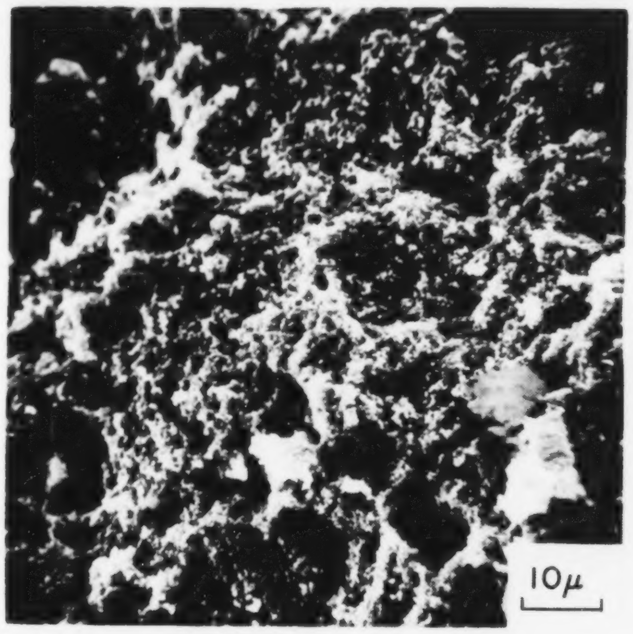

Fig. 35. Type 4 calcine; 12/16 mesh; shows general character of the material at low magnification; SEM, X1100.

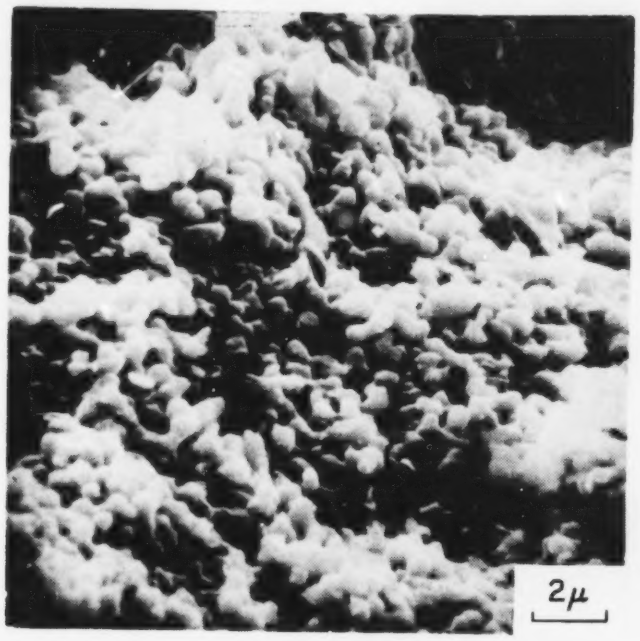

Fig. 36. Close-up of fig. 35, showing granular character of much of the lime; SEM, X5100.

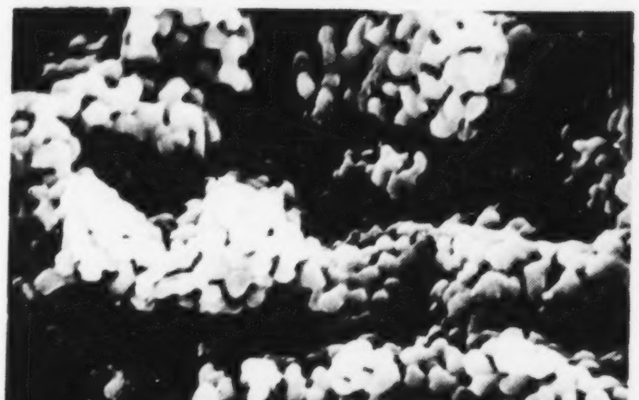

Fig. 37. Another area of specimen in fig. 35, showing spongy texture; SEM, X4890.

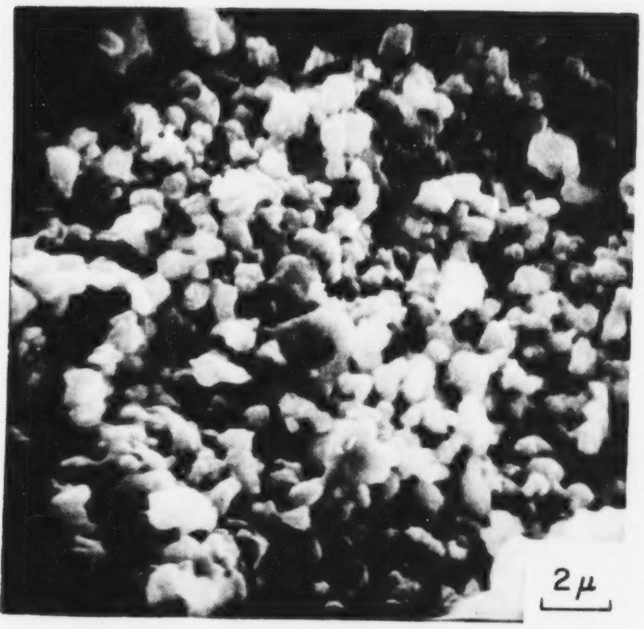

Fig. 38. Type 4 calcine; 42/65 mesh; shows mixed granular and spongy texture; SEM, X5000.

Type 5 calcines consist of lime and periclase in nearly equal proportions and crush very easily in the mortar and pestle. The texture of the original dolomite is commonly preserved in the calcined product (fig. 39). However, the calcines are very finely granular (figs. 40 and 41). Distinction between the lime and periclase in the electron micrographs cannot be made positively, but two groups of particle sizes can be seen in the calcine. One group is approximately 1 µ, the other is near 0.2 µ. As the magnesium carbonate of the dolomite loses $CO_2$ at a lower temperature than the calcium carbonate, the larger particles are probably periclase. In the electron micrographs, the larger particles appear to underlie the submicron grains. Most of the 0.2 µ particles, probably lime, appear to be attached individually to the surface of the larger particles (figs. 40 and 42). The term "subgrain" may be applicable to these attachments, or appendages.

Type 6 calcines consist of lime and periclase with quartz and other constituents derived from the small amounts of clay in the original dolomite. The texture of the calcine is uniformly finely granular and porous (fig. 43). The particles of calcine are found to be fairly soft in the mortar and pestle and consist of lime granules 1 µ or less in size.

Type 7 calcines are derived from fine-grained magnesite and are quite uniform in surface texture (fig. 44). The material consists entirely of periclase. The texture is finely granular, and resembles that of the 1700° F calcine of type 1 (fig. 19). The calcine particles of type 7 are moderately hard when ground in the mortar and pestle.

Type 8 (oolitic aragonite) calcines consist of lime. The lime is typified by its spongy texture (fig. 45); however, small areas of the samples have an interlocking grain texture (fig. 46). The figure also shows solid material, probably lime, occurring along some of the grain boundaries. Most of the calcined particles are colorless in reflected light, but many are pale green and are generally composed of grains about 5 µ in diameter. The colorless particles are generally in the range of 0.5 to 2 µ in diameter.

Type 9 calcines consist of lime and periclase derived from the original calcitic dolomite. The calcines are distinctly buff in color because they contain iron oxide. The calcines (figs. 47 and 48) are composed of 1 to 15 µ agglomerate particles and retain much of the granular character of the original stone. A highly magnified view of the larger particles (fig. 48) shows they have a granular texture much like the calcine of type 5 dolomite, and that the occurrence of many 1 µ grains (probably lime) are partly fused to, or incorporated in, larger "underlying" grains that are probably periclase.

## Discussion of Calcines

These studies do not show consistent or significant differences between the three grades, 12 by 16, 42 by 65, and 150 by 170 Tyler mesh sizes, of the calcined materials. The 1700° F calcine of Iceland spar calcite (type 1) has a low sorption capacity for $SO_2$, which will be discussed later. This low capacity probably is due to the large size and density of the lime particles. The anisotropism of this lime is unique and no doubt results from a high degree of strain in the Ca-O bonds of the lime's crystal structure. When the calcine is heated

## CALCINES FROM REEF DOLOMITE, TYPE 5, 1800° F

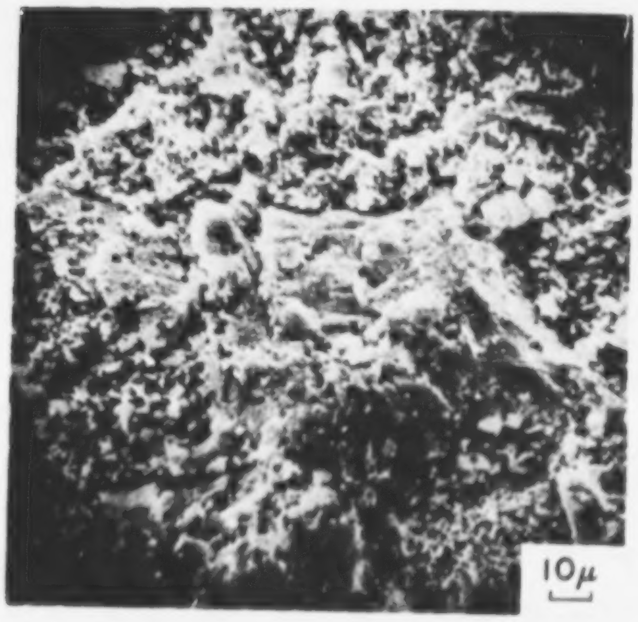

Fig. 39. Type 5 calcine; 12/16 mesh; original grain texture of the dolomite is preserved in the lime and periclase; SEM, X520.

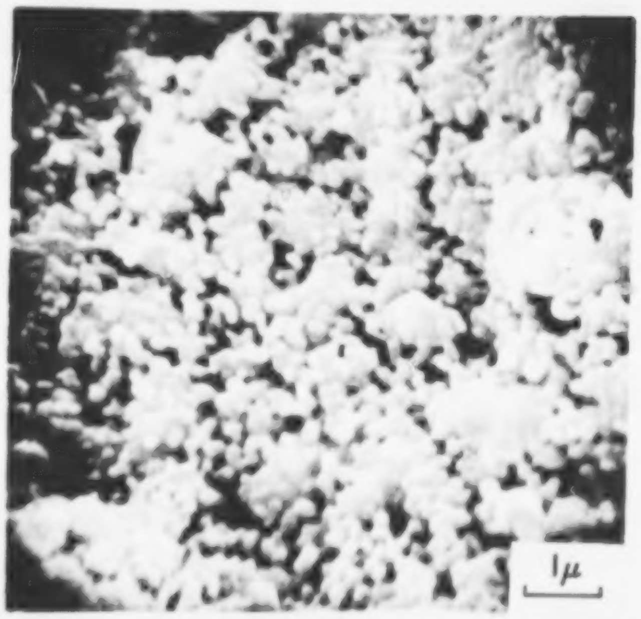

Fig. 40. Close-up of the center of fig. 39; numerous grains, 0.1 to 0.2 μ, are fused to form agglomerate particles about 1 to 2 μ in diameter; SEM, X10,240.

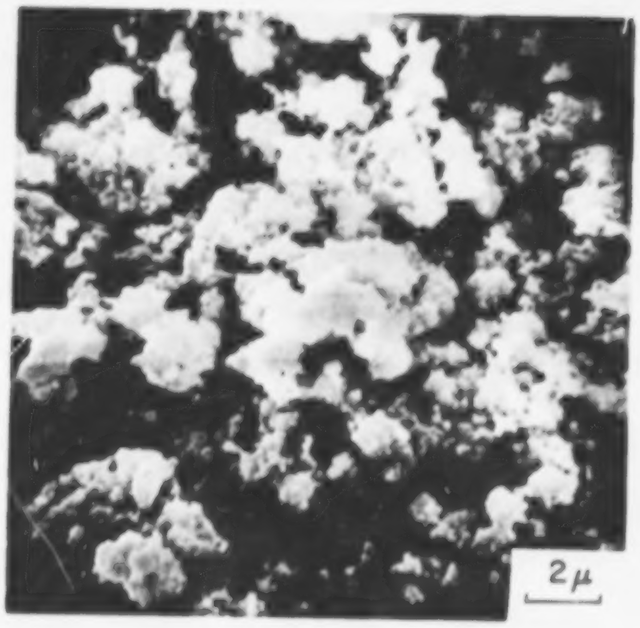

Fig. 41. Type 5 calcine; 150/170 mesh; general view, showing granular nature of the lime and periclase; SEM, X5000.

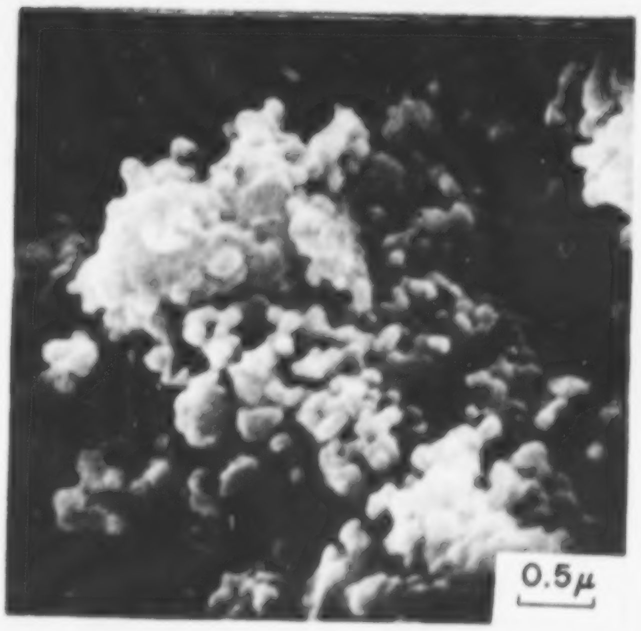

Fig. 42. Close-up of granular particles of sample in fig. 41; SEM, X20,000.

## CALCINES FROM TYPES 6 THROUGH 9, 1800° F

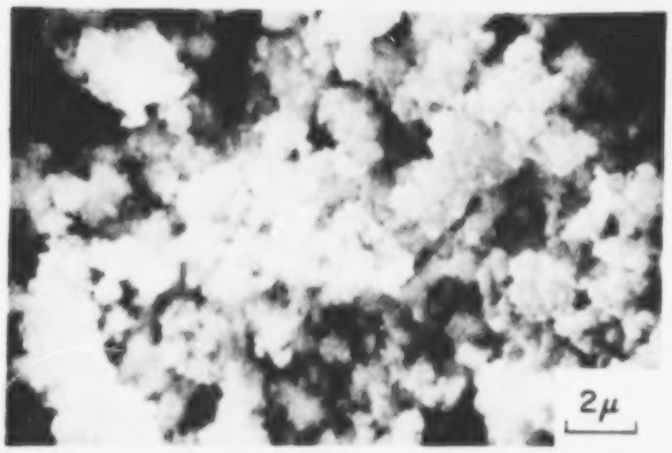

Fig. 43. Type 6 calcine of interreef dolomite; 12/16 mesh; typical view of very finely granular lime and periclase; SEM, X10,000.

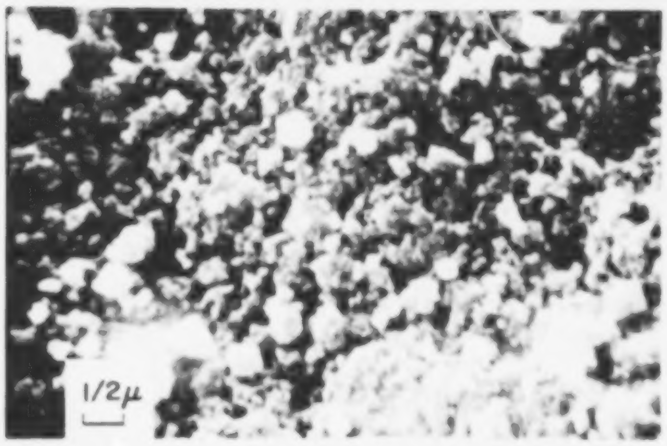

Fig. 44. Type 7 calcine of magnesite; typical view showing granular character of the periclase; SEM, X10,000.

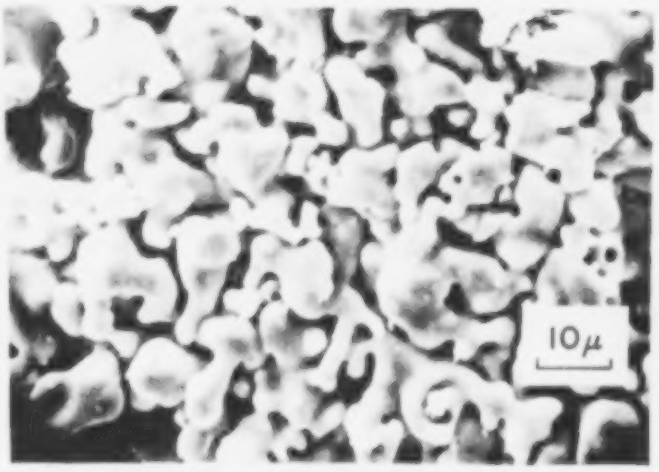

Fig. 45. Type 8 calcine of oolitic aragonite; the lime is typified by its spongy texture; SEM. X1000.

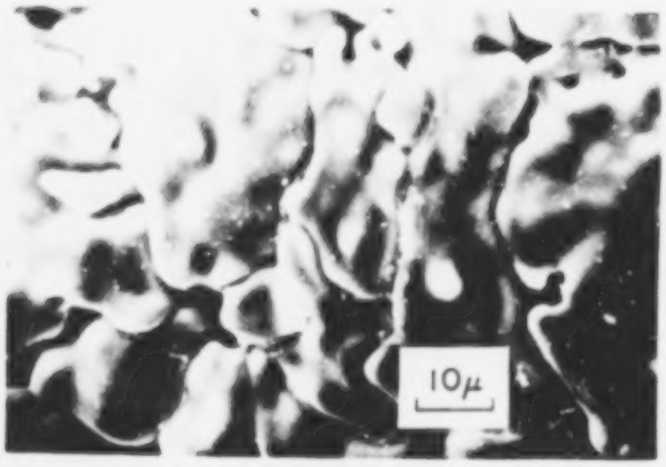

Fig. 46. Same as fig. 45; sintered lime forms an interlocking texture in small patches in the sample; SEM, X1000.

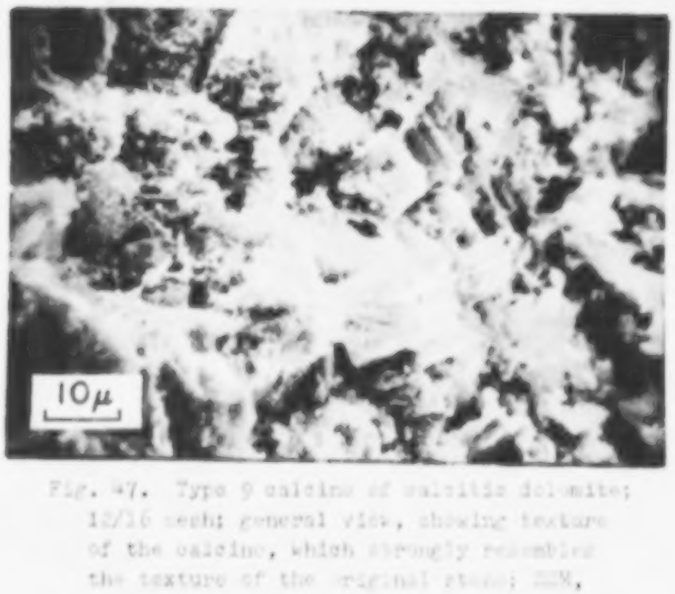

Fig. 47. Type 9 calcine of calcitic dolomite; 12/16 mesh; general view, showing texture of the calcine, which strongly resembles the texture of the original stone; SEM, X1000.

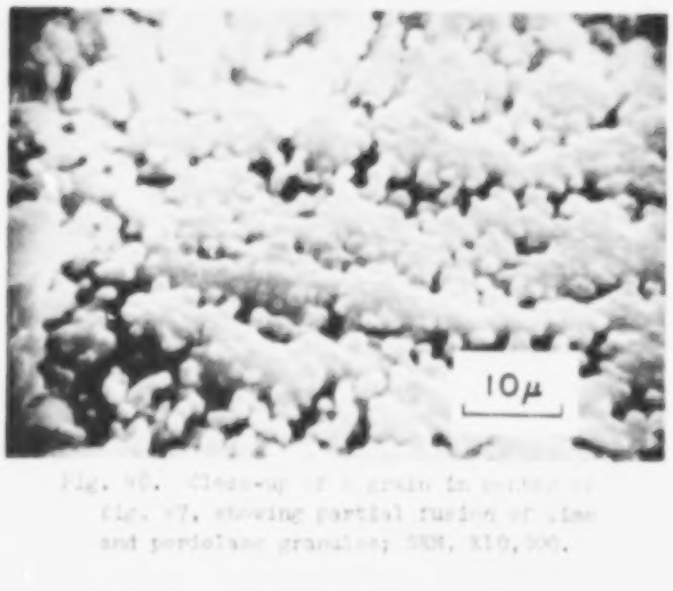

Fig. 48. Close-up of a grain in center of fig. 47, showing partial fusion of lime and periclase granules; SEM, X10,000.

further to 1800° F, the shape of the angular subgrains on the surface of the 1700° F calcine becomes rounded, the grain size is greatly reduced, and the lime becomes isotropic.

When the temperature of calcination is changed from 1700° to 2040° F, the SEM observations of types 1 and 2 calcines show porosity increases, then decreases. These porosity changes are accompanied by a series of changes in texture, starting from granular (with submicron angular grains), altering to rounded granular, then to spongy, and finally to an interlocking granular texture with blocky grains of lime.

It is postulated that the lime particles formed by calcination of dolomite are prevented from coalescing because of the presence of masses of periclase formed earlier, which tend to physically separate the nuclei of the lime and thereby produce a subgrain structure with a very high CaO surface area.

## PETROGRAPHIC STUDIES OF SAMPLES OF CERTAIN COMMERCIAL CARBONATE ROCKS (PHASE II)

### Samples and Methods

Seventeen commercially available crushed stone samples were examined and studied in the second phase of the project. Included in these samples are five poorly lithified and unconsolidated marls and chalks, each rich in calcite, a calcitic marble, six limestones, and five dolomites. All the limestones and dolomites contain more than 93 percent carbonates. One of the samples (2061) was the limestone injected into unit 10 of the Shawnee Steam Plant of TVA during the first stage of the dry limestone injection project.

The samples studied during this phase of the project were obtained from the Division of Process Control Engineering of APCO. They consist of crushed particles, most less than an eighth of an inch in diameter, considered to represent a commercial product. Representative sample splits were analyzed for their mineral content by HCl residue, X-ray diffraction, and microscope methods; they were also subjected to chemical analysis and petrographic studies. For the petrographic studies, 30 to 60 specimens, 12 to 16 mesh, were cast in epoxy molds. Three to six petrographic thin sections and two or more polished sections were then prepared for examination with the Quantimet. Also, selected specimens were examined with a scanning electron microscope (SEM). Grain and pore size measurements were made with both the Quantimet and electron microscope.

### Petrographic Characterization of Samples

Petrographic descriptions and source of the samples are given in table 8. Typical photomicrographs from the polarizing and scanning electron microscopes are shown in figures 49 to 51. In table 8, the term granularity refers to the degree of uniformity of the grain size of the rock as observed microscopically. The term inequigranular is used for a sample in which the majority

## TABLE 8—PETROGRAPHIC DESCRIPTION AND SOURCE OF SAMPLES

| Sample number | Granularity | Relative grain size | Grain shape | Degree of grain interlocking | Other textural features | Source |
|---|---|---|---|---|---|---|
|  | LIMESTONES |  |  |  |  |  |
| 1343 | Inequigranular | Fine to medium | Anhedral | High | Micro-fossiliferous and fragmental: algal, foraminifera, brachiopod shells etc., also pelletoidal. | Hooper Bros., Weeping Water, Nebraska (1/8" down aglime) |
| 1359 | Equigranular | Fine | Anhedral | High | Few veinlets of medium-grained sparry calcite. Few specimens are inequigranular, others limonite bearing. | Grove Lime Company, Stephens City, Virginia (aglime) |
| 2060 | Inequigranular | Fine to coarse | Anhedral | Moderate | Fossiliferous and fragmental; abundant coarse crinoid plates, other fine-grained fossils (see 2061), dolomite and quartz silt (24 μ) set in very fine calcite matrix. | Fredonia Valley Quarries, Fredonia Valley, Kentucky (Blue Ledge) |
| 2061 | Inequigranular | Fine and coarse | Anhedral - subhedral | Low | Oolitic and fossiliferous and fragmental: fine-grained brachiopods, echinoids, bryozoans, ostracods, and foraminifera fragments; and few coarse single grained crinoid plates. | Fredonia Valley Quarries, Fredonia Valley, Kentucky (Upper white ledge) |
| 2065 | Inequigranular | Fine to medium | Anhedral | Moderate | Pelletoidal, with sparry calcite (10 μ) cement; also irregular patches of medium-grained sparry calcite. | Longview Limestone (TVA) |
| 2071 | Inequigranular | Very fine and medium | Anhedral and rhombic | High | Mostly very fine-grained even textured with scattered dolomite rhombs throughout the stone particles. Few patches of sparry calcite in some specimens. | Marble Cliff, Carntown, Kentucky (TVA) |
|  | MARBLE |  |  |  |  |  |
| 1336 | Single crystal particles | Very coarse | Cleavage rhombs |  | Sparry calcite, intracrystalline inclusions and twin lamellae. Scattered grains of tremolite surrounded by calcite in some specimens. | Georgia Marble Company, Tate, Georgia (#2 crushed marble) |

TABLE 8—PETROGRAPHIC DESCRIPTION AND SOURCE OF SAMPLES (Continued)

| Sample number | Granularity | Relative grain size | Grain shape | Degree of grain interlocking | Other textural features | Source |
|---|---|---|---|---|---|---|
| | DOLOMITES | | | | | |
| 1377 | Equigranular | Coarse | Rhombic | High | Granular mosaic, microporous; few specimens are fine-grained. | Chas. Pfizer Company, Gibsonburg, Ohio (#10 Glasshouse stone) |
| 1378 | Inequigranular | Coarse, medium and fine | Sub-rhombic | High | Granular mosaic; grain boundaries tend to be stairstepped in many particles, others are curvilinear. | Verplanks Coal and Dock Fettysburg, Michigan (Fluxing fines) |
| 1380 | Equigranular | Medium | Sub-rhombic | High | Granular mosaic; grain boundaries tend to be stairstepped. | Rockwell Lime Company, Manitowoc, Wisconsin |
| 1688 | Inequigranular | Coarse and medium | Rhombic | High | Granular mosaic | Marblehead Lime Company, Chicago, Illinois |
| 2069 | Equigranular | Medium and fine | Rhombic and anhedral | High | Mixture of fine-grained (anhedral) and medium-grained (rhombic) stone particles. | James River Limestone, (TVA) |
| | MARLS AND CHALKS | | | | | |
| 2080 | Inequigranular friable | Fine | Anhedral and fibrous | Moderate | Banded algal (?) structures and foraminifera, also globular and irregular shaped agglomerates. Sparry calcite cement partly surrounding banded particles. The latter crystallites are generally parallel to one another (fibrous). | Ohio Geological Survey Columbus, Ohio (NE, OH) |
| 2109 | Inequigranular friable | Fine | Anhedral | Low | Variety of thin fossil shells and other microfossils and woody organic matter. Thin bands of organic-rich matter surrounds many dense very fine-grained calcite globules. Also some specimens with abundant quartz silt (20-50 μ). Pores largely in microfossil cavities. Scattered limonite grains. | Soil Conservation Service, Syracuse, New York (Canastota, Madison County, New York) |

### TABLE 8—PETROGRAPHIC DESCRIPTION AND SOURCE OF SAMPLES (Concluded)

| mple mber | Granularity | Relative grain size | Grain shape | Degree of grain interlocking | Other textural features | Source |
|---|---|---|---|---|---|---|
| 29 | Equigranular friable | Fine | Anhedral | Low | Predominantly fine, even textured calcite (1 $\mu$); few scattered thin shelled fossils and limonite-organic-rich particles and stringers. Few scattered quartz grains up to 1 mm diameter. | S. K. Vorres, R. R. 2, Fremont, Michigan (Newaygo County, Michigan) |
| 77 ustin halk) | Inequigranular friable | Fine | Anhedral | Low | Sparry calcite (up to .15 mm across) fossil materials scattered sparsely throughout a very fine-grained (micritic) calcite. Few green glauconite clay pellets and limonite-rich particles. | Longhorn Portland Cement, San Antonio, Texas (Austin chalk) |
| 81 ansas halk) | Inequigranular friable | Fine | Anhedral and fibrous | Moderate | Abundant foraminiferal tests (up to 0.5 mm across) consisting of very fine-grained calcite and medium-grained calcite spar filling voids in the tests. Also banded algal (?) structures, alternating very fine and medium-grained (fibrous) calcite (5-15 $\mu$). Some specimens mainly pelletoidal. Scattered quartz silt (10-25 $\mu$) and limonite. Few soft gray clay particles. | State Geological Survey, Lawrence, Kansas (Kansas chalk) |

## EXPLANATION OF FIGURE 49

1343 — TPL (Thin-section in transmitted crossed-polarized light); shows inequigranular and fossiliferous nature of the limestone. A foraminifera test is shown in the lower left and clear sparry calcite is scattered throughout the fine-grained calcite. The dark grains, near center and in upper left, are calcite oriented at optical extinction in crossed-polarized light.

1359 — SEM (Fracture surface in scanning electron microscope); shows equigranular character of the limestone sample and high degree of grain-interlocking.

2061 — TPL; shows oolitic and fossiliferous nature of the limestone. The dark areas are very fine-grained and the light areas are medium- to coarse-grained (crinoid fossil fragments) sparry calcite.

2061 — SEM; shows detail of the main components in the limestone: (1) large single crystal grain of calcite (crinoid fossil fragment) with intracrystalline voids on left, (2) very fine-grained and poorly interlocking calcite grains that form the outer bands of the oolites and fossil fragments (see 2061-TPL), and (3) the medium-sized and tightly interlocked grains of clear sparry calcite on the right.

2065 — TPL; shows the inequigranular character of the irregular patches of sparry calcite. SEM photographs of the pelletoids that occur in this sample appear as in 1359 above. The dark grains are mainly crystalline grains of calcite oriented at optical extinction and a few grains of opaque pyrite.

1336 — SEM; shows cleavage surface of a large grain of calcite in the marble. Note the presence of eight voids, approximately 0.5 to 2 microns across, shown in this micrograph.

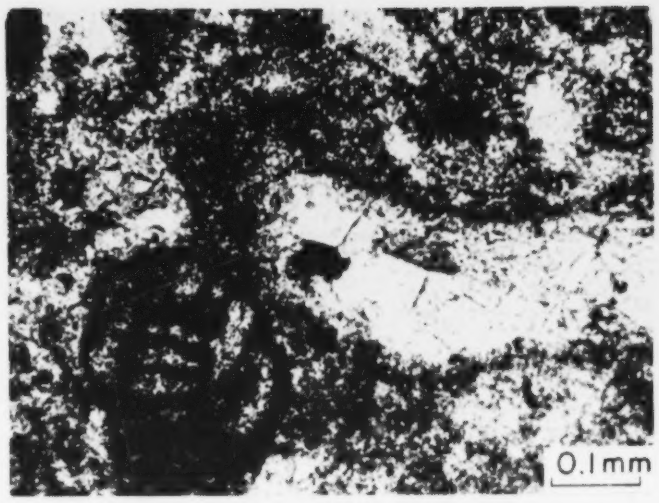

1343 - Limestone X150

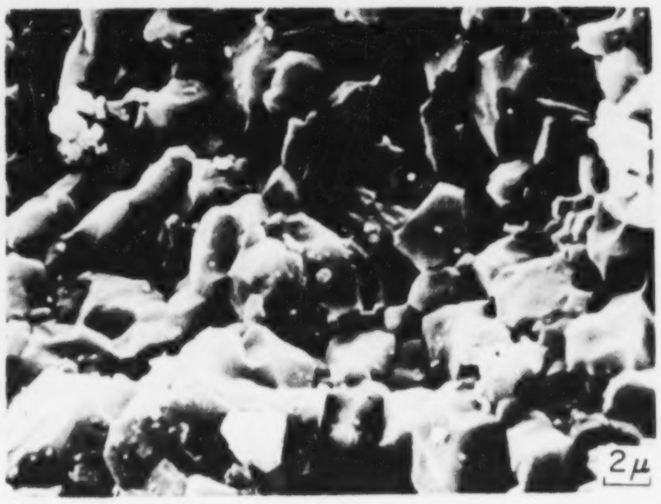

1359 - Limestone X3310

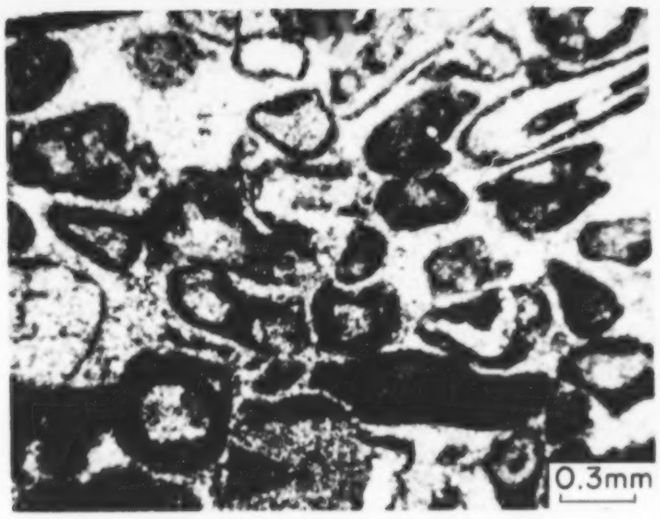

2061 - Limestone X30

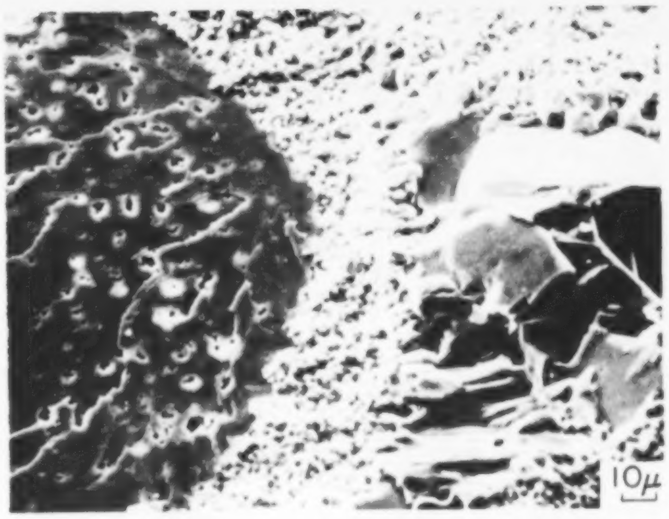

2061 - Limestone X430

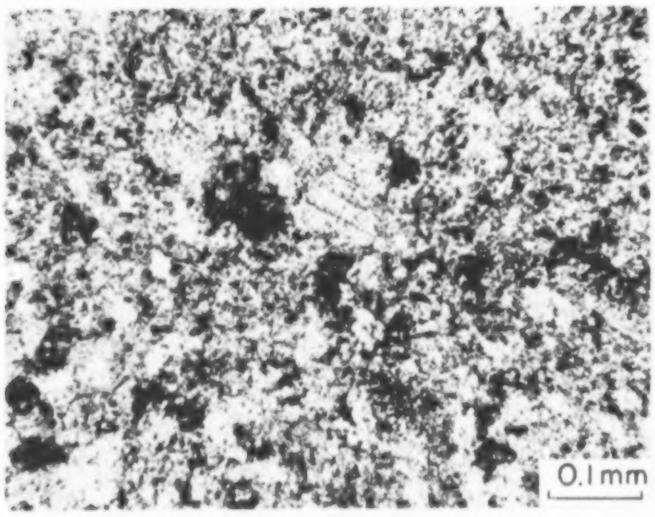

2065 - Limestone X130

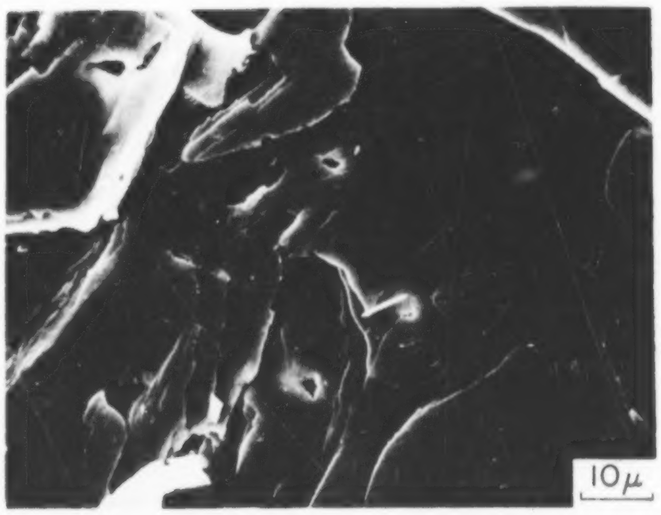

1336 - Marble X990

Fig. 49. Typical textures and grain characteristics of limestones and marble.

## EXPLANATION OF FIGURE 50

1337 — TPL; equigranular and coarse-grained dolomite. Dark grains oriented at optical extinction show very small crystallite inclusions. Several grains show characteristic rhombic angles by intersection of grain boundaries.

1378 — TPL; inequigranular dolomite showing few occurrences of "stairstep" grain boundaries. The dark inclusions abundantly shown in the grains are intragranular voids such as are shown in the SEM photograph of 1688 below. The larger dark areas are dolomite grains.

1380 — TPL; equigranular dolomite showing typical granular mosaic. Grain boundaries tend to be less linear than those in the other samples. Note also the abundance of very small and dark-appearing inclusions (voids) within the grains.

1688 — TPL; inequigranular dolomite.

1688 — SEM; shows detail of the type of intragranular voids common in all of the dolomite samples.

2069 — TPL; mosaic of equigranular dolomite.

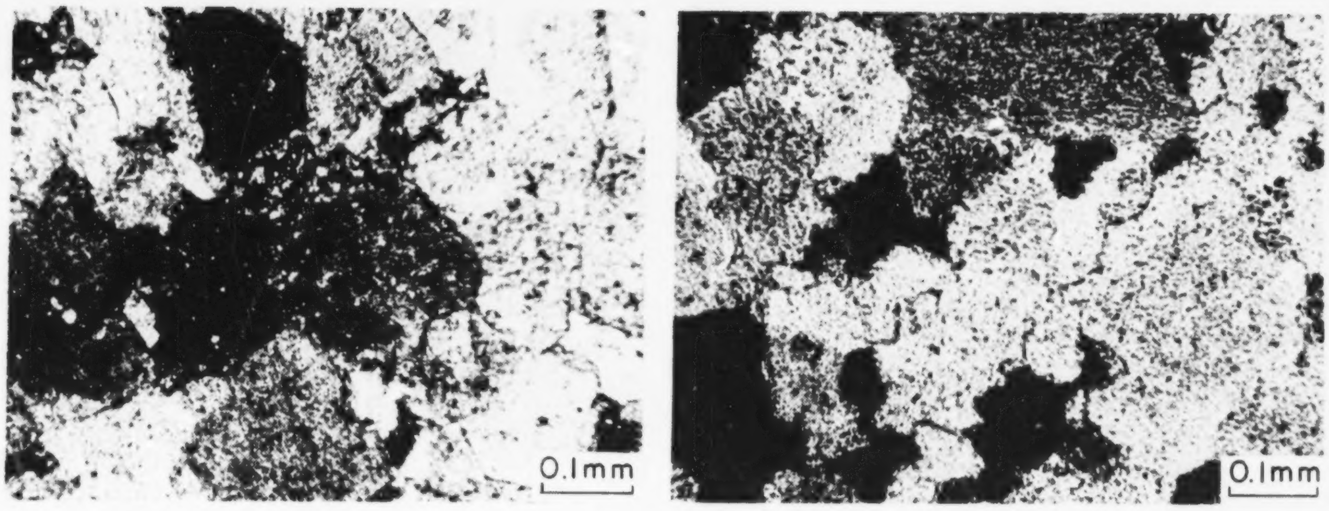

1337 - Dolomite X130 1378 - Dolomite X130

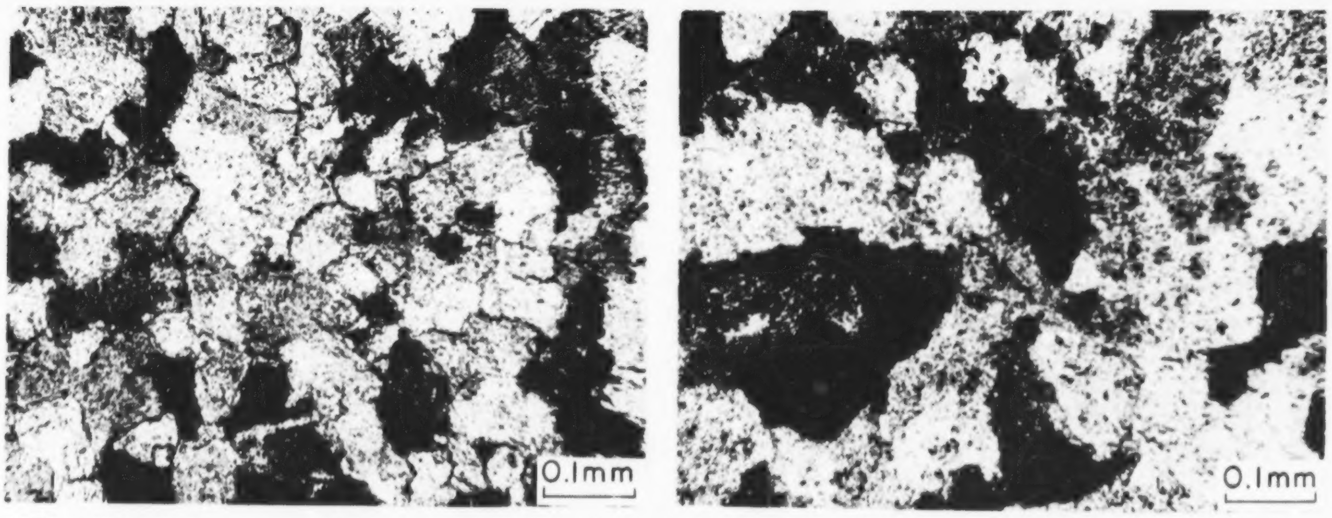

1380 - Dolomite X130 1688 - Dolomite X130

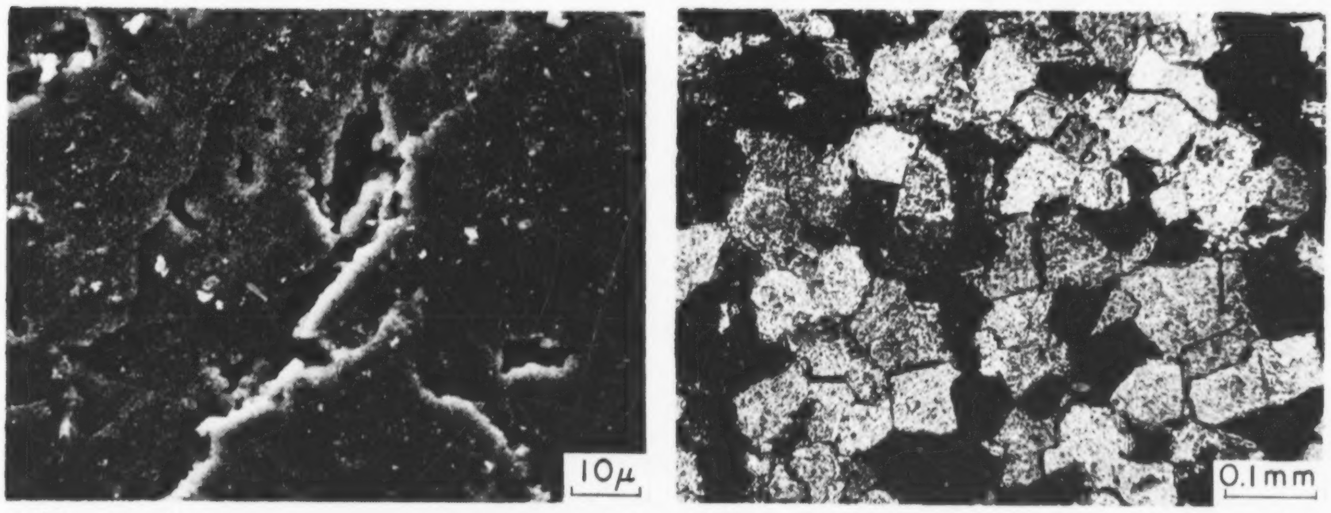

1688 - Dolomite X990 2069 - Dolomite X130

Fig. 50. Typical textures and grain characteristics of dolomites.

EXPLANATION OF FIGURE 51

2080 — SEM; shows fine-grained, partly fibrous, and porous character of the marl.

2109 — SEM; shows general texture of the marl. Note the uniformity of grain sizes compared with those of 2080.

2129 — SEM; shows the fine-grained and agglomerated character of the marl (X2800).

2129 — SEM; close-up view of one agglomerate particle showing the platy crystallites of calcite and the highly porous nature of the particle.

2077 — SEM; shows the granular nature of the chalk. The particles are single subrhombic grains 1 to 2 μ, or agglomerates of interlocking grains whose porosity appears to be less than those in 2129.

2081 — SEM; shows the character of the chalk. Note the presence of fibrous particles of calcite and the polygranular nature of the particles.

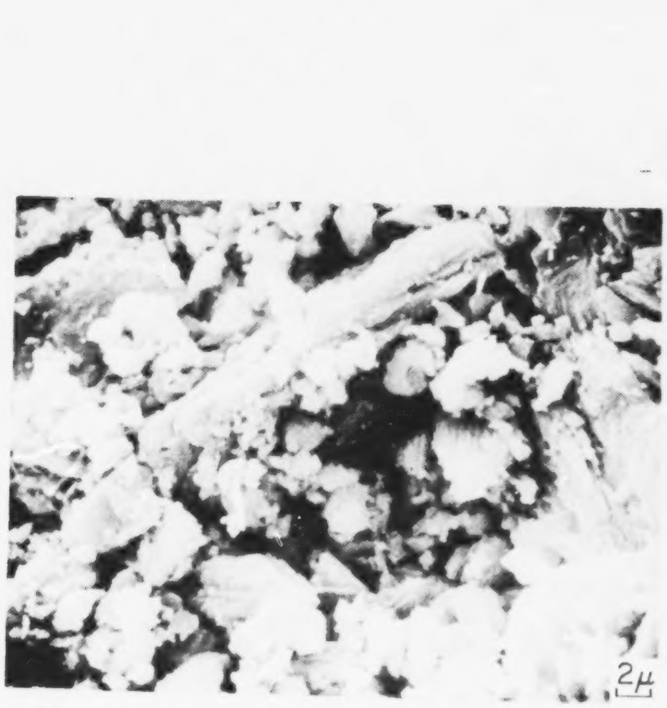

[illegible]0 - Marl X2400

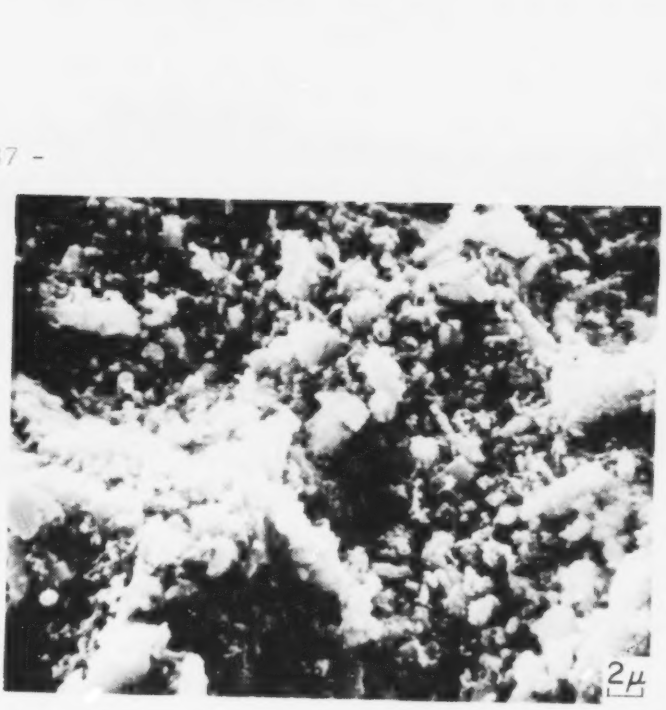

3109 - Marl X2400

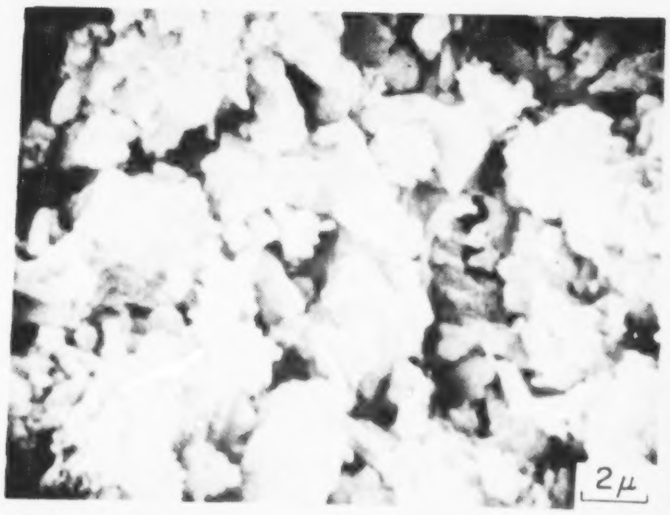

3129 - Marl X5000

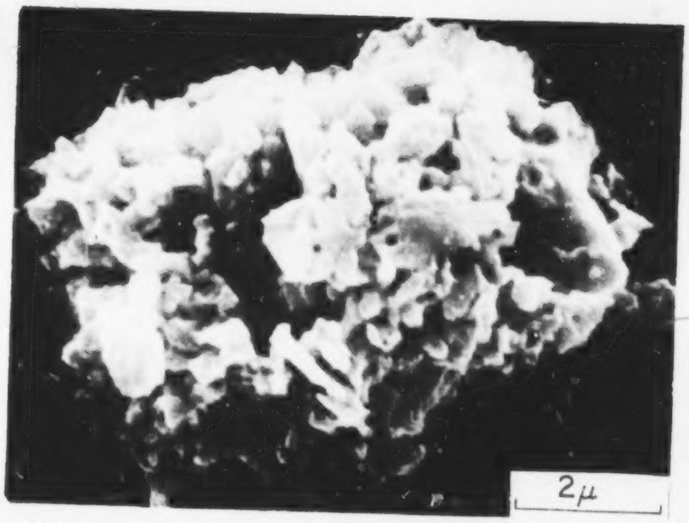

3129 - Marl X10,000

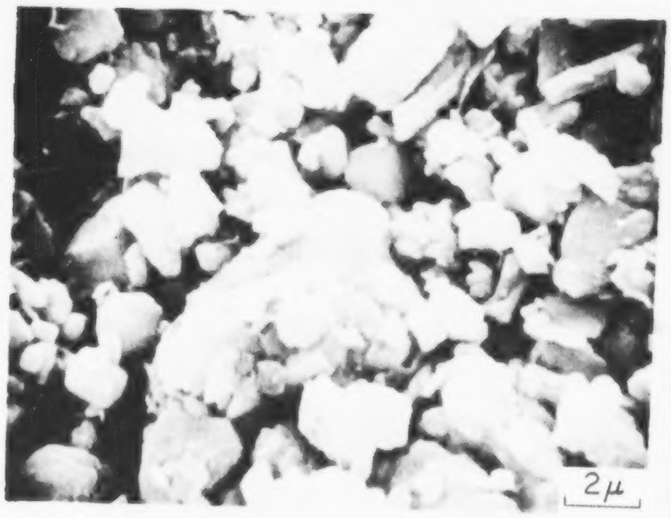

3097 - Chalk X5100

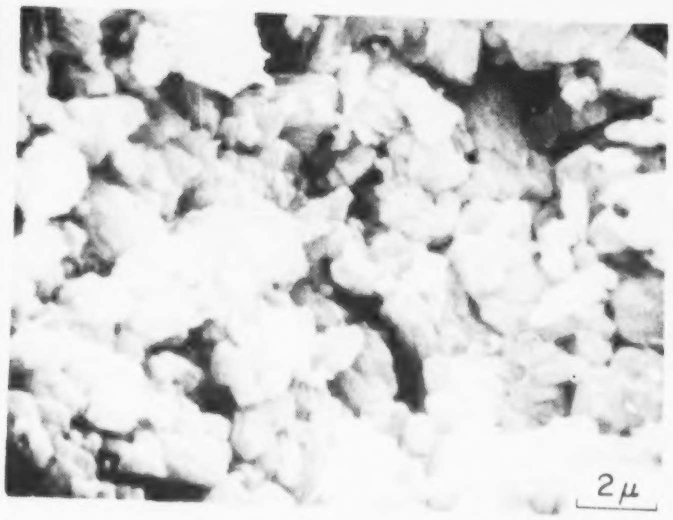

3098 - Chalk X5000

Fig. 11. Typical textures and grain characteristics of marls and chalks.

of the chip specimens (crushed particles) observed contains a wide range of grain sizes. Grain shapes are qualitatively referred to as rhombic, subrhombic, and anhedral. The two-dimensional granular fabric produced by interlocking of anhedral grains is termed a mosaic texture.

Petrographically, limestone samples 1343 and 2060 are very similar, being high-purity fossiliferous fragmental rocks with a micritic type of calcite matrix that is very fine grained (2 to 8 µ), dense, and anhedral. The fossil fragments consist of interlaminated grains of calcite (brachipods), large single crystalline grains (crinoid fossil plates), and fine-grained calcite (other remains of marine invertebrates). Abundant patches of clear (sparry) anhedral calcite grains occur in former fossil voids and in other irregular areas in the stone (fig. 49, 1343). In some cases the clear calcite has replaced parts of the original fossil material.

Sample 2061 is a soft, oolitic, and porous limestone. The oolites are mainly of a normal type in that they consist of spherical or ellipsoidal bodies 0.5 to 1 mm across, with a nucleus and concentric rings. Most nuclei are single crystals of calcite (crinoid fossil fragment); rarely, they are quartz sand grains. The concentric rings consist of very fine-grained calcite (poorly defined in 2061 of fig. 49 by the dark bands shown magnified 30 times (X30), and in the center area of 2061 at X430). Few of the oolites show radial structure in the outer rings. Many superficial oolites occur that have only one ring around the nucleus. Several oolites in 2061 are flattened, and others have deformed or ruptured outer rings. Fossils occurring in 2061 are mainly crinoid, brachiopod, bryozoan, and ostracode fragments. In addition, irregularly shaped, fine-grained intraclasts occur. The oolites, fossils, and intraclasts are cemented (lithified) together by clear, sparry, anhedral calcite (light-colored areas surrounding oolites in fig. 49, 2061, at X30; also shown on right side of 2061 at X430). The geologic occurrence and additional information on the source of sample 2061 is given in a later section, as this stone was used as limestone additive in the TVA tests.

Sample 1359 is a very fine-grained, even-textured, and dense limestone, which is almost entirely micritic calcite. This limestone is essentially the same as type 4 of phase I. The high degree of grain interlocking and the character of the grains are shown in figure 49, 1359.

Sample 2065 is a pelletoidal limestone. It consists predominantly of ellipsoidal pellets up to 0.5 mm across that are composed of a mixture of micritic and sparry calcite. Figure 49, 2065, shows detail of the interior structure of a pellet. The pellets are surrounded by sparry calcite.

Sample 2071 is dominantly micritic calcite (similar to 1359); however, rhomb-shaped crystals of dolomite, 35 to 40 µ in size, are scattered throughout the rock.

The marble, sample 1336 (fig. 49), is uniformly very coarse-grained calcite spar, and the crushed sample consists almost entirely of cleavage rhombs or irregularly broken fragments of a single crystal of calcite. Scattered through the particles are a few grains of tremolite (ideal composition: $Ca_2Mg_5Si_8O_{22}(OH)_2$), a mineral commonly associated with marbles. Few intragranular voids or inclusions were observed in specimens of the marble with the SEM (fig. 49, 1336).

The dolomite samples described in table 8 also are petrographically very similar. They all consist of more than 98 percent dolomite, and each appears to have a similar geologic origin: replacement of original limestones. Their textures are similar (fig. 50), each resulting from the replacement and recrystallization processes, and they differ mainly in grain size distribution and pore structures. Samples 1378 and 2069 are more inequigranular than the other samples, and 1337 has the highest porosity. These samples, with the exception of 1337, are quite similar to type 5, phase I.

## Marls and Chalks

The marls and chalks are grouped together because these two types of carbonate rocks are very similar in mineralogy and texture. Marl is defined as a "semifriable mixture of clay materials and lime carbonate" (Pettijohn, 1957, p. 369). The mineral composition of marls may vary greatly, and various limits of the carbonate and clay contents have been proposed, ranging from 25 to 75 percent carbonate and a complementary content of clay (Gillson, 1960). Quartz silt and organic matter are usually present, and in some deposits of marl calcite occurs only in fossil shells.

Chalk is a porous, fine-textured, and somewhat friable carbonate rock. Normally, it is light buff to white and consists almost wholly of calcitic shells of microfossils (Pettijohn, 1957, p. 400). Most chalks are 90 or more percent calcite, although, according to Gillson (1960), rocks that are classified as chalks may be as much as 25 percent noncalcite.

Most literature on the deposition of fresh-water lake marls of New York through Minnesota describes the importance of an alga (*Chara*) that causes $CaCO_3$ to precipitate on its surfaces. The carbonate, as very fine-grained calcite, is eventually sloughed off the alga and accumulates on the bottom of the lake where it forms marl.

The samples of marls and chalks studied in this phase are described in detail in table 8, and typical SEM micrographs are shown in figure 51. The samples are composed of a variety of microfossils, mainly shells (up to 0.5 mm) of foraminifera, plus a few gastropod shells and other fossil remains. The Kansas chalk (2081) and Ohio marl (2080) are petrographically very similar, as is shown in table 8 and figure 51. The marls 2109, 2129, and the Austin chalk (2077) also are similar, although the Austin chalk contains more coarse sparry calcite than do the marls. All the chalks and marls investigated here are characterized by their high calcite content, poor consolidation, high porosity, and very fine grain structure.

## Grain and Pore Size Distributions

The grain sizes of the limestone, marble, and dolomite samples were determined from thin sections with the polarized light microscope on the Quantimet, by methods described earlier. The grain size data are summarized in table 9. The modes listed in the third column of the table were determined by inspection of the histograms.

TABLE 9—GRAIN SIZE ANALYSES

| Sample | Distribution | Modes* (μ) major; minor | Graphic mean† (μ) | Graphic standard deviation (in log units) | Arithmetic mean‡ (μ) |
|---|---|---|---|---|---|
| | LIMESTONES | | | | |
| 1343 | Fine skew | 2 | 6.2 | 2.0 | 4 |
| 1359 | Bimodal | 2; 20 | 2.7 | 1.2 | 3 |
| 2060 | Irregular | 20, 2; 180 | 12.2 | 2.2 | 7 |
| 2061 | Bimodal | 2; 90 | 10.2 | 2.9 | 5 |
| 2065 | Irregular | 2; 10, 45 | 6.2 | 2.2 | 4 |
| 2071 | Fine skew | 2 | 4.1 | 0.3 | 3 |
| | MARBLE | | | | |
| 1376 | Normal | | 1300** | | |
| | DOLOMITES | | | | |
| 1337 | Coarse skew | 150 | 126.9 | 0.9 | 107 |
| 1378 | Irregular | 210, 50; 25 | 119.0 | 1.1 | 89 |
| 1380 | Normal (with very minor second mode) | 105; (25) | 117.2 | 0.9 | 94 |
| 1688 | Bimodal | 125; 50 | 119.0 | 0.8 | 108 |
| 2069 | Normal | 50 | 52.9 | 0.8 | 45 |
| | MARLS AND CHALKS | | | | |
| 2080 | Fine skew | 0.8; 25 | 0.9 | 1.1 | 1.1 |
| 2109 | Fine skew | 0.8; 5 | 0.8 | 1.1 | 1.1 |
| 2129 | Fine skew | 0.4; 10 | 0.4 | 1.2 | 0.6 |
| 2077 | Fine skew | 1; 15 | 1.1 | 1.0 | 1.4 |
| 2081 | Fine skew | 2; 10 | 1.6 | 1.4 | 2.9 |

* As observed from histogram plots of equal logarithmic size intervals.

† Folk and Ward, 1957.

‡ Krumbein and Pettijohn (1938, p. 240).

** Single grained particles (12 by 16 mesh). Average grain size = average particle size = 1300 μ.

Grain size measurements of the marls and chalks were made from electron micrographs. As the diameters were determined predominantly from whole grains, no corrections due to cross section effects are necessary. In thin sections, small patches consisting of grains up to 0.3 mm across are widely scattered throughout the marl and chalk samples.

The results (table 9) indicate the limestones are predominantly fine grained. Sample 2060 is the only limestone that does not have a major mode at 2 microns. The dolomites are much coarser than the limestones and show a wider range of major modes. However, four of the five dolomites have a graphical mean (geometric mean) near 120 microns. The fifth dolomite (2069) has a mean of 53 microns.

The marls and chalks are the finest grained samples, and of these the Michigan marl (2129) is the finest grained, having a graphic mean diameter of 0.4 microns. The Kansas chalk (2081) is the coarsest of this group, with a graphic mean diameter of 1.6 microns.

The volume of pores greater than 0.9 μ (QTM pore volume) and their size distribution were determined for the phase II samples by using the same methods described earlier for the phase I samples. The particle size of the phase II samples analyzed with the Quantimet was 12 by 16 mesh. The results in volumetric units (table 10) are the means of image analyses of 60 to 240 areas within different particles and are essentially equal to the total pore volume of the samples of limestones, dolomites, and marble. The QTM pore volume of two of the marls (2080 and 2109) and one chalk (2081) are thought to be erroneously low owing to the filling of several large pores with epoxy during preparation of the specimens and to the presence of many pores less than 0.9 μ.

The electron microscope showed abundant voids within dolomite grains in each of the dolomite samples. Image analyses with the Quantimet were made of scanning micrographs taken of cleaved rock surfaces of four samples (for example, fig. 50, SEM 1688) with the epidiascope and the Quantimet. The abundance and size distribution of void inclusions were measured, and the results are listed in table 11. Sample 1380 appears to contain about half as many inclusions as the other dolomites. Time did not permit the analyses of a sufficient number of specimens to determine how representative the data are.

## Mineralogy

Mineral composition of the samples was determined by the methods described earlier. The results are listed in table 12. The HCl-insoluble residues from 20-gram samples of the limestones and dolomites proved to be mainly quartz and clay in various amounts plus smaller amounts of organic matter and a grain or two of opaque minerals, mainly pyrite. Sample 2060 has the highest residue (5.92 percent) found in the limestones and dolomites. The residues from samples of the marls and chalks make up as much as 13 percent of the sample. Much of the residue from 2109 and 2129 is woody organic matter. In addition, HCl-soluble organic matter occurs in the marls and chalks. The calcite ranges from 76 to 98 percent by weight in the marls.

## TABLE 10—QUANTIMET ANALYSES OF PORE STRUCTURE

| Sample | Mean pore volume ($mm^3/g$) | Pore projection (mm) | Pore volume distribution† ($mm^3/g$) 0.9-2 | 2-2.8 | 2.8-3.9 | 3.9-5.5 | 5.5-7.8 | 7.8-11 | 11-16 | 16+ (μ) | Predominant position of pores‡ |
|---|---|---|---|---|---|---|---|---|---|---|---|
| | LIMESTONES | | | | | | | | | | |
| 1343 | 22 | 0.22 | 11.7 | 5.1 | 2.4 | 1.8 | 0.6 | 0.2 | 0.1 | < 0.1 | Between grains |
| 1359 | 10 | 0.09 | 6.9 | 2.2 | 0.5 | 0.3 | < 0.1 | < 0.1 | < 0.1 | 0 | Between grains |
| 2060 | 9 | 0.29 | 5.3 | 2.0 | 1.0 | 0.6 | 0.2 | 0.1 | < 0.1 | 0 | Between grains |
| 2061 | 21 | 0.32 | 12.8 | 4.7 | 1.5 | 1.0 | 0.4 | 0.4 | 0.1 | < 0.1 | Variable |
| 2065 | 9 | 0.09 | 5.1 | 2.5 | 0.8 | 0.6 | 0.2 | < 0.1 | < 0.1 | < 0.1 | Between grains |
| 2071 | 18 | 0.52 | 12.1 | 3.7 | 1.2 | 0.6 | 0.1 | < 0.1 | < 0.1 | < 0.1 | Between grains |
| | MARBLE | | | | | | | | | | |
| 1336 | 8 | 0.18 | 5.0 | 1.4 | 0.6 | 0.5 | 0.4 | 0.2 | 0.2 | 0.1 | Within grains |
| | DOLOMITES | | | | | | | | | | |
| 1337 | 51 | 0.46 | 30.9 | 11.2 | 4.5 | 4.6 | 3.9 | 1.3 | 1.3 | 0.8 | Variable |
| 1378 | 14 | 0.22 | 7.5 | 2.8 | 1.4 | 0.9 | 0.8 | 0.4 | 0.1 | < 0.1 | Within grains |
| 1380 | 18 | 0.38 | 11.5 | 3.4 | 2.2 | 0.9 | 0.5 | 0.2 | 0.2 | < 0.1 | Within grains |
| 1688 | 24 | 0.55 | 14.5 | 5.2 | 1.9 | 1.4 | 0.5 | 0.3 | 0.1 | < 0.1 | Within grains |
| 2069 | 15 | 0.40 | 8.4 | 2.8 | 1.3 | 1.1 | 0.6 | 0.4 | 0.1 | 0.1 | Within grains |
| | MARLS AND CHALKS | | | | | | | | | | |
| 2080 | 21 | 0.42 | 13.9 | 3.2 | 1.0 | 1.4 | 0.7 | 0.4 | 0.3 | 0.2 | Between grains |
| 2109 | 9 | 0.17 | 5.6 | 1.6 | 0.7 | 0.5 | 0.3 | 0.1 | < 0.1 | < 0.1 | Between grains |
| 2129 | 73 | 1.34 | 29.2 | 14.4 | 8.7 | 9.1 | 5.3 | 3.7 | 1.7 | 1.0 | Between grains |
| 2077 | 56 | 0.19 | 28.0 | 14.9 | 6.9 | 4.0 | 1.6 | 0.4 | 0.1 | < 0.1 | Between grains |
| 2081 | 17 | 0.36 | 10.8 | 2.8 | 1.4 | 0.9 | 0.6 | 0.3 | 0.1 | < 0.1 | Between grains |

---

* Image analyses of pores larger than 0.9 μ. Quantimet magnification of 1300X.

† The intervals, in microns, correspond to a constant interval of 1/2 phi units.

‡ Determined by scanning electron microscopy.

TABLE 11—VOID INCLUSIONS IN DOLOMITE GRAINS

| Sample | Frequency percentage of voids larger than (μ) | | | | | | | No. of voids/mm$^2$ | Median size (μ) |
|---|---|---|---|---|---|---|---|---|---|
| | 0.1 | 0.2 | 0.4 | 0.8 | 1.6 | 3.3 | 4.9 | | |
| 1378 | 90.3 | 78.9 | 65.4 | 43.6 | 19.7 | 5.3 | 0.2 | 17,400 | 0.65 |
| 1380 | 92.5 | 79.3 | 64.2 | 30.2 | 13.2 | 1.9 | 0 | 8,000 | 0.53 |
| 1688 | * | 83.4 | 69.1 | 50.7 | 26.1 | 7.4 | 2.6 | 17,300 | 0.82 |
| 2069 | 87.6 | 68.8 | 53.2 | 34.4 | 15.6 | 0 | 0 | 16,760 | 0.45 |

* Not determined.

## Chemical Analyses

The results of analyses of the major and minor elements present in the samples are listed in table 13. The methods of analyses used were described earlier in this report. The data show that, of the limestone samples, 2060 contains the most silica (4.42 percent) and the least CaO (49.2 percent). The composition of the dolomite mineral as calculated from the chemical analyses is given in table 12. The analyses indicate there is slightly more calcium than magnesium in all samples except 1688, which has the ideal dolomite composition (Ca/Mg = 1/1).

Chemical analyses of the marls and chalks show a wide range of organic matter and silica content. Sulfur contents range from 0.01 to 0.62 percent. The sulfur occurs mainly in very rare, small grains of pyrite. Less than 0.1 percent of the sulfur is organic in these samples. The marl from Michigan (2129) has high $Na_2O$ and $H_2O$ contents.

## DISCUSSION OF RESULTS RELATED TO SULFUR DIOXIDE SORPTION TESTS

The samples of carbonate rocks investigated were tested for their $SO_2$ reactivity by personnel of the Division of Process Control Engineering, APCO, Cincinnati, Ohio. Two methods were used to evaluate the relative reactivity of carbonate rock samples with $SO_2$ in flue gases. Their capacity for reaction was measured in a fixed-bed reactor (Potter, 1969), and an indirect assessment of the rate of reaction was made with a differential reactor, according to the Borgwardt method (1970a).

For the capacity test a weight of uncalcined sample equivalent to 20 grams of calcine, 16 to 20 Tyler mesh, was exposed in a fixed-bed reactor to a flue gas containing 2700 ppm $SO_2$ for 3½ hours at 1800° F. The gain in weight

TABLE 12—MINERAL ANALYSES

| Sample | Major component (%) | Minor and trace components | HCl insoluble residue (%) |
|---|---|---|---|
| LIMESTONES | | | |
| 1343 | 98 Calcite | 1.4% kaolinitic clay; trace of quartz | 1.65 |
| 1359 | 99 Calcite | Traces of illitic clay and dolomite | 0.65 |
| 2060 | 81 Calcite | 12% dolomite; 3.5% quartz; 2% illitic clay; trace of limonite | 5.92 |
| 2061 | 98+ Calcite | < 1% kaolinitic clay; < 1% quartz sand | 1.11 |
| 2065 | 94 Calcite | 5% dolomite; trace of quartz as sand and silt; trace of clay | 0.95 |
| 2071 | 95 Calcite | 3.8% dolomite; < 1% quartz; traces of feldspar and clay | 1.73 |
| MARBLE | | | |
| 1336 | 98 Calcite | 1+ % tremolite; < 1% mica | 1.95 |
| DOLOMITES | | | |
| 1337 | 99+ Dolomite*<br>$Ca_{1.14}Mg_{.86}(CO_3)_2$ | Traces of quartz and clay | 0.34 |
| 1378 | 98 Dolomite<br>$Ca_{1.03}Mg_{.97}(CO_3)_2$ | 1% quartz sand; < 1% clay | 1.88 |
| 1380 | 99 Dolomite<br>$Ca_{1.03}Mg_{.97}(CO_3)_2$ | < 1% cherty quartz; < 1% clay | 0.76 |
| 1688 | 99+ Dolomite<br>$Ca_{1.00}Mg_{1.00}(CO_3)_2$ | Traces of quartz and clay | 0.35 |
| 2069 | 98 Dolomite<br>$Ca_{1.08}Mg_{.92}(CO_3)_2$ | 1.5% kaolinitic clay; trace of limonite | 1.94 |
| MARLS AND CHALKS | | | |
| 2080 | 98 Calcite | 1% organic matter; 1% illitic clay; < 1% silty quartz | 1.19 |
| 2109 | 92+ Calcite | 5% woody and HCl-soluble organics; 2% clay; 2% dolomite | 2.58 |
| 2129 | 76+ Calcite | 11% organics, mainly woody; 3% illitic clay; 4% silty quartz; 4% dolomite | 13.07 |
| 2077 | 87+ Calcite | 6% glauconitic clay; 3% quartz; 1% limonite; trace of feldspar | 8.11 |
| 2081 | 92+ Calcite | 2% organic matter; 1% clay; 1% quartz; trace of feldspar | 2.82 |

* The proportions of $Ca^{++}$ and $Mg^{++}$ in the dolomite, calculated from analyses in table 13, are as shown. Ideal dolomite is $Ca_{1.0}Mg_{1.0}(CO_3)_2$.

### TABLE 13—CHEMICAL ANALYSES IN WEIGHT PERCENTAGE
(Analyses by Analytical Chemistry Section, Illinois State Geological Survey)

| Sample | $SiO_2$ | $Al_2O_3$ | $Fe_2O_3$ | MnO | MgO | CaO | $Na_2O$ | $K_2O$ | S | $H_2O+$ | $CO_2$ | Organic C | Total |
|---|---|---|---|---|---|---|---|---|---|---|---|---|---|
| LIMESTONES | | | | | | | | | | | | | |
| 1343 | 0.11 | 0.57 | 0.14 | * | * | 54.8 | 0.031 | 0.06 | 0.04 | * | 43.10 | * | 98.8 |
| 1359 | * | 0.14 | 0.07 | 0.011 | trace | 55.5 | 0.007 | 0.01 | * | 0.25 | 43.27 | 0.15 | 99.5 |
| 2060 | 4.42 | 0.64 | 0.23 | 0.016 | 2.79 | 49.2 | 0.047 | 0.15 | trace | 0.26 | 41.58 | * | 100.3 |
| 2061 | 0.29 | 0.47 | 0.14 | 0.013 | * | 55.0 | 0.012 | * | * | 0.22 | 43.63 | * | 99.8 |
| 2065 | 0.25 | 0.04 | 0.28 | 0.009 | * | 55.0 | 0.004 | 0.14 | 0.01 | * | 43.48 | * | 99.2 |
| 2071 | 0.56 | 0.33 | 0.11 | 0.005 | 0.92 | 54.3 | 0.034 | 0.06 | 0.03 | * | 43.52 | * | 99.9 |
| MARBLE | | | | | | | | | | | | | |
| 1336† | 0.08 | 0.40 | 0.12 | 0.005 | 1.01 | 54.1 | 0.011 | 0.03 | * | * | 43.25 | * | 99.0 |
| DOLOMITES | | | | | | | | | | | | | |
| 1337 | * | 0.15 | 0.19 | 0.004 | 18.0 | 33.2 | 0.044 | 0.11 | < 0.01 | 0.04 | 47.17 | * | 98.9 |
| 1378 | * | 0.43 | 0.02 | * | 20.82 | 30.7 | 0.066 | 0.01 | 0.01 | 0.01 | 46.42 | * | 98.5 |
| 1380 | * | 0.27 | 0.19 | * | 20.67 | 30.5 | 0.044 | 0.02 | < 0.01 | 0.23 | 46.97 | * | 98.7 |
| 1688 | * | 0.21 | 0.02 | * | 21.57 | 30.0 | 0.048 | 0.01 | < 0.01 | 1.10 | 47.09 | 0.01 | 101.1 |
| 2069 | 0.44 | 0.61 | 0.23 | 0.020 | 19.2 | 31.4 | 0.031 | 0.22 | 0.04 | 0.84 | 44.93 | 0.60 | 98.6 |
| MARLS AND CHALKS | | | | | | | | | | | | | |
| 2080 | * | 0.67 | 0.03 | * | * | 54.8 | 0.024 | 0.05 | 0.62 | 1.23 | 40.99 | 0.35 | 98.8 |
| 2109 | * | 0.84 | 0.01 | * | 1.88 | 51.7 | 0.033 | 0.02 | 0.55 | 1.47 | 40.16 | 2.77 | 99.4 |
| 2129† | 5.10 | 0.88 | 0.47 | 0.01 | 3.08 | 43.9 | 0.160 | 0.01 | 0.19 | 4.66 | 35.38 | 6.18 | 100.0 |
| 2077 | 6.34 | 2.17 | 0.82 | 0.01 | * | 49.2 | 0.035 | 0.49 | 0.01 | 1.13 | 38.31 | 0.19 | 98.8 |
| 2081† | 2.48 | 1.09 | 0.15 | * | 1.41 | 51.4 | 0.060 | 0.11 | 0.57 | 1.16 | 39.44 | 0.95 | 98.8 |

* None detected.

† Mercury in 1336 = 0.19 ppm, in 2129 = 0.07 ppm, and in 2081 = 0.77 ppm; not determined in other samples.

TABLE 14—$SO_2$ REACTIVITIES
($SO_2$ tests by Division of Process Control Engineering, APCO)

| Sample | Rock classification | Sorption capacity, fixed bed (g/20 g) | Reactivity, differential (mg $SO_3$/30 mg calcine) |
|---|---|---|---|
| Type 1 | Iceland spar (calcite) | 5.46 | 8.3 |
| Type 2 | Calcite spar | 11.65 | 9.6 |
| Type 3 | Limestone | 10.73 | 13.9 |
| Type 4 | Limestone | 6.97 | 14.0 |
| Type 5 | Dolomite | 9.03 | 17.0 |
| Type 6 | Dolomite | 13.68 | 12.1 |
| Type 7 | Magnesite | 1.78 | — |
| Type 8 | Aragonite | 18.30 | 7.1 |
| Type 9 | Dolomite | 14.91 | 15.8 |
| 1343 | Limestone | 6.06 | 5.08 |
| 1359 | Limestone | 4.94 | — |
| 2060 | Limestone | 12.25 | 8.98 |
| 2061 | Limestone | 9.52 | 4.84 |
| 2071 | Limestone | 7.40 | 4.42 |
| 1336 | Marble | 7.50 | 3.86 |
| 1337 | Dolomite | 11.53 | 9.28 |
| 1378 | Dolomite | 11.90 | 7.08 |
| 1380 | Dolomite | 8.70 | 6.53 |
| 1688 | Dolomite | 11.35 | — |
| 2069 | Dolomite | 9.08 | 8.82 |
| 2080 | Marl | 15.60 | 6.60 |
| 2109 | Marl | 15.38 | 7.12 |
| 2129 | Marl | 14.83 | 14.92 |
| 2077 | Chalk | 12.54 | 8.62 |
| 2081 | Chalk | 13.37 | 11.73 |

of the sample after the test period was taken as the measure of the sample's $SO_2$ sorption capacity. The results of the fixed-bed capacity tests of the samples appear in table 14.

For the differential reactor tests, the stone was precalcined at 1800° F for 2 hours, and a 150- to 170-mesh calcine was exposed at 1800° F for various periods of time to a flue gas containing 2700 ppm $SO_2$. The plot of the amount of $SO_3$ sorbed by the sample versus time was constructed and evaluated at 120 seconds to give the differential reactivity. These values, supplied by the Division of Process Control Engineering, for the samples investigated are given in table 14.

In the discussions that follow, samples of all the carbonate rocks studied will be considered.

## Petrography Related to $SO_2$ Sorption

No consistent correlation is apparent between the results of fixed-bed and differential $SO_2$ reactivities and the mineralogy of the samples. A clayey and silty nonreef-type dolomite, selected for study because of its impurity, contains about 25 percent inert oxides in its calcine, yet this sample was among the highest in $SO_2$ capacity. On the other hand, Borgwardt (1970b) found the rate of reaction of this sample notably reduced, compared to rates of high-purity calcines, at a particular degree of sulfation. Considered in terms of capacity for sorption of $SO_2$, the textural properties of the calcine and, presumably, the raw stone outweigh a moderate degree of impurity.

In the fixed-bed capacity tests, the dolomites averaged 11.27 grams per 20 grams of calcine and the limestones averaged 6.84. The marls and chalks had a high average of 14.34 g/20 g. The oolitic aragonite (type 8) adsorbed the largest amount of $SO_2$ (18.3 g/20 g) and the magnesite (type 7) the least (1.78 g/20 g). The limestones containing abundant crinoidal fossil fragments had higher $SO_2$ sorption capacities than other limestones. The crinoid fragments are generally the coarser crystalline grains in limestones and the abundance of crinoids is generally reflected in the mean grain size of the stone.

In differential reactivity tests the dolomites averaged 10.9 mg of $SO_3$ per 30 mg of calcine, whereas, the limestones averaged 8.5 mg of $SO_3$/30 mg of calcine. The comparable values for the marls and chalks are 9.55 and 10.68 mg, respectively. Two of the marls had rather low differential reactivities, while sample 2129 had a high value (14.9 mg of $SO_3$/30 mg of calcine). The reef dolomite, type 5, had the highest differential reactivity (17.0) and the marble, sample 1336, the lowest (3.86). The very fine-grained limestone with scattered dolomite rhombs (2071) tested very low (4.42); limestone sample 2061, very similar to 2071 but lacking the dolomite rhombs, also had a very low differential reactivity. However, the fine-grained, type 4 limestone, which is similar petrographically to 2061 and 2071, had a rather high reactivity (14.0 mg of $SO_3$/30 mg calcine). Such diverse differential reactivities are thought to result from slight differences in pore structure of the calcines of these samples, which gives rise to differences in the rate of reaction during the first few tens of seconds of exposure to $SO_2$, with a resultant significant difference in the degree of sulfation after a reaction period of 120 seconds. Determination of the rate of reaction of calcines at a constant degree of sulfate loading enabled Borgwardt (1970b) to correlate the differential reactivity with the surface area measurements of the calcines. As the surface area of the calcine increased, a linear increase in the differential reactivity was observed for calcines having a constant degree of sulfation.

## Grain Size and Pore Structure Related to Sorption

The interim report on this project gave results on the nine type samples that showed the $SO_2$ capacity tended to increase with increasing pore volume and decreasing grain size of the stone. These relations are more conclusively demonstrated by the data on all samples studied except the magnesite. Graphs of the various petrographic parameters showing notable correlations appear in figures 52 to 56.

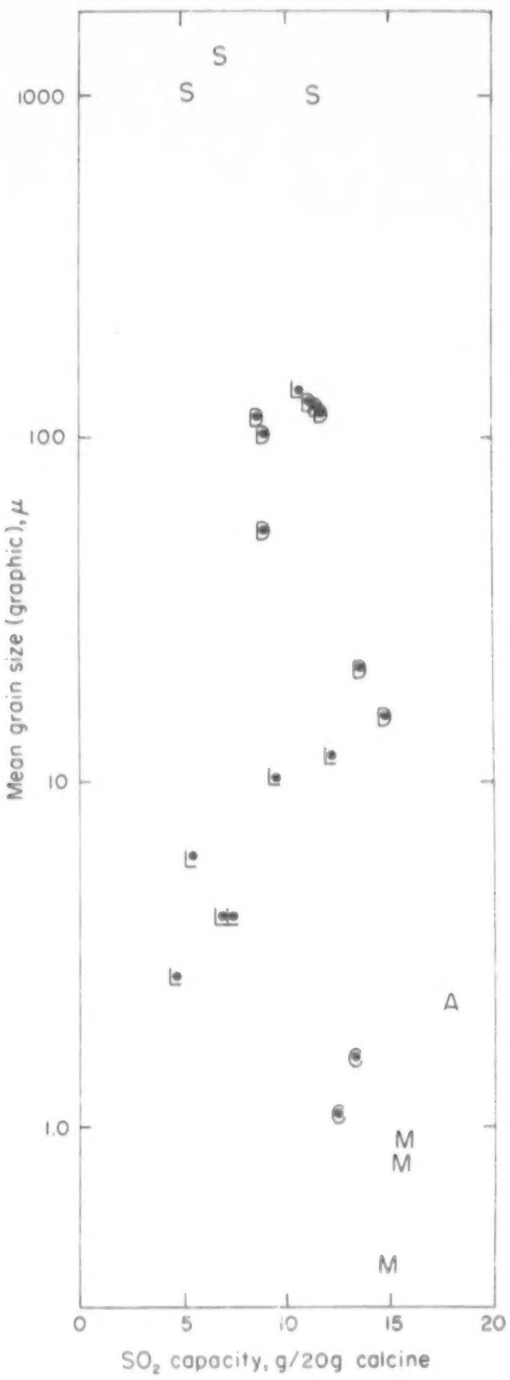

Fig. 52. $SO_2$ capacity as measured in fixed-bed tests versus mean grain size of carbonate rocks. L = limestones, D = dolomites, S = calcite spars, C = chalks, and M = marls.

The finer grained rocks, in general, tend to have greater $SO_2$ capacities (fig. 52). The measure of the grain size plotted is the graphic mean from table 9; a similar distribution is apparent when the arithmetic mean is substituted for the graphic mean. In figure 52 four clusters of data points occur. The cluster of points near 10 μ are for the micritic limestones and two petrographically similar dolomites (types 6 and 9). This cluster shows increasing $SO_2$ capacity as grain size increases. This behavior, which is contrary to the general trend, is related to the occurrence of crinoid grains in the limestones as discussed above. The coarse-grained crinoidal limestone (type 3) is associated with the coarse-grained dolomites near 100 μ on the graph (fig. 52), and each of these samples contain abundant intragranular voids. The chalks and marls and the oolitic aragonite samples constitute the cluster (fig. 52) with the finest grain size and show the highest average $SO_2$ capacity of the various groups. The three coarsest samples (top of fig. 52) are calcite spar and related types. The grain size of the carbonate rocks shows no significant correlation with their differential reactivity (120-second reaction period).

Measurements of the mean QTM pore volume (tables 5 and 10) show certain correlations with $SO_2$ capacities (fig. 53). With exception of the aragonite sample and the chalk and marl samples that had pore volumes thought to be erroneously low (2080, 2109, and 2081, each circled in fig. 53), there is a significant linear increase in pore volume with increasing sorption capacity. The correlation coefficient is 0.71. The pore volume (QTM) within the 2 μ to 16 μ size interval plotted against the $SO_2$ capacity (fig. 54) also shows increasing sorption capacity as pore volume increases. The 2 μ to 16 μ pore volume has a correlation coefficient of 0.97 with the QTM pore volume.

The differential reactivity data plotted against the QTM pore volume of the uncalcined samples (fig. 55) and against the pore projection (fig. 56) show little significant correlation. Other petrographic properties show even less correlation with differential reactivity.

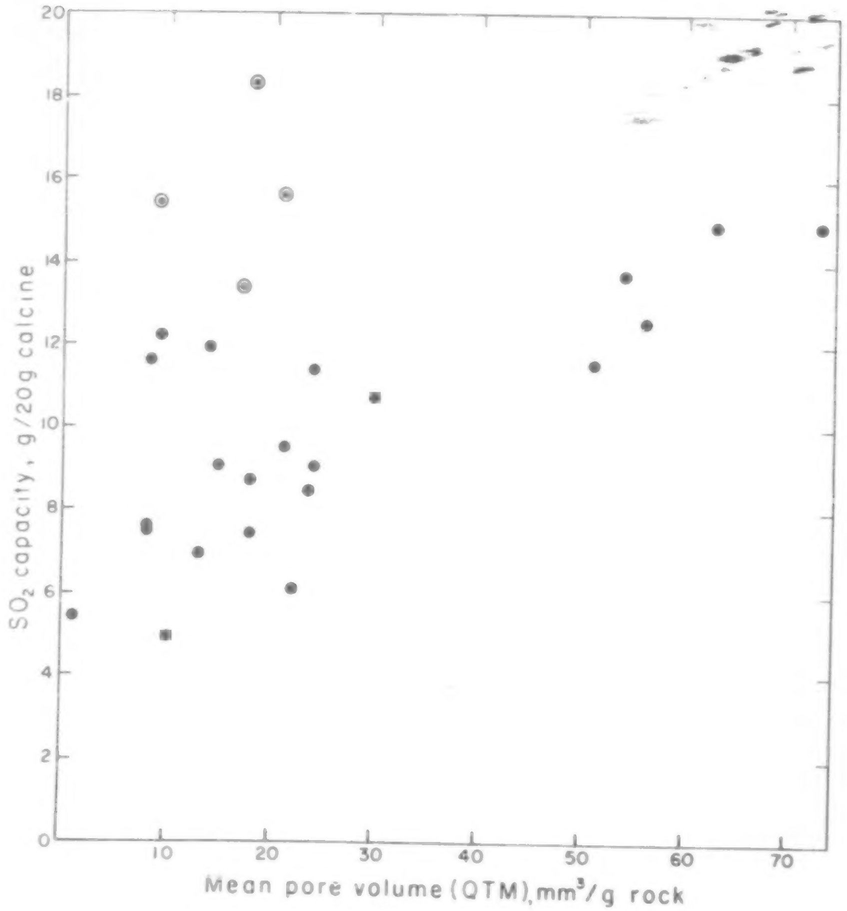

Fig. 53. SO$_2$ capacity as measured in fixed-bed tests versus volume of pores larger than 0.9 µ in diameter (tables 5 and 10) in carbonate rocks, determined by Quantimet methods. The pore volumes of samples that are circled are believed to be erroneously low. Correlation coefficient, disregarding circled samples, is 0.71.

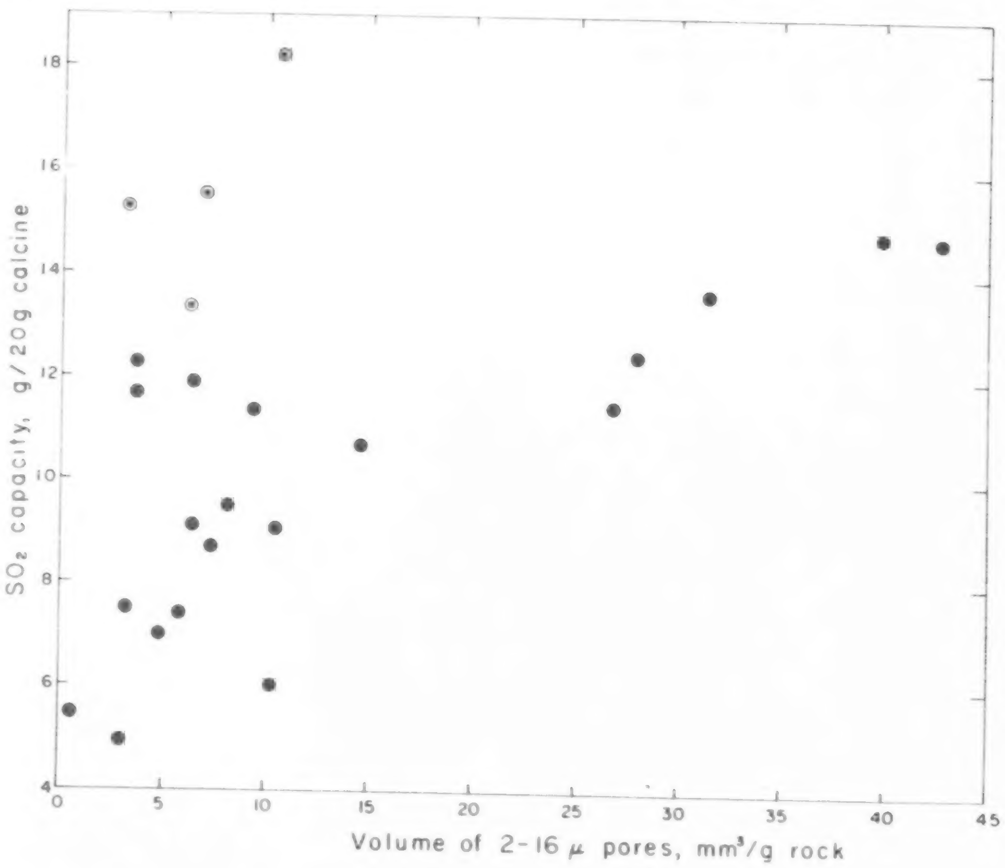

Fig. 54. SO$_2$ capacity in fixed-bed tests versus volume of 2 to 16 µ in "diameter" pores of carbonate rocks, as determined by Quantimet methods.

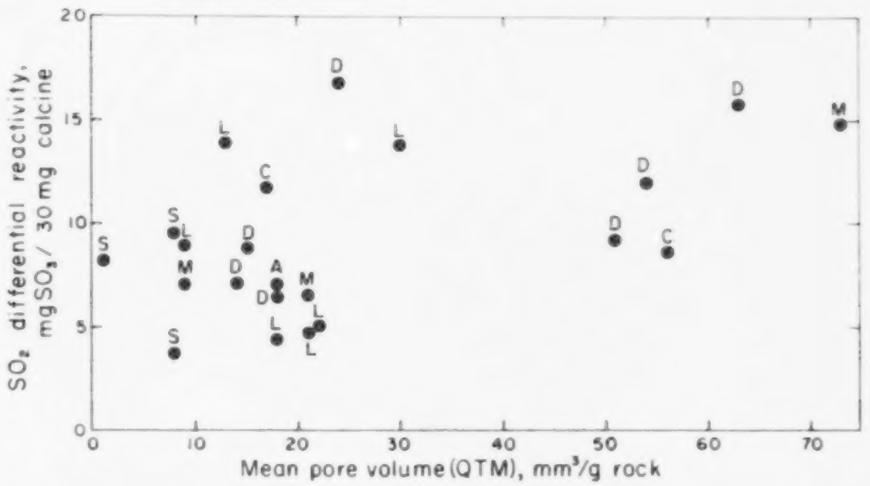

Fig. 55. $SO_2$ reactivity in differential tests versus volume of pores larger than 0.9 µ in diameter in carbonate rocks, as determined by Quantimet methods. L = limestones, D = dolomites, S = Iceland spar, calcite spar, and marble, C = chalks, M = marls, and A = aragonite. Correlation coefficient is 0.48.

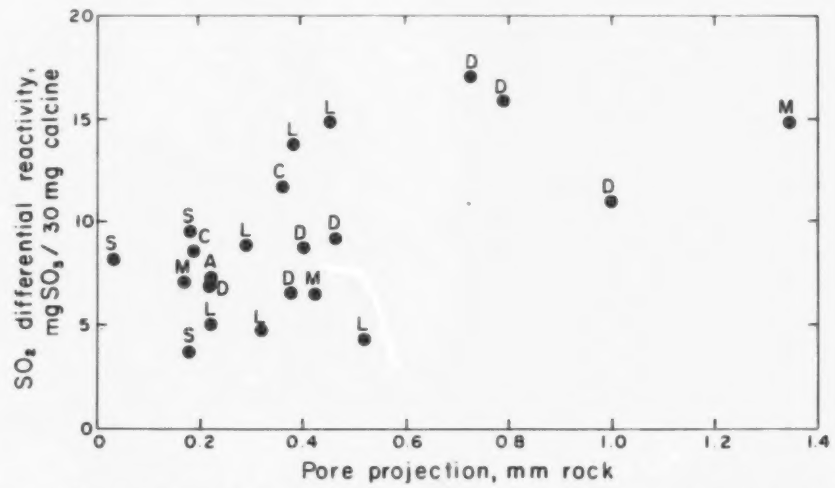

Fig. 56. $SO_2$ reactivity in differential tests versus pore (boundary) projection of carbonate rocks, as determined by Quantimet methods. L = limestones, D = dolomites, S = Iceland spar, calcite spar, and marble, C = chalks, M = marls, and A = aragonite. Correlation coefficient is 0.67.

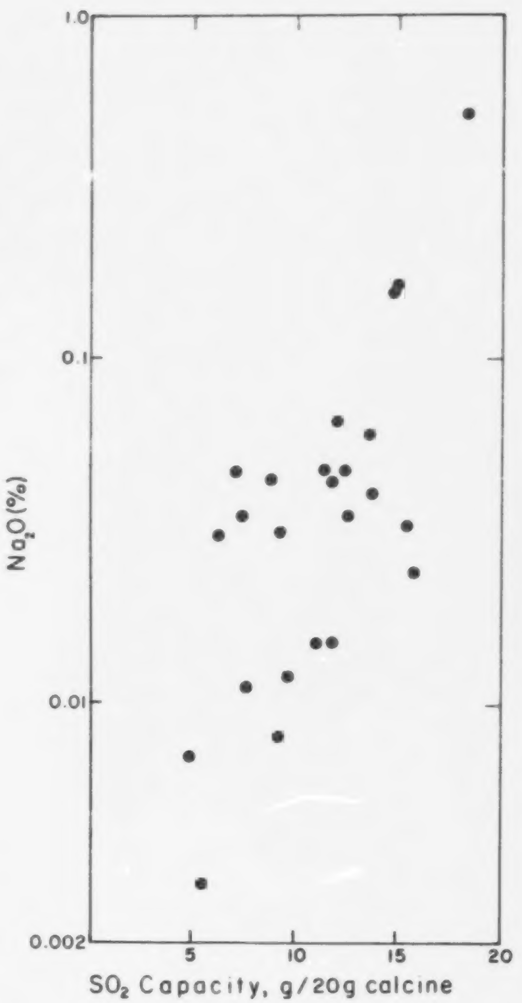

Fig. 57. $SO_2$ capacity in fixed-bed tests versus $Na_2O$ content of carbonate rocks. Correlation coefficient is 0.78.

## Chemical Analyses and Sorption

Graphic plots of the weight percentages of the chemical elements present in the samples versus the $SO_2$ reactivities show no correlations, except for the plot of the sodium content. The capacity to react with $SO_2$ tends to increase with the amount of sodium (measured analytically as $Na_2O$) in the sample (fig. 57). The figure shows the logarithm of $Na_2O$, determined by neutron activation methods, plotted against the $SO_2$ capacity test results. The correlation coefficient is 0.78. Sodium is considered only as an index, not as a reactant with $SO_2$; however, it may be acting as a catalytic or fluxing agent to produce a more reactive calcine. For all the type samples except types 6 and 9, the sodium is thought to be in the form of soluble salts rather than inert clays; analysis shows that 77 percent of the $Na_2O$ of type 6 is a soluble salt, as is 97 percent of the $Na_2O$ of type 9. Similarly high proportions of the minor amounts of $Na_2O$ present in the phase II samples are probably also in the form of soluble salts. These salts are probably located along grain boundaries and in void inclusions in the dolomite samples (Lamar and Shrode, 1953). Sodium salts of chloride and carbonate were reported by Murray (1956) to result in decreased shrinkage of limestone and dolomite particles during calcination.

Comparison between the two calcite spar samples (types 1 and 2) shows that type 2 contains the highest concentration of all trace elements (table 4). These impurities may have contributed to the higher sorption capacity observed for type 2.

## REACTION PRODUCTS

Fundamental differences in the reactions of calcines with $SO_2$ were observed by analyses of the X-ray spectrum of sulfur from reacted specimens examined in the SEM (fig. 58). The 1700° F calcine of Iceland spar calcite (type 1) exposed to $SO_2$ for 600 seconds was converted to anhydrite ($CaSO_4$) only at the edges of the particles (fig. 58B), whereas, under the same conditions, the calcine of the coarse-grained crinoidal limestone reacted to form anhydrite throughout the particles (fig. 58D). This difference in behavior is thought to be due to the difference in porosities of the calcined particles. Anhydrite was the reaction product in every reacted sample studied. No magnesium-sulfur compounds were detected in any of the samples, but periclase (MgO) was abundant in the reacted calcines of the dolomite samples.

The anhydrite on the exterior surfaces of $SO_2$-reacted particles (3½ hours at 1800° F) is granular, with grains ranging from about 1 to 6 microns. The particles of anhydrite are smooth surfaced, and their boundaries tend to be linear in reacted dolomites (fig. 59). Examination of the SEM micrographs of reacted type 5 dolomite indicates a moderate number of pore channels lead from the external surfaces into the particles. SEM studies of reacted calcines of type 4, an example of the limestones, show larger grains (up to 30 $\mu$) of anhydrite that are generally smooth and anhedral and have a tightly interlocking granular fabric that is essentially impervious (fig. 60).

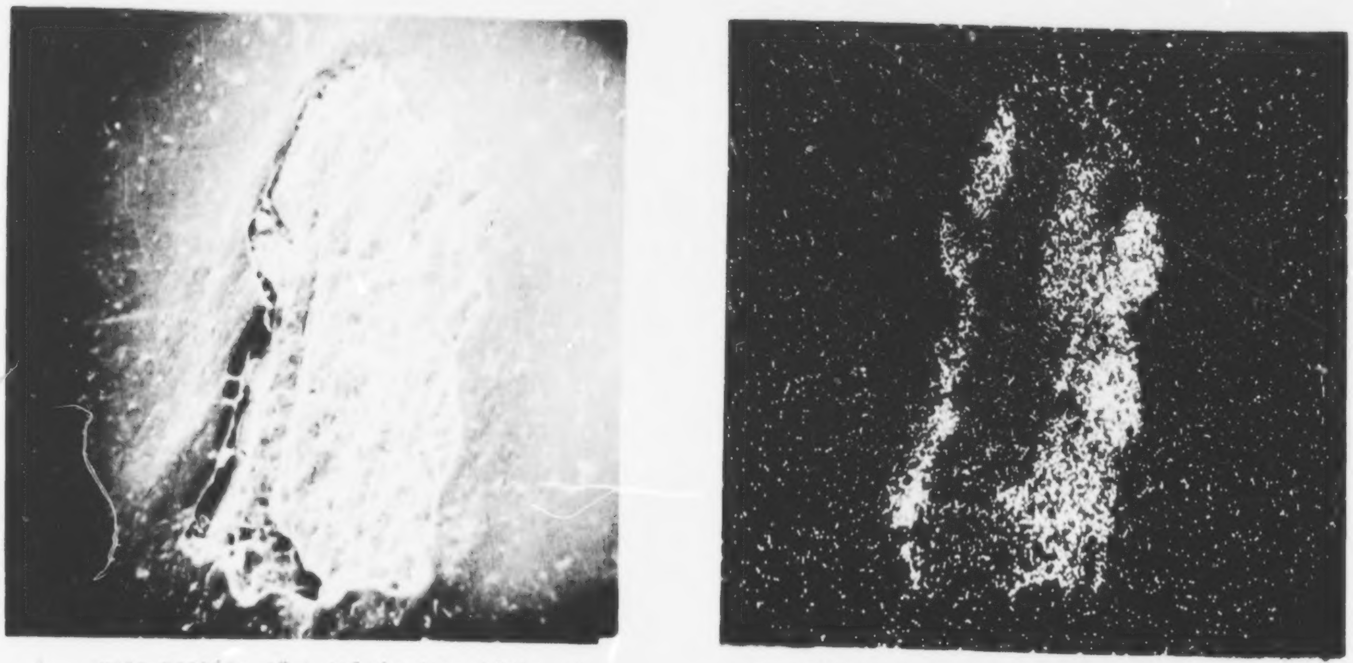

A. Cross section of a calcined particle of Iceland spar (type 1) reacted with $SO_2$ for 600 seconds; embedded in expoxy. Polished section of particle is 0.67 by 0.25 mm; SEM, X120.

B. Sulfur X-ray scan of A, showing sulfated lime on outer rim.

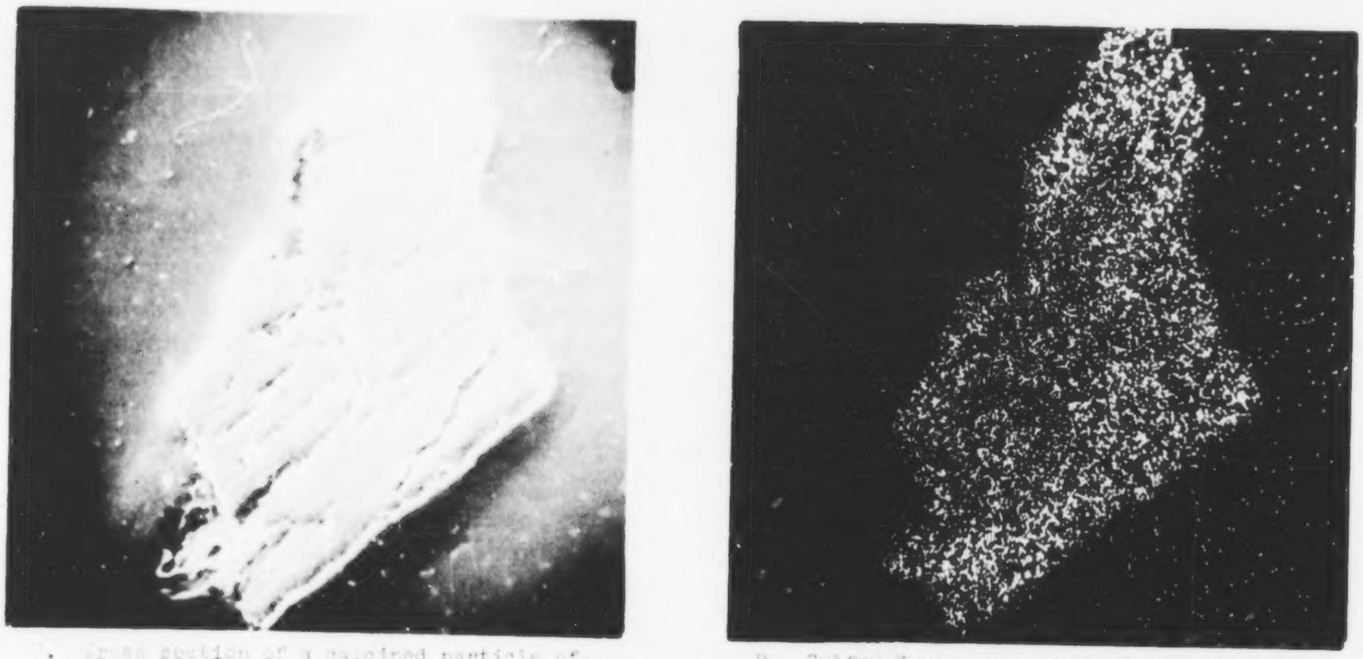

C. Cross section of a calcined particle of coarse limestone (type 3) reacted with $SO_2$ for 600 seconds. Polished section of particle is 0.48 by 0.25 mm; SEM, X200.

D. Sulfur X-ray scan of C, showing complete sulfate permeation.

Fig. 30. Distribution of sulfur in two types of carbonate rocks showing different reaction behavior.

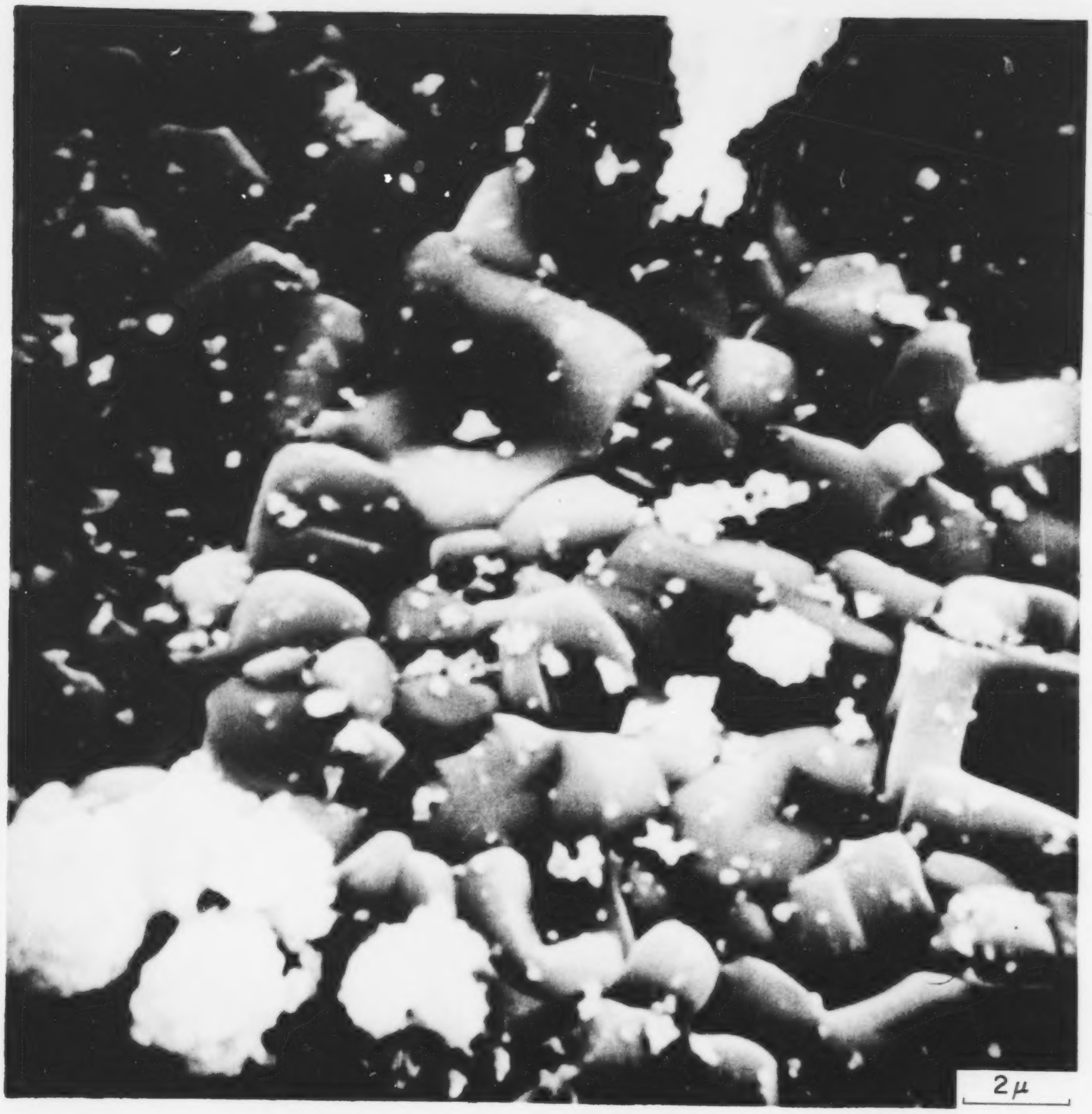

Fig. 59. Exterior surface of $SO_2$-reacted calcine of a high-purity reef dolomite (type.5), showing blocky texture of anhydrite (gray). The highlighted grains are dust particles derived from the sample. SEM, X9350.

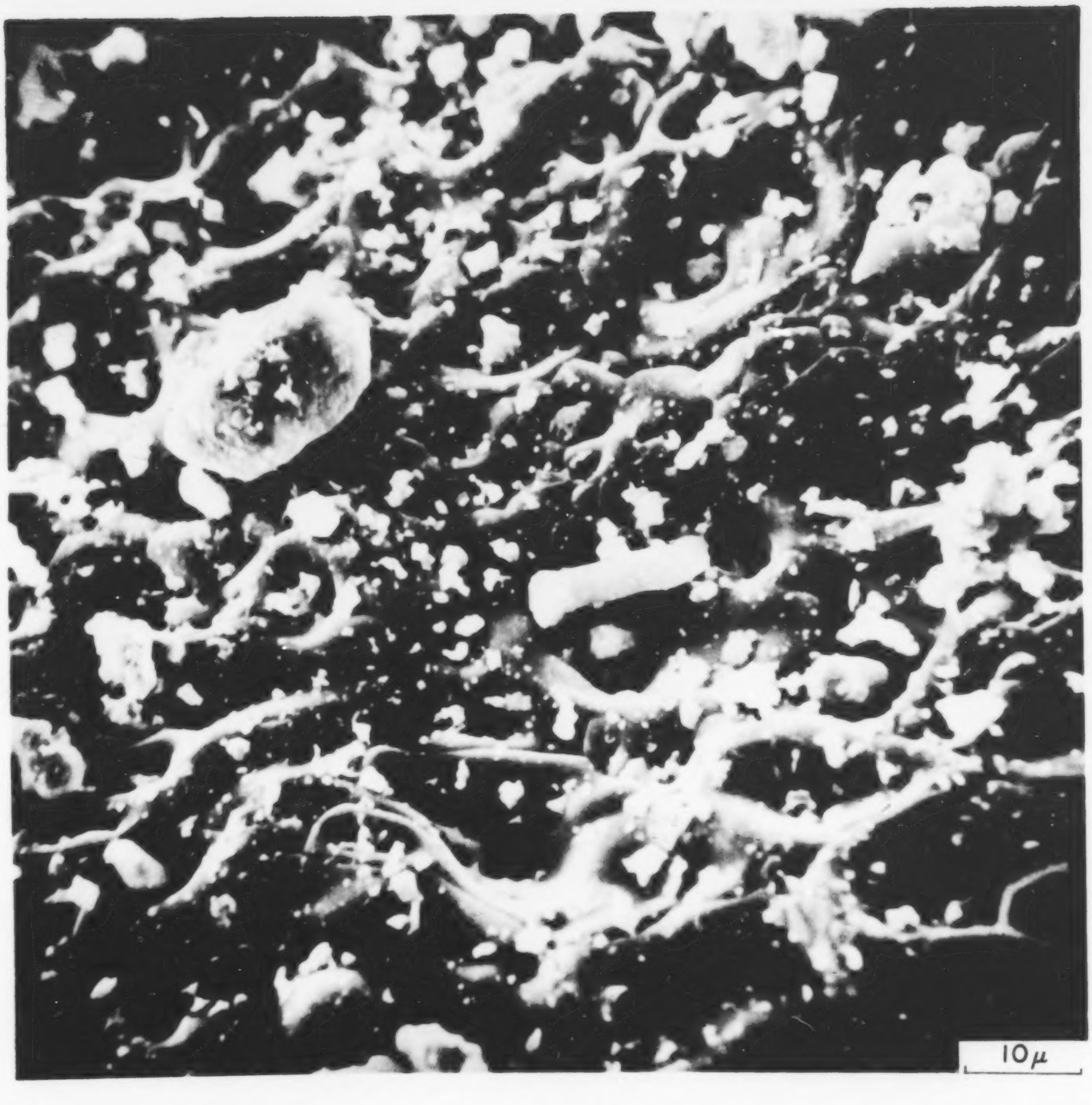

Fig. 60. Exterior surface of $SO_2$-reacted calcine of a fine-grained limestone (type 4), showing dense mosaic of anhedral grains of anhydrite (gray). The highlighted grains are dust particles derived from the sample. SEM, X2080

## PETROGRAPHIC STUDIES OF LIMESTONE-MODIFIED FLY ASH AND BOILER DEPOSITS

The limestone injected into boiler number 10 of the Tennessee Valley Authority's (TVA) Plant, Paducah, Kentucky, was taken from the "Upper white oolitic limestone" ledge in the quarry of Fredonia Valley Quarries, Inc., located about one mile south of Fredonia, Kentucky. During the summer of 1969, three distinct ledges of stone were being exploited in the quarry, an "Upper white oolitic limestone" ledge 35 to 40 feet thick, a middle "Blue limestone" ledge 29 to 30 feet thick, and a "Lower white oolitic limestone" about 33 feet thick. These units are diagrammed and a field description of the upper strata are given in figure 61. The limestone beds exposed in the quarry are geologically classified as part of the Fredonia Member of the Ste. Genevieve Formation (Dever and McGrain, 1969). This member consists mainly of oolitic, gray, fossiliferous limestone, which occurs in the western parts of Kentucky and Tennessee, in the southern parts of Indiana and Illinois, and in southeastern Missouri (Keroher and others, 1966). The oolitic beds in the Fredonia Member are characteristically high-calcium limestones. Sample 2061, previously described, was taken from the upper white oolitic limestone beds, and sample 2060 was taken from the "blue," fossiliferous limestone beds that underlie the upper oolite in the quarry.

Recently, TVA has been injecting oolitic aragonite into the boiler. Sample type 8, described earlier, was taken from the same source as the stone used in the TVA tests.

Samples of the normal fly ash were obtained from the mechanical hopper of the test boiler so that the constituents derived from the coal consumed in the boiler could be identified and characterized. Limestone-modified fly ash samples were obtained from the various positions in the boiler.

Sample plane AA is nearly horizontal across the upper part of the boiler at an elevation of 376 feet and about 20 feet above the points of limestone injection. Plane CC is horizontal across the down-draft section of the boiler, behind the exchanger section. Samples from these two planes across the gas stream were collected by special probes introduced into the planes to various sampling points. Samples were also taken from the mechanical and electrostatic hoppers (dust collectors). Details of the boiler and sampling procedures were given by Womble and Reese (1970). The samples for the following petrographic studies were supplied by personnel of TVA and APCO. Identifications of the samples of fly ash materials studied are given in table 15.

The injection test conditions were:

| | |
|---|---|
| Injection temperature | 3000° F |
| Particle size of injected limestone | 70% < 200 mesh |
| Average temperature at plane AA | 2190° F |
| Average temperature at plane CC | 650° F |
| Stoichiometry (number of molecules of CaO injected divided by number of atoms of S in coal) | 1.3 to 1.5 |

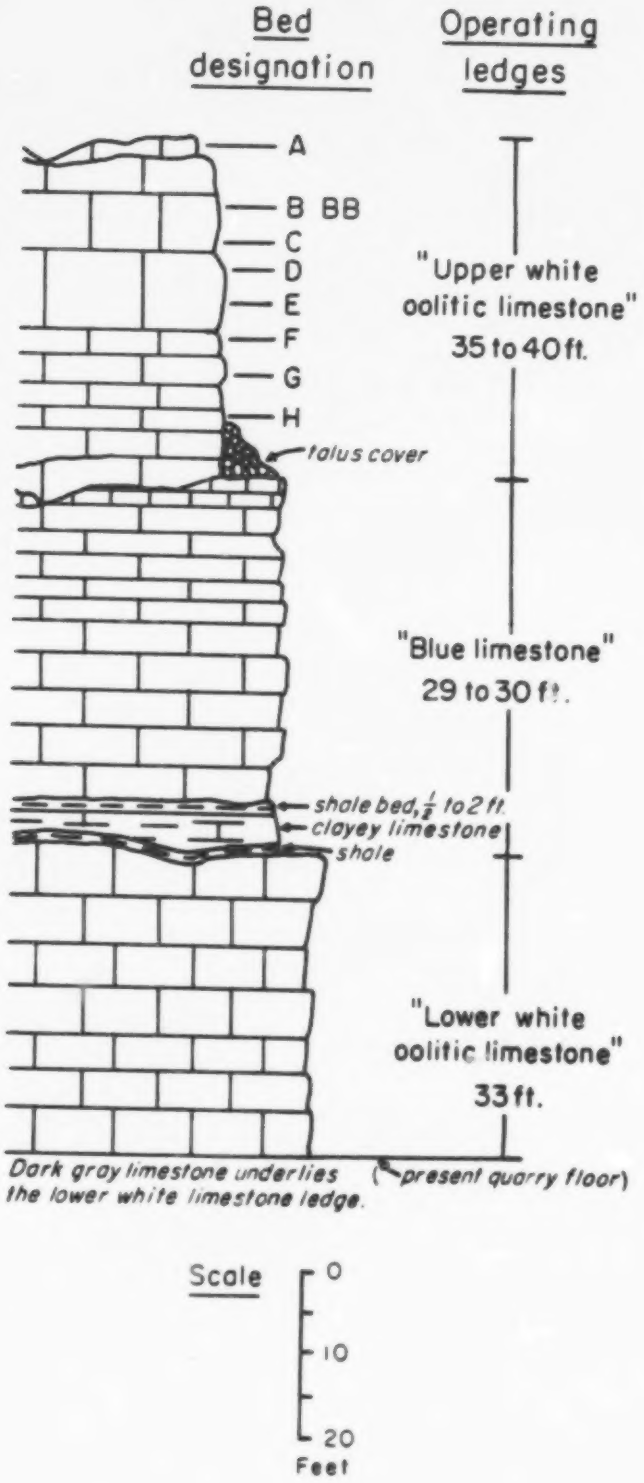
Bed designation
Operating ledges
A
B BB
C
D
E
F
G
H
talus cover
"Upper white oolitic limestone" 35 to 40 ft.
"Blue limestone" 29 to 30 ft.
shale bed, $\frac{1}{2}$ to 2 ft.
clayey limestone
shale
"Lower white oolitic limestone" 33 ft.
Dark gray limestone underlies the lower white limestone ledge.
(present quarry floor)
Scale
0
10
20
Feet

DESCRIPTION OF BEDS

Overburden consists of 2 to 14 feet of clay, silt, and soil. A gray limestone ledge up to 40 feet thick has been quarried from above the upper oolitic limestone ledge currently being produced. On the face of the quarry that was examined in detail there was 1 to 2 feet of the gray limestone remaining (sample A).

A. Gray limestone with calcite spar nests in micrite, biomicrite thin shell-oolitic, stylolitic, irregular patches of lithographic beds interbedded—irregular thickness 1-2 feet.

B. White limestone highly oolitic, fossiliferous, few sparry cement patches. Soft porous, homogeneous stone sample 5-6 feet from top of unit. Varies slightly laterally to somewhat harder stone—sample BB—crinoidal, brown, coarse crystalline.

C. 2-3 feet below B; same as B.

D. 2 feet below C. Contains 3 mm gray ellipsoidal fossils of unknown type. 18 inches to iron-stained beds.

E. White oolitic limestone, as in B, with iron-stained beds about 4 feet thick; iron stain most intense along vertical joints.

F. White oolitic limestone as in B.

G. White oolitic limestone, mixture of fine- and coarse-grained stone with notable porosity in some beds.

H. White oolitic limestone; porous adjacent to joints, fine-grained and non-porous a few feet laterally from the joints.

Floor of upper ledge

Fig. 61. Cross section of the quarry of Fredonia Valley Quarries, Inc., Fredonia, Kentucky.

TABLE 15—FLY ASH SAMPLES STUDIED

| Sample identification | Type of fly ash | Boiler locations and test date |
|---|---|---|
| 45 | Normal | Mechanical hopper |
| 66-71 | Limestone-modified | Plane AA, probe 5AW |
| 92-3, 97-8 | Limestone-modified | Plane CC, composite of 3 probes on the east side of boiler |
| 104 | Limestone-modified | Mechanical hoppers 1-3 |
| 106 | Limestone-modified | Electrostatic hoppers 5-8 |
| Test 2, I-IV | Limestone-modified | Plane AA, 4 composite samples in each test from certain probes taken during 4 different tests: 2(5-13-70), 4(5-21-70), 6(5-27-70), and 8(6-2-70). |
| Test 4, I-IV | Limestone-modified | |
| Test 6, I-IV | Limestone-modified | |
| Test 8, I-IV | Limestone-modified | |
| Test 2, V-VI | Limestone-modified | Plane CC, 2 composite samples each from certain probes during same tests as above. |
| Test 4, V-VI | Limestone-modified | |
| Test 6, V-VI | Limestone-modified | |
| Test 8, V-VI | Limestone-modified | |
| Test 25, I-IV | Limestone-modified | Plane AA, 4 composite samples each from certain probes taken on 8-31-70. |
| Test 25, V-VI | Limestone-modified | Plane CC, 2 composite samples each from certain probes taken on 8-31-70. |
| Test N | Normal | Taken on 6-1-70 |
| I | Normal | Electrostatic hopper 7 |
| II | Normal | Electrostatic hopper 3 |
| III | Normal | Mechanical hopper 3 |

## Mineral Analyses

The minerals occurring in the fly ash samples were identified by X-ray diffraction methods. The iron-rich particles were removed from the nonmagnetic fraction in the samples by repeated use of a very strong hand magnet. Most samples were further separated into eight size classes with sieves of the following mesh: 100, 140, 170, 200, 230, 325, and pan. Each class was further pulverized and mixed with a small amount of mineral oil, and the mixture was spread on a glass slide and X-rayed. The results are tabulated in table 16, and two partial X-ray tracks are shown in figure 62.

The only sulfur-bearing compound positively detected that is believed to have formed in the boiler by reaction with limestone-derived materials is anhydrite ($CaSO_4$). Some calcium sulfite ($CaSO_3$) may have formed, but, if so, most of it must have been converted to the sulfate form prior to analysis of the

### TABLE 16—MINERALOGY OF FLY ASH SAMPLES DERIVED BY X-RAY DIFFRACTION

| | Nonmagnetic fraction | | | Magnetic fraction | | | |
|---|---|---|---|---|---|---|---|
| Sample | Relative abundance: High | Medium | Low | High | Medium | Low | Total mag. (%) |
| 45<br>(normal ash) | Quartz | Lime | Portlandite<br>Anhydrite<br>Pyrite (?) | Magnetite | Hematite | Periclase (?) | 51.6 |
| 66-71<br>(plane AA) | Lime | Quartz | Portlandite<br>Anhydrite | Magnetite | — | Lime<br>Anhydrite<br>Periclase (?) | 8.1 |
| 92-3, 97-8<br>(plane CC) | Lime | Anhydrite | Quartz<br>Portlandite<br>Calcite<br>Periclase (?) | — | — | — | 6.6 |
| 104<br>(mechanical hopper) | Lime | Anhydrite | Quartz<br>Portlandite (?) | Magnetite | Hematite | Anhydrite (?)<br>Pyrite (?) | 17.5 |
| 106<br>(electrostatic hopper) | Lime | Anhydrite | Quartz<br>Portlandite | — | — | — | 0.4 |

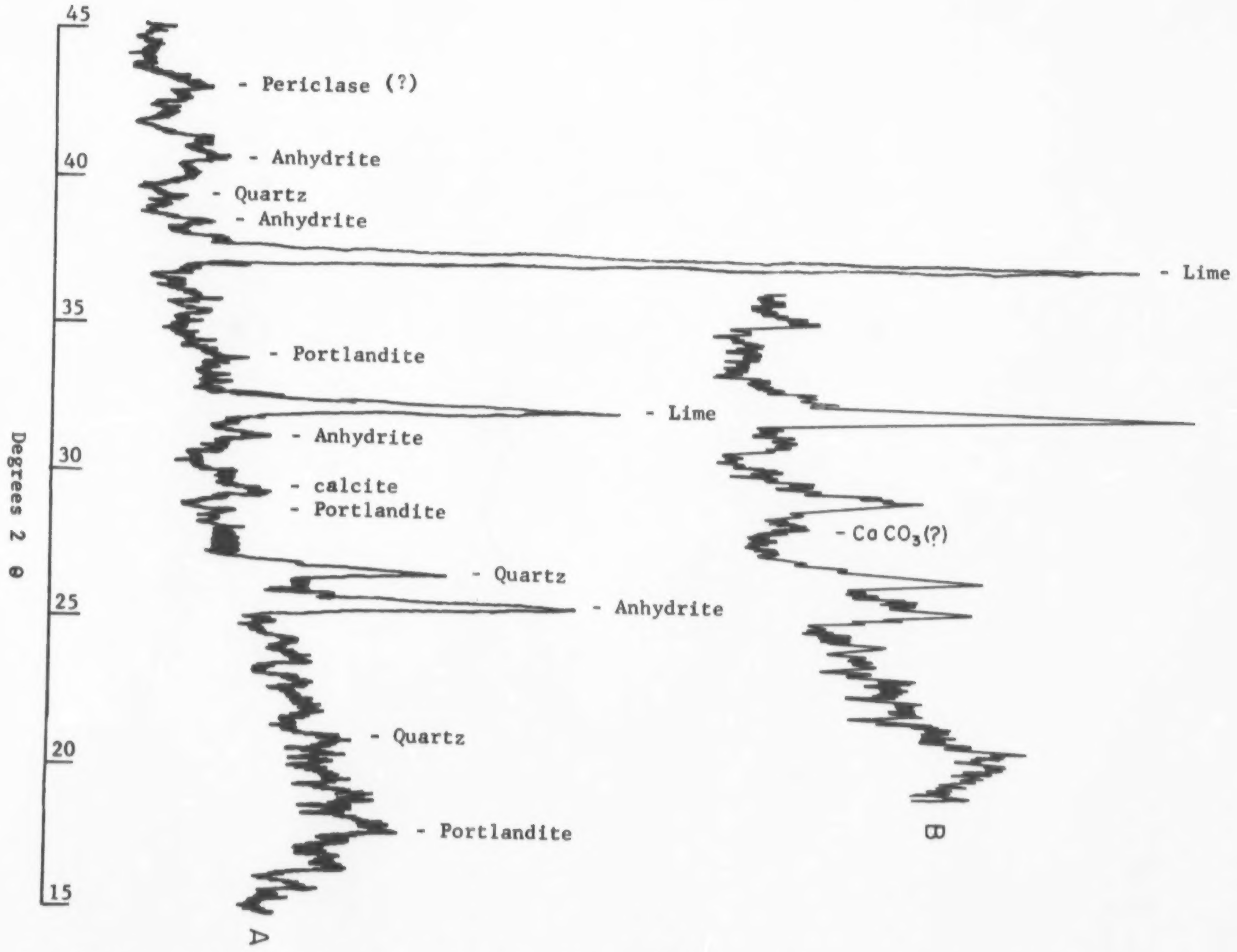

Fig. 62. X-ray diffraction tracks of nonmagnetic fraction of limestone-modified fly ash from plane CC. (A) sample 92-3, 97-8; (B) the +100 mesh of test 25, probes 8E-1,2,3, showing possible trace occurrence of $CaSO_3$.

samples. The identification of very small amounts of $CaSO_3$ is complicated by the partial masking of the main diffraction peak of $CaSO_3$ by a moderate peak of portlandite ($Ca(OH_2)$), a very small peak from anhydrite, and a peak from magnetite. The main peak of $CaSO_3$ occurs at 28.6 degrees, and secondary peaks occur at 30.8 and 35.4 degrees. The small anhydrite peak also occurs at 28.6 degrees, the main peak of magnetite occurs at 35.4 degrees, and one peak of $Ca(OH_2)$ occurs at 28.7 degrees. To add to the difficulty, anhydrite, portlandite, and magnetite occurred to some extent in nearly every sample. Four samples had X-ray tracks that suggest the possible occurrence of $CaSO_3$: the 100- to 140-mesh and the +100-mesh samples from probes 8E and 8W, all from plane CC (test 25, 8-31-70). One of these tracks is shown in figure 62B. Portlandite appears to be absent in this sample (fig. 62B), the anhydrite content is low (small peak at 25.5 degrees), and the peak at 28.8 degrees appears too large to be accounted for solely from anhydrite. Therefore, the 28.8 degree peak indicates a minor amount of $CaSO_3$ is present. However, the 30.8 degree peak of $CaSO_3$ is absent, and the 35.4 peak on the sample track could be produced from a small amount of magnetite that remained in the sample.

The X-ray peak heights from the samples indicate anhydrite occurs in nearly the same abundance in both electrostatic and mechanical hoppers; less anhydrite was found in the CC plane, and the least occurs in samples from plane AA.

The separation of magnetite and hematite from the ashes by repeated passing of the sample through the magnetic field was successful in that no iron oxides were detected by X-ray diffraction in the nonmagnetic fraction. Small amounts of lime and traces of anhydrite were captured by the magnetic particles and were detected in the magnetic fraction. The weight percentage of the magnetic fraction separated from the samples is given in table 16. Microscope examination reveals numerous glassy and spherical particles in both magnetic and nonmagnetic fractions. Those in the magnetic fraction were dark gray to black, while most of the nonmagnetic spherulites were colorless. These glassy and amorphous particles account for the broad hump in the base line of the X-ray pattern between 15 and 22 degrees $2\theta$ (fig. 62).

The mineral composition of the fly ash samples taken from plane AA in test 25 differed from that of the first series (66-71). Calcite was abundant in the coarse fractions in plane AA samples taken during test 25, whereas it was not detected in samples 66-71. The amount of limestone injected into the boiler or the temperature of injection probably differed for the two tests.

Certain mineralogical changes in the fly ash apparently occurred during cooling. The occurrence of portlandite in the fly ash is the result of the reaction of small amounts of moisture with the lime, probably during handling of the sample. The X-ray data suggest that pyrite is present in trace amounts in samples 45 and 104. This pyrite either survived combustion or reformed during cooling of the ash-gas mixture by reaction of gaseous $SO_2$ and certain Fe-rich particles. The increase of approximately 0.5 percent of sulfate sulfur in the samples from the electrostatic and mechanical hoppers over that of plane CC (table 17) indicates some growth of anhydrite occurs in the dust below plane CC.

Studies were made of samples of the normal fly ash of test N (I, II, and III) to develop a method for rapid analysis of anhydrite-lime relations in

TABLE 17—CHEMICAL ANALYSES OF FLY ASH MATERIALS IN WEIGHT PERCENTAGE*
(Analyses by Analytical Chemistry Section, Illinois State Geological Survey)

| | | Limestone-modified fly ash | | | | Normal fly ash |
|---|---|---|---|---|---|---|
| | Boiler position: | AA | CC | Electrost. hopper | Mech. hopper | Mech. hopper |
| Oxide | Sample number: | 66-71 | 92-3<br>97-8 | 106 | 104 | 45 |
| $SiO_2$ | | 31.2 | 33.4 | 46.5 | 38.8 | 39.0 |
| $Al_2O_3$ | | 11.19 | 15.0 | 18.99 | 13.94 | 15.63 |
| $Fe_2O_3$ | | 8.62 | 8.75 | 8.07 | 14.89 | 31.68 |
| CaO | | 39.8 | 30.7 | 17.1 | 24.5 | 10.8 |
| $CO_2$ | | 0.49 | 1.90 | 0.93 | 1.00 | 0.28 |
| Organic C | | 4.29 | 1.00 | 1.19 | 0.66 | 1.32 |
| Sulfate S | | 0.26 | 1.52 | 1.65 | 1.68 | 0.43 |
| Pyritic S | | 0.07 | 0.03 | 0.05 | 0.10 | 0.09 |
| Organic S | | 0.03 | 0.32 | 0.33 | 0.07 | ‡ |
| TOTAL† | | 95.95 | 92.62 | 94.81 | 95.64 | 99.23 |
| Calculated compounds (%) | | | | | | |
| Anhydrite ($CaSO_4$) | | 1.1 | 6.46 | 7.0 | 7.1 | 1.8 |
| Calcite ($CaCO_3$) | | 1.1 | 4.3 | 2.1 | 2.3 | 0.6 |

* CaO was determined by X-ray, $CO_2$ by gravimetric methods, total C by hi-temp methods, total S by ESCHKA, sulfate S by dilute HCl treatment, pyritic S by measurement of Fe in nitric acid solution, organic S and C by difference.

† Minor amounts of $TiO_2$, MnO, MgO, and $K_2O$ probably are present and account for the low totals.

‡ None detected.

limestone-modified ash. Oil-immersed, powdered samples were examined in crossed-polarized light with the Quantimet. Under these conditions, the glassy components (isotropic) of the ash appear black, and anhydrite and a few other anisotropic components (principally quartz) appear in their characteristic interference colors. Image analysis of the quantity and size of anisotropic particles in normal and limestone-modified samples should provide a means of determining the content and particle size of anhydrite in limestone-modified ash samples. However, the amount of quartz and other anisotropic grains varied greatly in the normal ashes, and the anhydrite grains in modified ashes were too small for rapid identification and accurate analysis by this method.

## Chemical Analyses

Chemical analyses of the fly ash samples are shown in table 17, along with the percentage of anhydrite in the samples, as calculated from the chemical data. These values for anhydrite are in close agreement with the X-ray diffraction data. Calcite percentages also were calculated (table 17). The presence of small amounts of $CO_2$ in the samples substantiates the presence of calcite, especially in sample 92-3, 97-8.

The percentages of the sulfur as $SO_4$ and of the organic sulfur in unburned coal particles are related to the total sulfur in the ash samples, as follows:

| Sample | Percentage of total S as: Organic S | $SO_4$ |
|---|---|---|
| 66-71 (plane AA) | 8 | 72 |
| 92-3, 97-8 (plane CC) | 17 | 81 |
| 106 (electrostatic hopper) | 16 | 81 |
| 104 (mechanical hopper) | 4 | 91 |
| 45 (normal ash, mechanical hopper) | 0 | 83 |

The reason for the relatively low proportion of organic sulfur in plane AA compared to that in the other limestone-modified ash samples is not known. Because of fairly wide variation in these figures, detailed analyses of the various species of sulfur in fly ash samples, including organic S, should be made in future studies.

The average of the analytical results of the nonmagnetic and magnetic fractions of normal fly ash samples from mechanical hopper 3, test N, III (table 18) show only slight differences in composition from sample 45. Two samples from electrostatic hoppers 3 and 7 also were analyzed (table 18). The particles from the electrostatic hoppers were too fine for a good magnetic separation. The analyses of these two samples are very similar; none of the elements differ significantly. The magnetic fraction in the sample from mechanical hopper 3 was found to contain 66.5 percent iron oxide, which is equivalent to 46.5 percent iron.

Another series of limestone-modified fly ash samples (tests 2 through 8) was selected to evaluate the characteristics of the lime-anhydrite particles. Initially, special attention was to be given to the differences in crystal morphology of particles obtained from the AA and CC planes within the TVA boiler; however, the X-ray diffraction data indicated much of the lime in the samples had been hydrated to portlandite. Therefore, only chemical analyses were performed on these samples. These data (table 19) were subjected to statistical analyses to evaluate the dispersion of particles in planes AA and CC because various areas in the two boiler planes were sampled by a number of different probes.

Statistical analyses of the results from standard analysis of variance methods (Snedecor, 1946) led to the following conclusions:

1. There was no significant differences in CaO in plane AA between tests 2, 4, 6, and 8, as evaluated by the means of the various probe samples.

### TABLE 18—CHEMICAL ANALYSES OF NORMAL FLY ASHES (TEST N) TAKEN FROM SHAWNEE UNIT 10, JUNE 1, 1970

(Analyses by Analytical Chemistry Section, Illinois State Geological Survey)

| Test N: | I | II | III | | |
|---|---|---|---|---|---|
| | | | Mechanical hopper 3 | | |
| Oxide | Electrostatic hopper 7 | Electrostatic hopper 3 | Magnetic | Nonmagnetic | Average |
| $SiO_2$ | 50.8 | 52.1 | 19.7 | 50.6 | 35.1 |
| $TiO_2$ | 1.10 | 1.10 | 0.40 | 0.85 | 0.6 |
| $Al_2O_3$ | 23.5 | 23.3 | 8.46 | 20.8 | 14.7 |
| $Fe_2O_3$ | 12.0 | 12.1 | 66.5 | 5.38 | 36.0 |
| MnO | 0.15 | 0.15 | 0.80 | 0.07 | 0.4 |
| MgO | 0.44 | 0.83 | 0.53 | 0.17 | 0.4 |
| CaO | 4.98 | 3.89 | 2.17 | 15.3 | 8.8 |
| $K_2O$ | 2.61 | 2.61 | 0.77 | 2.29 | 1.5 |
| $P_2O_5$ | 0.23 | 0.34 | 0.09 | 0.01 | 0.05 |
| $CO_2$ | 0.19 | 0.10 | 0.23 | 0.50 | 0.4 |
| Organic C | 3.46 | 2.90 | 0.35 | 3.89 | 2.1 |
| $SO_3$ | 0.01 | 0.03 | 0.03 | 0.03 | 0.03 |
| Pyritic S | 0.11 | 0.10 | 0.17 | 0.01 | 0.09 |
| Organic S | 0.32 | 0.45 | 0 | 0.32 | 0.16 |
| TOTAL | 99.90 | 100.0 | 100.2 | 100.22 | |

2. There was no significant difference in CaO as sampled at the various probe positions in plane AA at the 99 percent confidence level. At the 95 percent confidence level the difference between probes 6AE + 7AE and 4AE + 5AE may be important, for it implies there may be some degree of nonuniformity of CaO in plane AA as sampled by the probes.

3. There was a significant increase in the sulfur content in plane AA between test runs 2 and 8, test run 8 being high in sulfur.

4. No significant differences were found in the sulfate sulfur from various probes in plane AA.

5. No significant differences in level of sulfate sulfur was found to occur in probes 8W 1, 2, 3 and 8E 1, 2, 3.

6. Plane CC contains significantly higher levels of sulfate sulfur and $CO_2$ than plane AA.

TABLE 19—CHEMICAL ANALYSES OF LIMESTONE-MODIFIED FLY ASH SAMPLES FROM PLANES AA AND CC FROM UNIT 10, SHAWNEE STEAM PLANT
(Analyses by Analytical Chemistry Section, Illinois State Geological Survey)

| Sample identification and date | Plane | Probes | Weight percentage |  |  |  |  |  |  |
|---|---|---|---|---|---|---|---|---|---|
|  |  |  | CaO | $CO_2$ | $SO_3$ | Organic C | Total S* | S as $SO_4$ | Organic S |
| Test 2 (5-13-70) |  |  |  |  |  |  |  |  |  |
| I | AA | 6AE + 7AE | 34.6 | 3.56 | 1.30 | 5.77 | 0.87 | 0.52 | 0.24 |
| II |  | 6AW + 7AW | 37.7 | 2.57 | 1.20 | 2.82 | 0.78 | 0.48 | 0.30 |
| III |  | 4AW + 5AW | 41.0 | 2.38 | 1.12 | 4.58 | 0.73 | 0.45 | 0.28 |
| IV |  | 4AE + 5AE | 36.7 | 2.18 | 0.80 | 5.02 | 0.58 | 0.32 | 0.26 |
| V | CC | 8W 1,2,3 | 31.3 | 3.56 | 5.04 | 2.52 | 2.64 | 2.02 | 0.62 |
| VI |  | 8E 1,2,3 | 36.6 | 3.96 | 4.72 | 2.71 | 2.39 | 1.89 | 0.50 |
| Test 4 (5-21-70) |  |  |  |  |  |  |  |  |  |
| I | AA | 6AE + 7AE | 37.8 | 3.56 | 0.87 | 4.95 | 0.54 | 0.35 | 0.19 |
| II |  | 6AW + 7AW | 36.6 | 3.37 | 0.87 | 4.91 | 0.57 | 0.35 | 0.22 |
| III |  | 4AW + 5AW | 42.9 | 2.57 | 0.82 | 7.61 | 0.63 | 0.33 | 0.30 |
| IV |  | 4AE + 5AE | 44.6 | 3.56 | 0.90 | 3.60 | 0.47 | 0.36 | 0.11 |
| V | CC | 8W 1,2,3 | 32.8 | 4.36 | 2.80 | 3.51 | 1.90 | 1.12 | 0.78 |
| VI |  | 8E 1,2,3 | 35.6 | 4.16 | 3.15 | 2.71 | 1.66 | 1.26 | 0.39 |
| Test 6 (5-27-70) |  |  |  |  |  |  |  |  |  |
| I | AA | 6AE + 7AE | 34.7 | 2.18 | 0.80 | 4.53 | 0.44 | 0.32 | 0.12 |
| II |  | 6AW + 7AW | 39.7 | 1.98 | 0.60 | 4.67 | 0.29 | 0.22 | 0.06 |
| III |  | 4AW + 5AW | 37.3 | 1.98 | 0.80 | 9.00 | 0.63 | 0.32 | 0.30 |
| IV |  | 4AE + 5AE | 45.1 | 1.78 | 0.47 | 4.10 | 0.44 | 0.19 | 0.24 |
| V | CC | 8W 1,2 | 39.9 | 2.77 | 2.07 | 1.34 | 1.16 | 0.83 | 0.33 |
| VI |  | 8E 1,2 | 29.4 | 2.77 | 2.07 | 5.08 | 1.07 | 0.83 | 0.23 |
| Test 8, run 2 (6-2-70) |  |  |  |  |  |  |  |  |  |
| I | AA | 6AE + 7AE | 35.1 | 1.58 | 0.57 | 3.84 | 0.33 | 0.23 | 0.09 |
| II |  | 6AW + 7AW | 40.3 | 1.98 | 0.70 | 4.07 | 0.39 | 0.28 | 0.10 |
| III |  | 4AW + 5AW | 39.4 | 1.39 | 0.75 | 6.02 | 0.51 | 0.30 | 0.20 |
| IV |  | 4AE + 5AE | 47.2 | 1.98 | 0.90 | 5.24 | 0.66 | 0.36 | 0.30 |
| V | CC | 8W2 + 8W3 | 43.9 | 2.57 | 2.00 | 2.05 | 1.51 | 0.80 | 0.70 |
| VI |  | 8E2 + 8E3 | 24.9 | 2.97 | 2.87 | 3.31 | 1.19 | 1.15 | 0.03 |

* S as pyritic sulfur was found to be less than 0.01% in all samples except Test 4-I, in which none was detected.

7. The ratios of the mean sulfate sulfur in planes CC to AA in tests 2, 4, 6, and 8 indicate the order of increasing amount of reaction between lime and $SO_2$ in the boiler:

   $$\text{test } 6 < \text{test } 4 = \text{test } 8 < \text{test } 2.$$

   Thus the conditions in the boiler were most favorable for sorption of sulfur during test 2.

## Grain Size Distribution

Particle size analyses of the samples taken during test 25 are given in table 20. The samples were sieved by ultrasonic vibration, and the weight percentage of the various intervals was determined. The size distribution of particles smaller than 44 μ were analyzed by number of particles with the Quantimet.

Differences in the particle size distribution from the various probes in plane AA are not significant, but the difference between the distribution of probes in planes AA and CC are considerable. The data in table 20 indicate there is nearly twice as much material in the range 44 to 63 μ in plane CC as in plane AA. This fact is more clearly shown by the histograms in figure 63. In CC samples, 37.5 percent (by weight) of the material is coarser than 44 μ, whereas in AA samples, 25.5 percent is coarser than 44 μ. This enlargement of grains is likely due to agglomeration of normal fly ash dust particles (fig. 64) and possibly also to the conversion of the surface of some of the lime particles. However, the average frequency (by number) of particles less than 4 μ in the CC plane is somewhat larger than in the AA plane (table 20).

The anhydrite content of the samples taken during test 25 varies according to particle size of the ash. In plane CC the anhydrite-to-lime ratio is high for the particles greater than 149 μ and for those less than 63 μ, compared with those in the 63 to 149 μ range. The anhydrite grains are mainly submicron to, possibly, 2 microns in size. The high anhydrite content in the coarser sieve fraction is due to the adherence of very small particles to the surfaces of large particles of lime.

## Electron Microscopy of Limestone-Modified Fly Ash

Observations from scanning electron microscope studies of limestone-modified fly ash samples, in connection with phase III of the project, were made from approximately 130 micrographs, 25 of which were selected and reproduced herein (figs. 64-68) to show the surface character of typical particles and certain special features. The discussion and interpretation of the micrographs are partly based on recent results obtained from the X-ray spectrometer attached to the scanning electron microscope. However, the specific samples illustrated were not analyzed with the X-ray apparatus.

Figure 64 shows typical particles found in normal fly ash obtained from the mechanical hopper (sample 45). They consist of very small spherulites with a fairly smooth-textured outer surface and some larger spherulites

TABLE 20—PARTICLE SIZE ANALYSES OF FLY ASH SAMPLES FROM VARIOUS PROBES INTO PLANES AA AND CC. TEST 25, AUGUST 31, 1970, SHAWNEE PLANT, KENTUCKY.

| Screen and particle size (µ) | 6AE-7AE AA Plane | 4AE-5AE AA Plane | 5AW-4AW AA Plane | 6AW-7AW AA Plane | 8E-1,2,3 CC Plane | 8W-1,2,3 CC Plane | Average |  |
|---|---|---|---|---|---|---|---|---|
|  | Weight percentage retained on screen |  |  |  |  |  | AA | CC |
| +149 | 1.36 | 1.68 | 2.55 | 3.21 | 2.09 | 0.70 | 2.20 | 1.4 |
| +105 | 1.68 | 2.07 | 2.46 | 2.57 | 2.71 | 1.11 | 2.20 | 1.9 |
| + 88 | 2.38 | 3.34 | 3.16 | 3.74 | 3.93 | 5.20 | 3.2 | 4.6 |
| + 74 | 2.77 | 4.30 | 4.18 | 3.89 | 5.41 | 4.42 | 3.8 | 4.9 |
| + 63 | 2.13 | 2.93 | 3.11 | 2.50 | 3.84 | 2.30 | 2.7 | 3.1 |
| + 44 | 10.58 | 13.80 | 10.85 | 10.55 | 22.55 | 20.67 | 11.4 | 21.6 |
| Pan | 79.10 | 71.88 | 73.69 | 73.54 | 59.47 | 65.60 | 74.6 | 62.5 |
| Size intervals (µ) | Number of particles in percent |  |  |  |  |  |  |  |
| 44-31 | 2 | 4 | 4 | 4 | 1 | 1 | 3.5 | 1 |
| 31-16 | 9 | 7 | 15 | 11 | 6 | 8 | 10.5 | 7 |
| 16-8 | 27 | 24 | 27 | 28 | 20 | 35 | 26.5 | 28 |
| 8-4 | 50 | 46 | 43 | 47 | 53 | 37 | 46.6 | 45 |
| 4-0 | 12 | 19 | 11 | 10 | 20 | 19 | 12.9 | 19 |

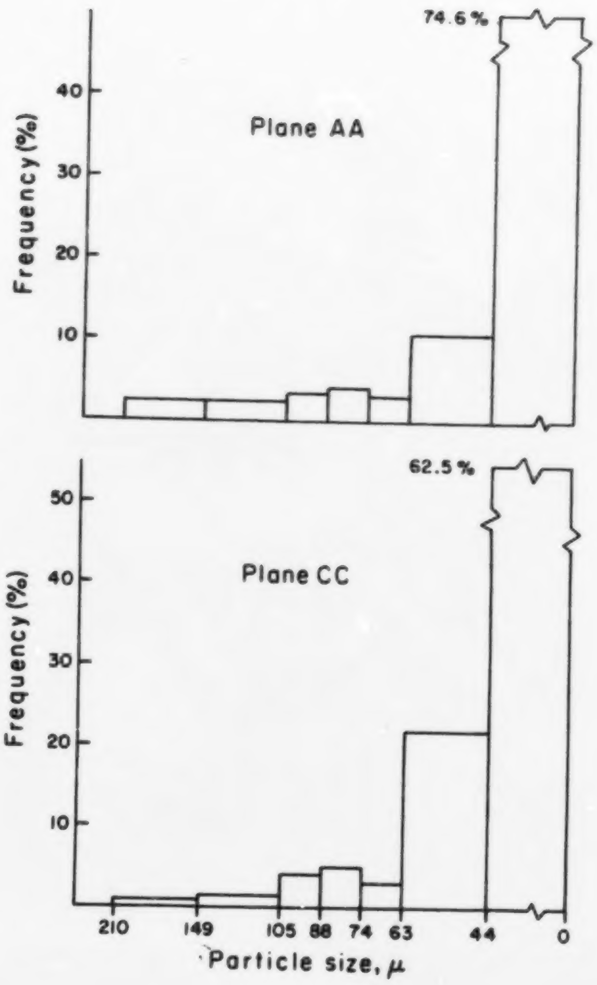

Fig. 63. Particle-size distribution of limestone-modified fly ash in boiler planes AA and CC, test 25.

with scattered pits and small holes (fig. 64A, B, and C). Larger spheres are hollow and usually contain smaller particles of fly ash (fig. 64B, C, and D). Many spheres of various sizes have a granular-textured surface, best shown in figure 64B. The iron content of these particles probably varies considerably, as their color in ordinary light ranges from colorless to dark black. Qualitative chemical analyses of a number of relatively smooth and spherical fly ash particles indicate they are mainly Si, Al, and Fe, in order of relative abundance.

The next most abundant type of particle is one characterized as vesicular slag (fig. 64D and fig. 65A and B). These particles are irregular in shape, but broken shells of the smooth spherulites may also be vesicular, as shown by the large particle in the lower right quarter of figure 64D. Figure 65 shows typical micrographs of limestone-modified fly ash from the mechanical hopper (sample 104). Over 90 percent of this sample appears to consist of normal ash particles. A few black and vesicular particles were observed in sample 104 (fig. 65A) that closely resemble slag, but because of their color it is thought these are unburned coal fragments. A variety of surface textures occur on particles in the limestone-modified fly ash samples that were not observed on normal particles (fig. 65C, D, and E).

Positive identification of the crystallites shown as epitaxial growths on spherulite surfaces in these pictures cannot be made at this time; however, the crystallites may be anhydrite. Figure 65F is a close-up view of a portion of a spherulite that is partly smooth and partly granular. The granularity may be due to the presence of lime and/or sulfated lime. The cavity in the center of this sphere contains platy and spherical fly ash particles. The two large spherulites (fig. 65H) have granular coatings that might be sulfated lime; however, the larger one resembles others observed in normal ash (fig. 64B).

Figure 66 shows particles in modified fly ash (sample 104). Micrographs B and C are typical views of the sample; C is mainly slag-type ash and B is mainly spherulites. Micrographs A and D are of particles thought to consist of lime and sulfated lime. Figure 66 A indicates some degree of sintering of the constituent grains on the surface of the particle; D shows less sintering and a more porous particle with normal ash spherulites attached to it.

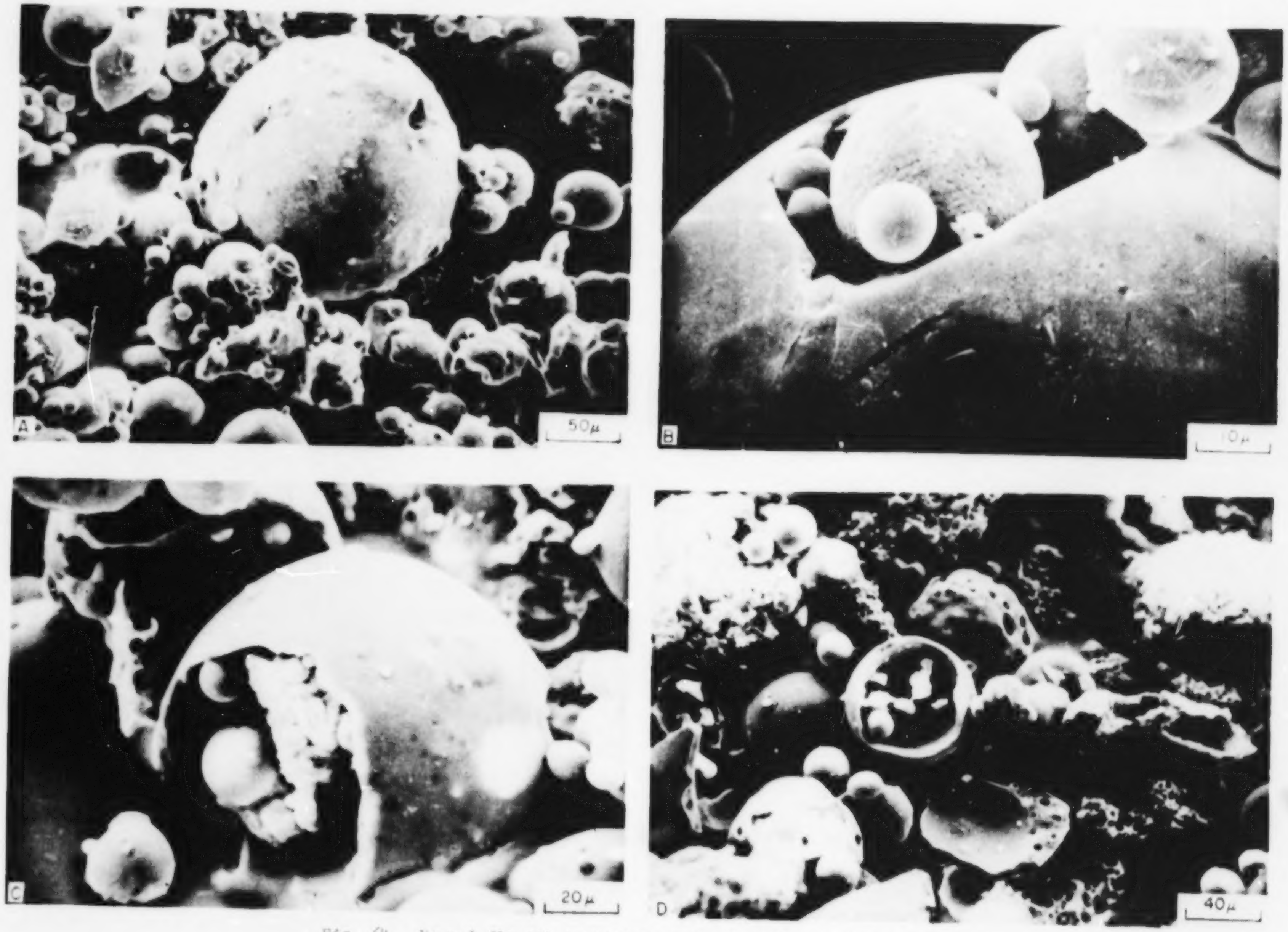
A
50μ
B
10μ
C
20μ
D
40μ

Fig. 64. Normal fly ash particles, mechanical hopper (sample 45).

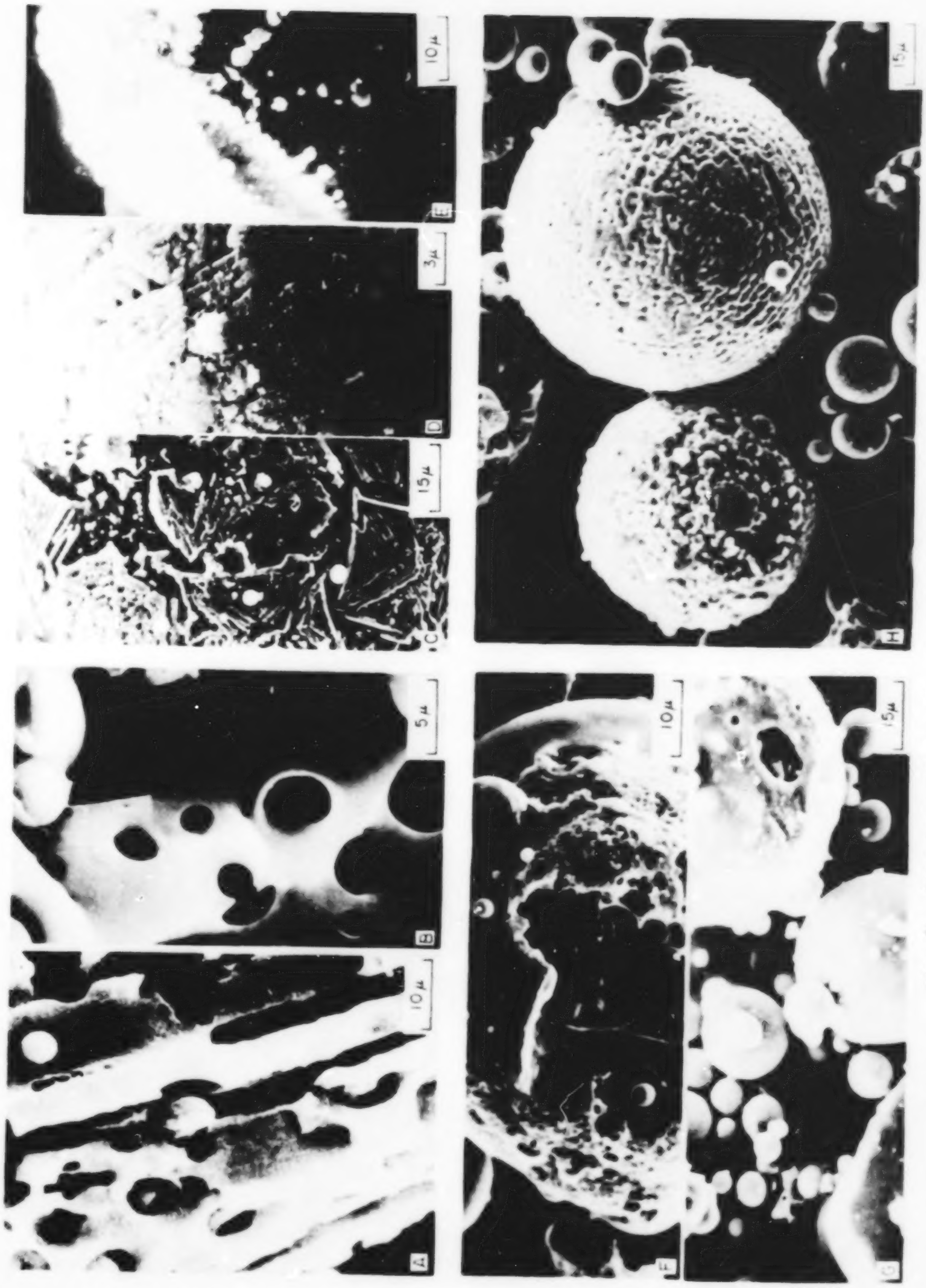
A
10μ
B
5μ
C
15μ
D
3μ
E
10μ
F
10μ
G
15μ
H
15μ

Fig. 65. Limestone-modified fly ash, mechanical hopper (sample 104).

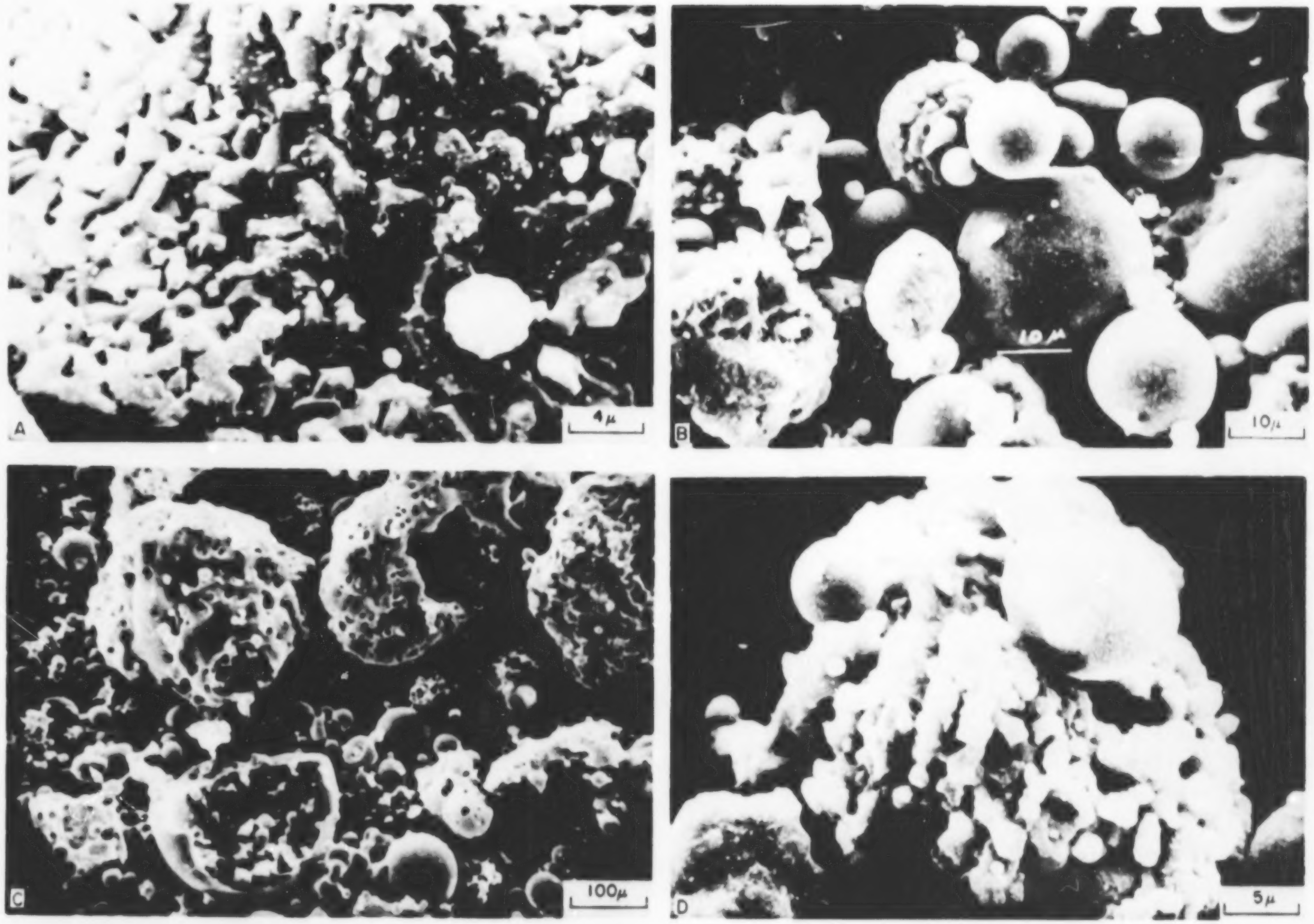
A
4μ
B
10μ
10μ
C
100μ
D
5μ

Fig. 66. Limestone-modified fly ash, mechanical hopper (sample 104).

Figure 67 shows particles that occur in limestone-modified ash from plane AA inside the boiler (sample 66-71). The granular (nonspherical) particles in A and B may be limestone-derived material. Micrographs C and D show mainly siliceous spherulite material; however, the coating on the lower part of the 10 μ spherulite near the center of C shows evidence of chemical activity, possibly sulfation. The large spherulites shown in C and D prove that pitting and complex cavities in fly ash spherulites develop very early in the formation of the ash, plane AA being at the top of the fire box in the boiler.

Figure 68A and C show particles taken from plane CC, probes 8E-1, 2, and 3, during test 2 of limestone injection on May 13, 1970. The micrographs are close-up pictures of particles that appear to contain sulfated lime. The granular and partly sintered texture is the basis of this interpretation. None of the particles from the CC plane could be identified from SEM observations as $CaSO_3$. The insert in A shows fibrous portlandite (CaOH) in the sample. Moisture was permitted to react with the lime in this sample prior to examination.

Figure 68B and D show typical particles that occur in samples taken from the electrostatic hopper (sample 106). They consist mainly of alumina-silica spherulites. Sulfated lime particles (anhydrite) are known from X-ray diffraction data to occur in this sample, but none could be positively identified under the scanning electron microscope. Possibly the very fine particles that are attached as granular dust on larger spherulites, shown in the lower half of figure 68D, are anhydrite.

## Studies of Boiler Deposits

During the course of injection of pulverized limestone into the boiler at the Shawnee Steam Plant it was noted in May 1970 by TVA engineers that a build-up of deposits was occurring. Inspection of the boiler in June showed considerable deposits had formed on the fire side of the reheat section. Petrographic examination of a few specimens of these deposits was made by the author. Since the specific orientation of the specimens relative to the steam pipes was not known and was considered important to the interpretation of the data, additional specimens were collected from the boiler during the next scheduled shut-down in September 1970. The results of petrographic and chemical studies of the specimens follow.

### Deposits Collected September 1970

The spatial relation of the pipes in the reheat section is indicated in figure 69A. By and large, the front side of the pipes was as free of deposits as the back side shown in the photograph. However, a few areas on the front and rear sides of the reheat section, about midway from the sides of the boiler, did have a hard material deposited on the fire side of the pipes. Eleven samples of these deposits were taken. Several specimens were separated into subsamples after preliminary microscope study, and chemical and mineralogical analyses were made of these subsamples. The results of these tests are given in table 21.

The deposits extended along the axis of the pipes for several feet and were triangular in cross section, as shown in figure 69B. Their shape is

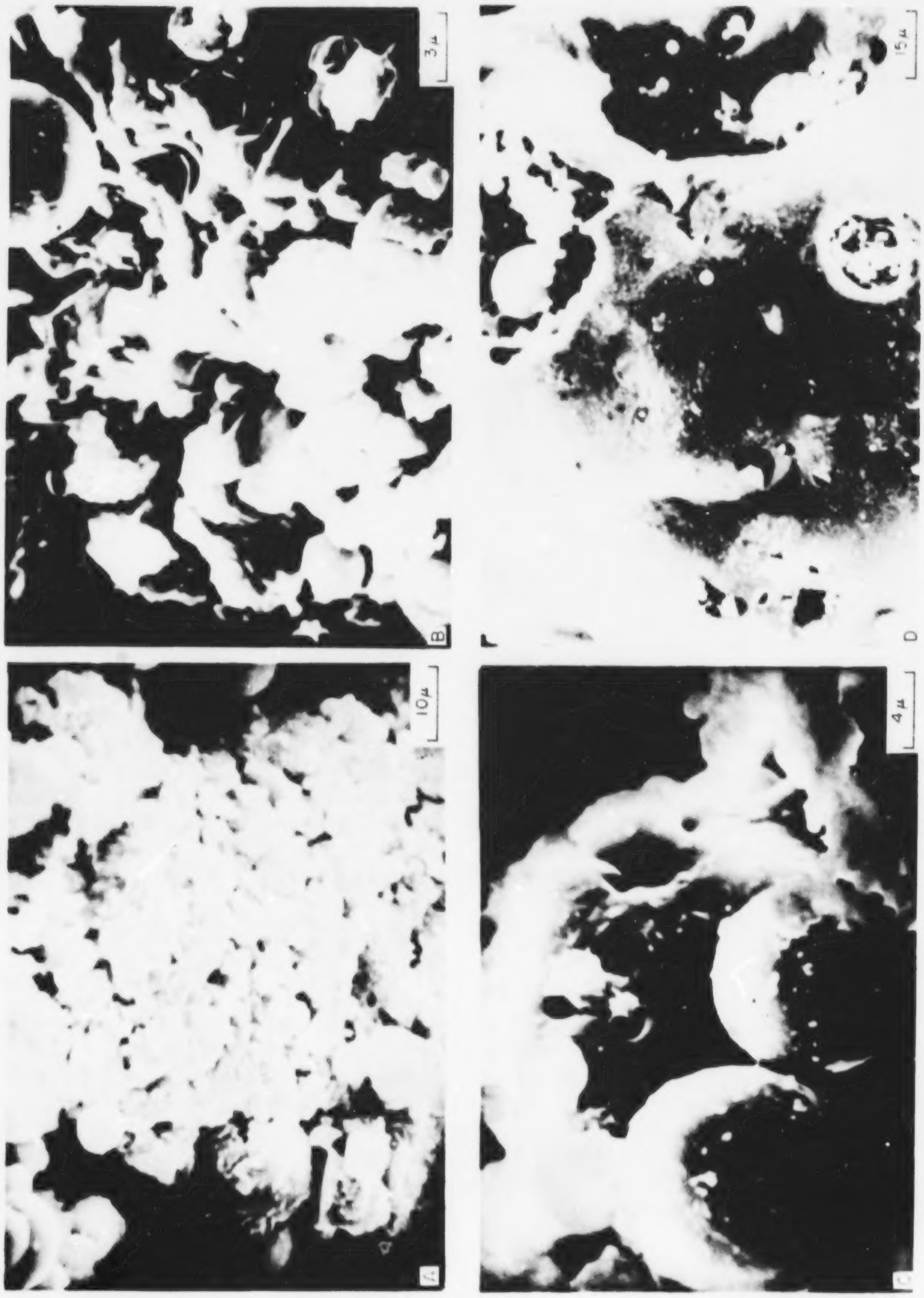
A
10μ
B
3μ
C
4μ
D
15μ

Fig. 67. Limestone-modified fly ash, plane AA (sample 66-71).

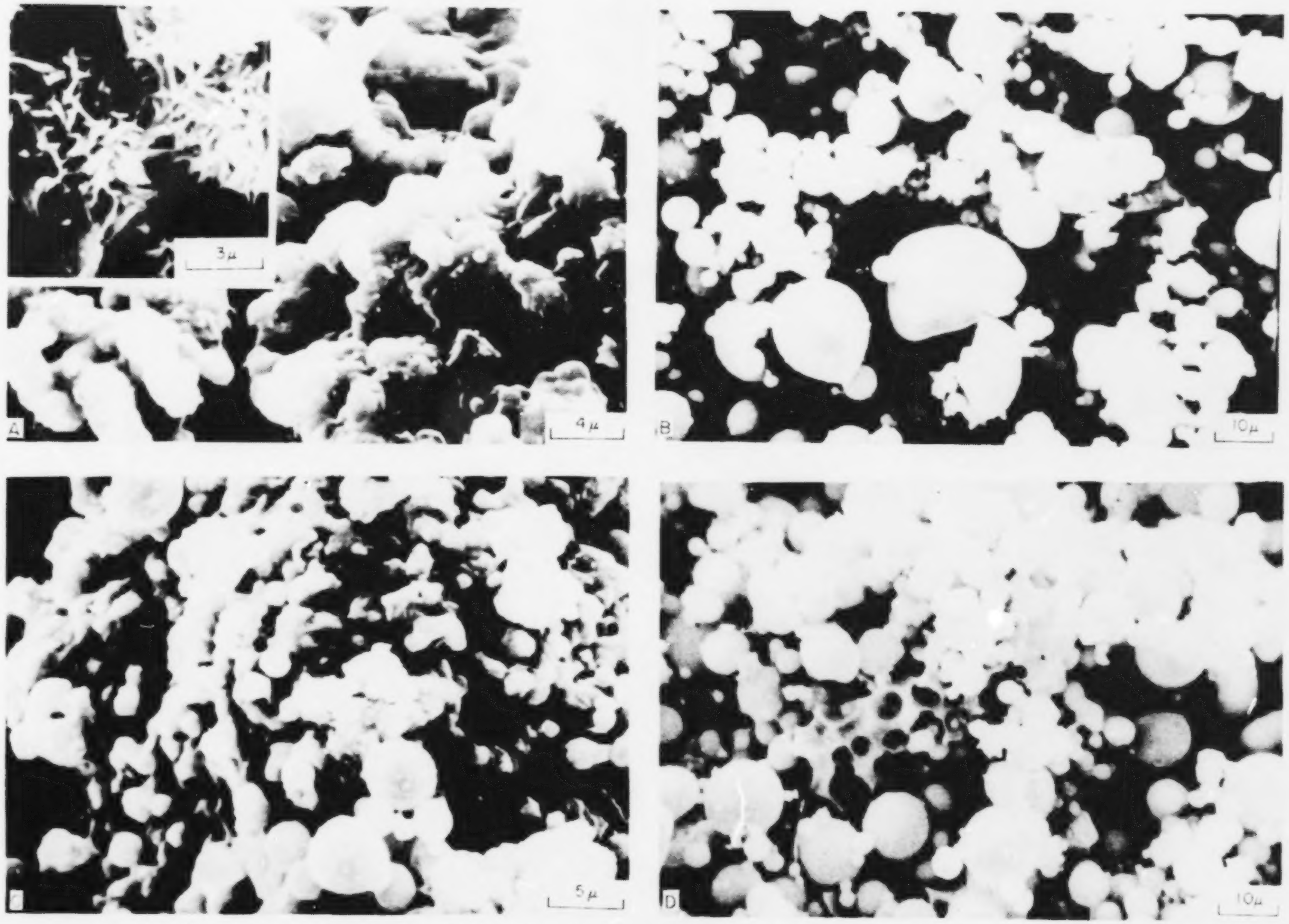
A
3μ
4μ
B
10μ
C
5μ
D
10μ

Fig. 68. A and C - Limestone-modified fly ash, plane CC (sample 92-3, 97-8); B and D - Limestone-modified fly ash, electrostatic hopper (sample 106).

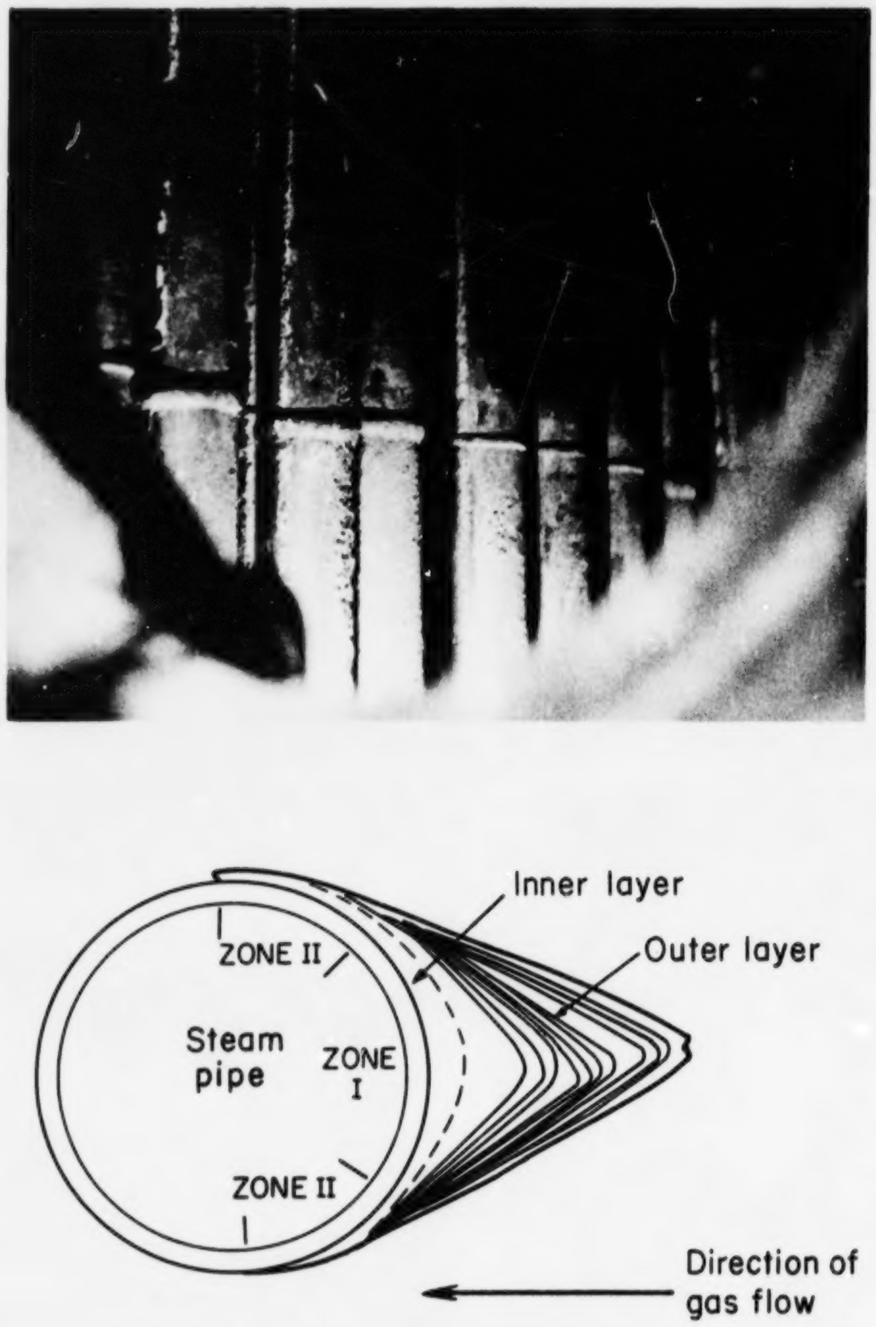
Inner layer
Outer layer
ZONE II
Steam pipe
ZONE I
ZONE II
Direction of gas flow

Fig. 69. A. View of the back side of the reheat section through an entry port. B. Cross section of a steam pipe with its attached deposit, showing the shape and layered structure of the deposit. Note the location of zones I and II in relation to the inner layer deposits.

TABLE 21—CHEMICAL AND MINERAL ANALYSES OF FIRE-SIDE BOILER DEPOSITS IN WEIGHT PERCENTAGE

| | Inner layer | | | | | | Outer layer | | | | Mixed layer | | | Dark gray front screen‡ |
|---|---|---|---|---|---|---|---|---|---|---|---|---|---|---|
| | White (Zone I) | | | Reddish brown (Zone II) | | | Buff + brown† | | Buff | Brown† | | | | |
| Position:* | F | B | B | F | F | F' | F | F | F | F | F | F' | B | |
| Sample: | 4A | 1 | 2 | 3A-1 | 5A-1 | 8B | 3A-2 | 4B | 3B-2 | 3B-1 | 5B | 8A | 6 | 7B |
| $SiO_2$ | 8.73 | 10.50 | 9.91 | 22.73 | 17.20 | 16.68 | 8.20 | 7.12 | 7.16 | 8.96 | 27.22 | 45.70 | 43.36 | 42.15 |
| $Al_2O_3$ | 3.93 | 4.16 | 3.89 | 10.57 | 7.50 | 7.57 | 4.50 | 2.89 | 2.90 | 4.20 | 10.64 | 17.28 | 19.44 | 18.07 |
| $Fe_2O_3$ | 2.74 | 2.42 | 2.04 | 6.37 | 7.42 | 5.23 | 2.29 | 2.01 | 2.43 | 2.60 | 10.69 | 14.90 | 14.81 | 17.18 |
| MgO | — | 0.05 | 0.52 | — | 0.25 | 1.08 | — | 0.54 | — | 0.29 | 0.55 | 1.19 | 1.12 | 0.83 |
| CaO | 36.26 | 35.96 | 35.26 | 22.95 | 25.63 | 31.40 | 36.74 | 41.23 | 36.79 | 36.34 | 18.52 | 7.40 | 6.11 | 14.33 |
| $K_2O$ | 0.44 | 0.62 | 0.56 | 1.40 | 0.97 | 0.96 | 0.43 | 0.28 | 0.39 | 0.47 | 1.56 | 2.27 | 2.61 | 1.84 |
| $Na_2O$ | 0.31 | 0.15 | 0.56 | 0.50 | 0.46 | 0.38 | 0.09 | 0.22 | 0.20 | 0.27 | 0.66 | 1.13 | 1.24 | 1.20 |
| $SO_3$ | 46.73 | 43.27 | 45.51 | 33.66 | 35.74 | 31.06 | 42.69 | 44.73 | 47.48 | 41.40 | 26.28 | 8.67 | 7.89 | 1.99 |
| TOTAL | 99.41 | 97.13 | 98.25 | 98.18 | 95.17 | 94.36 | 94.94 | 99.02 | 97.35 | 94.53 | 96.12 | 98.54 | 96.58 | 97.59 |
| Anhydrite | XXX** | XXX | XXX | XX | XX | XX | XXX | XXX | XXX | XXX | XX | X | X | X |
| Quartz | X | X | X | | | X | X | X | X | X | XX | XX | XX | XX |
| Hematite | X | | | X | X | X | X | X | | X | X | XX | XX | XX |
| Magnetite (?) | | | | | | | | | | | | X | XX | X |
| Calcite | X | X | X | | | | | X | | | | | | |
| Lime | X | X | X | | | | | | X | X | | | X | XX |

* Samples from the front of the reheat section of the boiler are indicated by F, those from the back side by B. F' indicates the sample came from the second row of pipes in the front of the reheat section.

† The brown material is the outermost crust of the deposit.

‡ The section of pipes in front of the reheat section. This sample is vesicular slag.

** The number of X's indicate the relative abundance based on X-ray data, XXX is the most abundant and X the least.

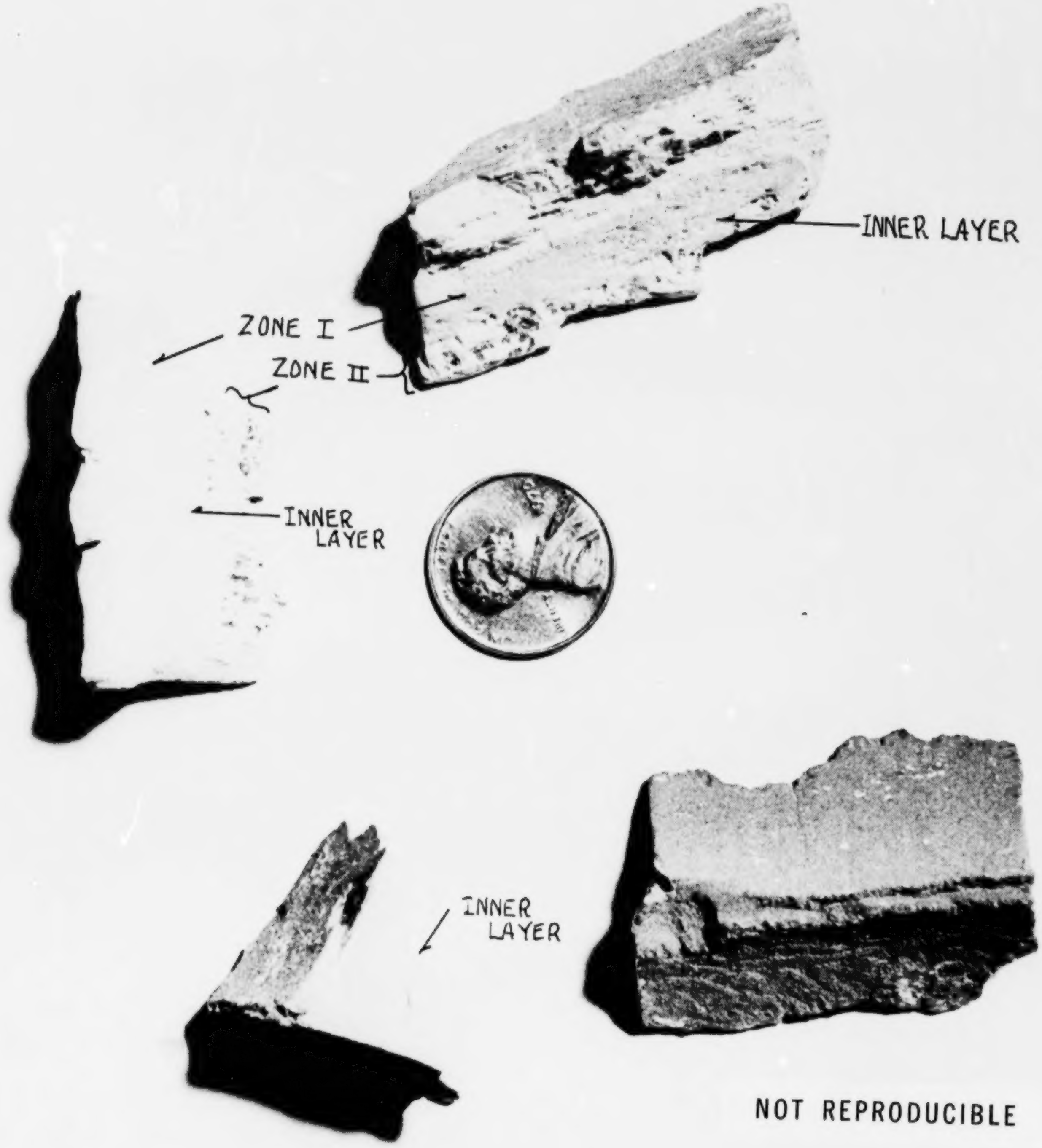
INNER LAYER
ZONE I
ZONE II
INNER LAYER
INNER LAYER

NOT REPRODUCIBLE

Fig. 70. Typical specimens of the boiler deposit obtained in September 1970 showing the occurrence of iron oxide blebs in zone II of the inner layer (sample 4).

essentially isosceles, with the apex pointing toward the fire side of the boiler, opposite to the direction of gas flow. The base of the triangle is attached to the pipe and is concave, owing to the curvature of the pipe. The typical shape of the samples is illustrated in figure 70. The specimen in the lower right of the figure shows a small double ridge on the apex of the triangle. This shape was observed by Bishop (1968) in laboratory tests simulating boiler deposition within a period of one hour after start of the test.

The deposits are characterized by two layers: an inner layer (Anderson and Diehl, 1955), also known as the primary layer (Bishop, 1968), which occurs adjacent to the steam pipe (fig. 69B), and an outer layer that forms the main body of the deposit. The outer layer is itself finely laminated and the outermost surface of the outer layer forms a brown and relatively hard crust. The inner and outer layers are distinguished by differences in color. The inner layer is primarily off-white, whereas the outer layer is mainly buff. Distinction between the two layers is not obvious on the sides of the pipes where the deposit is thinnest, and the boundary between the two layers grades from about 1 to 2 mm on the front side of the pipe where the deposit is thickest.

### *Inner Layer Material*

The composition of the material adjacent to the pipe depends on its position on the surface of the pipe. The various positions of the pipe surface were divided into zones (fig. 69B). The actual distribution of the materials deposited in the various zones can be seen on the specimens (figs. 70 and 71). Zone I is on the front side of the pipe and generally extends through an arc of about 100 degrees. The inner layer material in zone I is white to light gray, soft, microporous, and granular. X-ray studies indicate it is largely anhydrite. Electron microscopy of the inner white material shows irregularly shaped anhydrite grains 0.2 to 1 μ across and spherical ash particles (fig. 72A). Many anhydrite particles occur as individual grains and others are agglomerates of 2 to 10 grains. The surfaces of the glassy fly ash spheres (fig. 72A) are coated with a granular material, probably anhydrite. The electron microscope examination also shows the white material has a relatively high porosity, which accounts for the observed softness. The white layer was not observed on one sample (3A), which was collected on the front of the reheat section, just 1½ feet below sample 4, which had a well developed white layer. In sample 3A, an iron-rich scale occurred partly on the front side of the pipe.

The chemical analyses and mineral components of three different samples of the white inner layer are given in table 21. The X-ray and chemical data show these samples consist of 74 to 80 percent anhydrite ($CaSO_4$) and traces of quartz, hematite, calcite, and lime. The spherical particles of fly ash occurring in this zone account for the alumina and most of the silica in the chemical analyses. Sodium and potassium oxide contents are low in zone I.

Zone II of the inner layer is characterized by a deposit of a mottled, reddish brown, scale-like material about 1 mm thick (fig. 71), or by small blebs of reddish brown material interspersed with white anhydrite, as shown on the two upper fragments in figure 70. It may be significant that the iron-rich scale was not observed in samples that had the white inner layer, whereas iron blebs were always associated with the white layer. Electron microscope studies show the reddish brown scale has a matted appearance (fig. 72B). Observations at

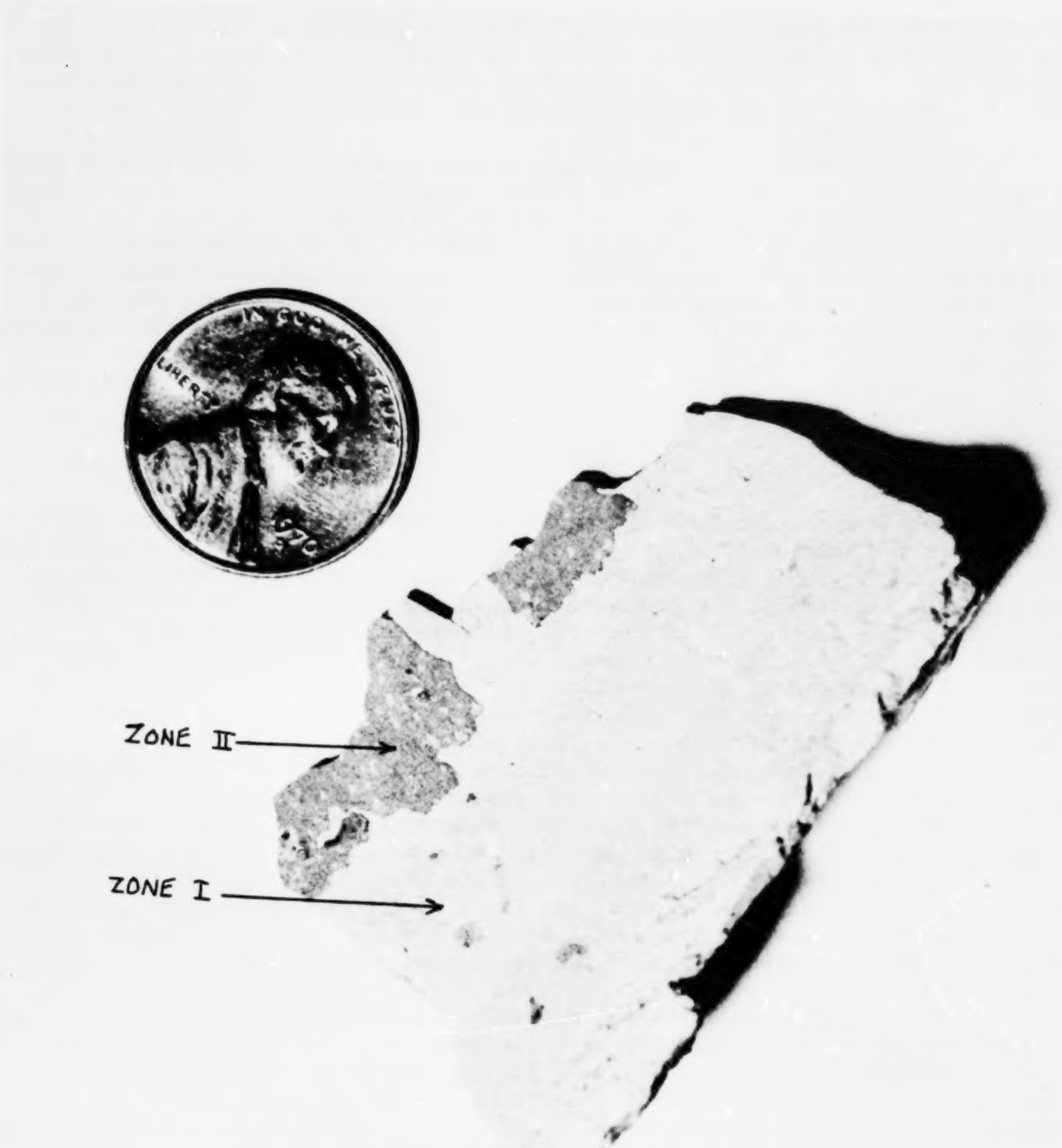
ZONE II
ZONE I
IN GOD WE TRUST
LIBERTY
1970
NOT REPRODUCIBLE

Fig. 71. Inner layer of deposit showing the iron-oxide scale in zone II.

ultra-high magnifications (not illustrated) show a high degree of interlocking of grains within these matted areas. The matted and interlocked grains may be anhydrite or hematite, and the texture indicates notable sintering of the material has occurred. Figure 72B shows that normal fly ash spherulites also occur in zone II of the inner layer.

Chemical analyses of the reddish brown scale are listed under samples 3A-1, 5A-1, and 8B in table 21. This material is characterized by its high iron oxide, silica, and alumina contents. Anhydrite represents only 53 to 61 percent of the brown scale in zone II.

Examination of the brown blebs in zone II shows the material has distinct, platy grain shape (fig. 72C), and X-ray data suggest the main constituent in these blebs is hematite. The white areas around the iron blebs in zone II are essentially the same as those in zone I. The hematite blebs are observed in samples from both the front and back of the reheat section.

### *Outer Layer Material*

The outer layer grades from a light buff next to the inner layer through deepening shades of buff to a brown on the outer surface. The contact between the inner white and the outer buff layers is gradational for a distance of about 2 mm in the center of the fire side of the steam pipe. The contact of the outermost brown crust and the main buff material is quite sharp. The outermost crust of the outer layer is relatively hard, but chemically does not differ significantly from the buff material (compare chemical data on samples 3B-1, 3B-2, 3A-2, and 4B). The outer layer is porous and composed of agglomerates of individual 1 μ grains of anhydrite (fig. 72D and E). Few of the grains have well formed crystal surfaces (fig. 72E), most are subrounded, and little fusion of grains (sintering) occurred.

## Deposits Collected June 1970

Several specimens were obtained from the boiler during the shut-down period in June 1970. By comparison with the oriented specimens, the June samples, with few exceptions, are judged to consist of only the outer layer. The specimens are a buff to brown, very fine grained, soft, porous mixture of anhydrite and normal fly ash components. Thin sections examined in transmitted light and magnified 25 times appear in figure 73A. Interlayered with these particulate materials are a few very thin dark gray bands composed of ultrafine-grained or amorphous matter (upper left corner of fig. 73A). These thin dark gray bands may consist of hematite or, possibly, carbonaceous matter. A few specks of transparent fly ash particles are enclosed in the dark bands (fig. 73A). Two, three, or four such bands could be recognized in cross sections of the specimens examined. The main body of the buff material is finely laminated, as in the outer layer in samples obtained in September.

The outermost crust of several of the specimens has a corrugated surface coated with a dark gray material that appears identical to the interior bands. Under the microscope this surface has a smooth texture and the anhydrite grain boundaries are very indistinct (lower right corner in fig. 73B). The upper left of figure 73B shows the edge of one of several pits that occur on the corrugated surfaces. Fly ash spherulites can be recognized in these pits.

## EXPLANATION OF FIGURE 72

A. Broken surface of the light gray inner layer of zone I showing the fine granularity of the anhydrite (0.2 to 1 μ diameter) and spherical fly ash particles coated with anhydrite. Electron micrograph of sample 4A, X5500.

B. Innermost surface of reddish brown scale showing mixture of normal fly ash components and recrystallized iron mat in center, probably compound of hematite and anhydrite. Electron micrograph of sample 3A-1, X4500.

C. Innermost surface of a reddish brown bleb showing platy form of the iron, probably hematite. Electron micrograph, specimen separated from sample 4 (see fig. 69), X4680.

D. Broken surface of the buff-colored outer layer showing the granular character of the anhydrite grains that constitute 80 percent of the specimen. $CaSO_4$ occurs mainly as individual grains and as a few small agglomerated grains. The specimen also has considerable porosity. Electron micrograph, sample 4, X1300.

E. Close-up view of same specimen as in D showing the occurrence of individual grains and small agglomerates of several grains. Electron micrograph, X4760.

F. Broken surface of white anhydrite adjacent to hematitic bleb in zone II. Note the presence of several agglomerate particles showing little or no porosity. This is probably due to incipient sintering of the anhydrite in this area of the deposit. Electron micrograph, X1870.

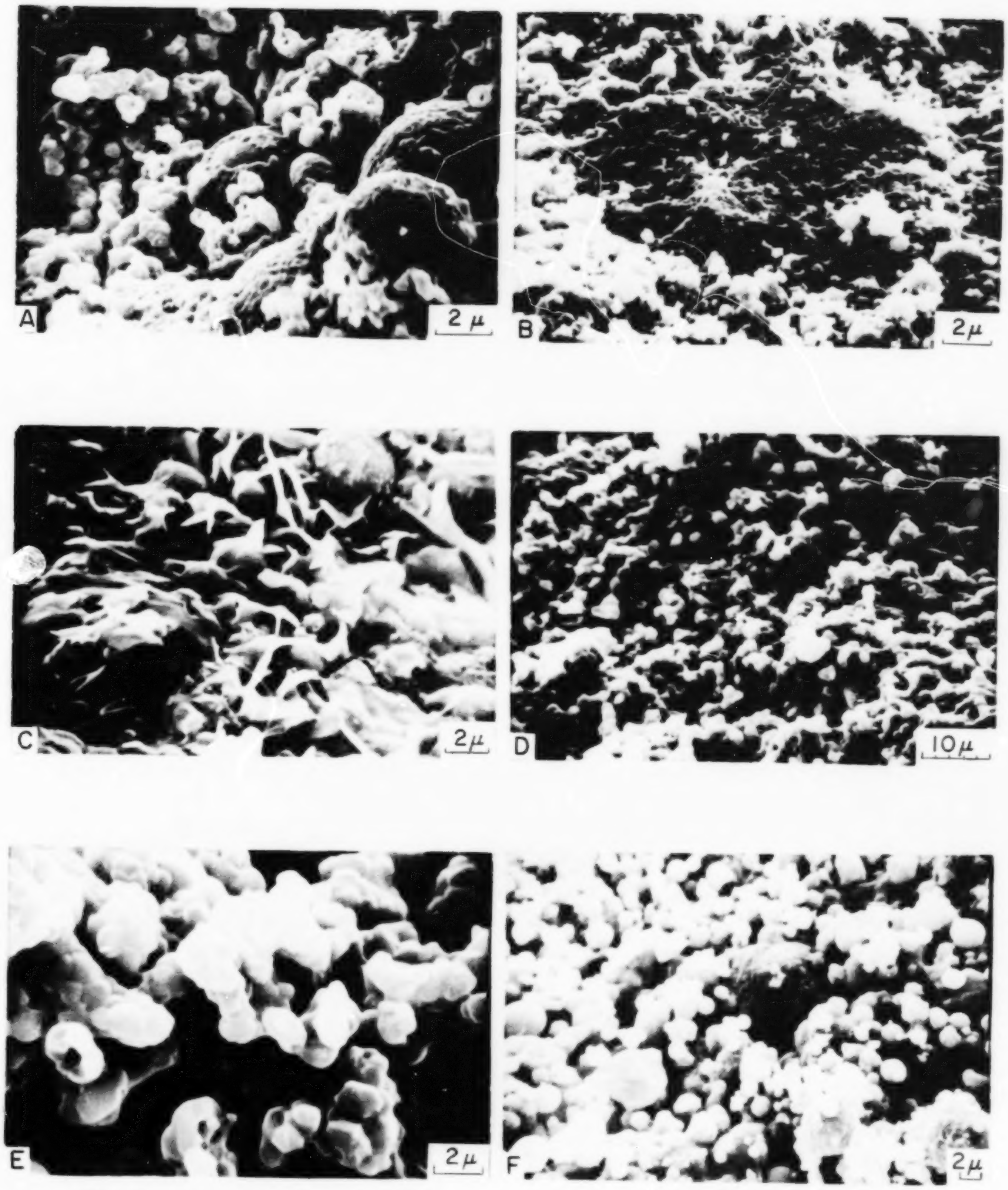
A
2 μ
B
2μ
C
2μ
D
10μ
E
2μ
F
2μ

Fig. 72 - Scanning electron micrographs showing the nature of inner layer (A, B, and C) and outer layer (D, E, and F) of boiler deposits collected September 1970.

## EXPLANATION OF FIGURE 73

A. Finely laminated structure in the buff outer layer. The dark bands probably contain some hematite and possibly carbonaceous matter. The small light grains are anhydrite and transparent fly ash particles. Few opaque fly ash particles are embedded in anhydrite in the lower left. The two circles in the upper right are air bubbles in the immersion oil. Transmitted light, X26.

B. Outer surface of a corrugated outer crust showing a smooth surface in the lower right and the edge of a pit in the upper left with normal fly ash particles coating the pit surface. Electron micrograph, X5525.

C. Fracture surface of buff outer layer showing well crystallized and interlocking grains of anhydrite. This texture is indicative of sintering action. Electron micrograph, X2660.

D. Same specimen as figure 13, showing the variability of the porosity and grain size of the recrystallized anhydrite. Electron micrograph, X2465.

E. Anhydrite crystal on a fracture surface of a glassy area, probably in inner layer, zone II. Electron micrograph, X2465.

F. Detail of same specimen as figure 15, showing the smooth and partly granular character of the iron-rich inner layer. Electron micrograph, X5355.

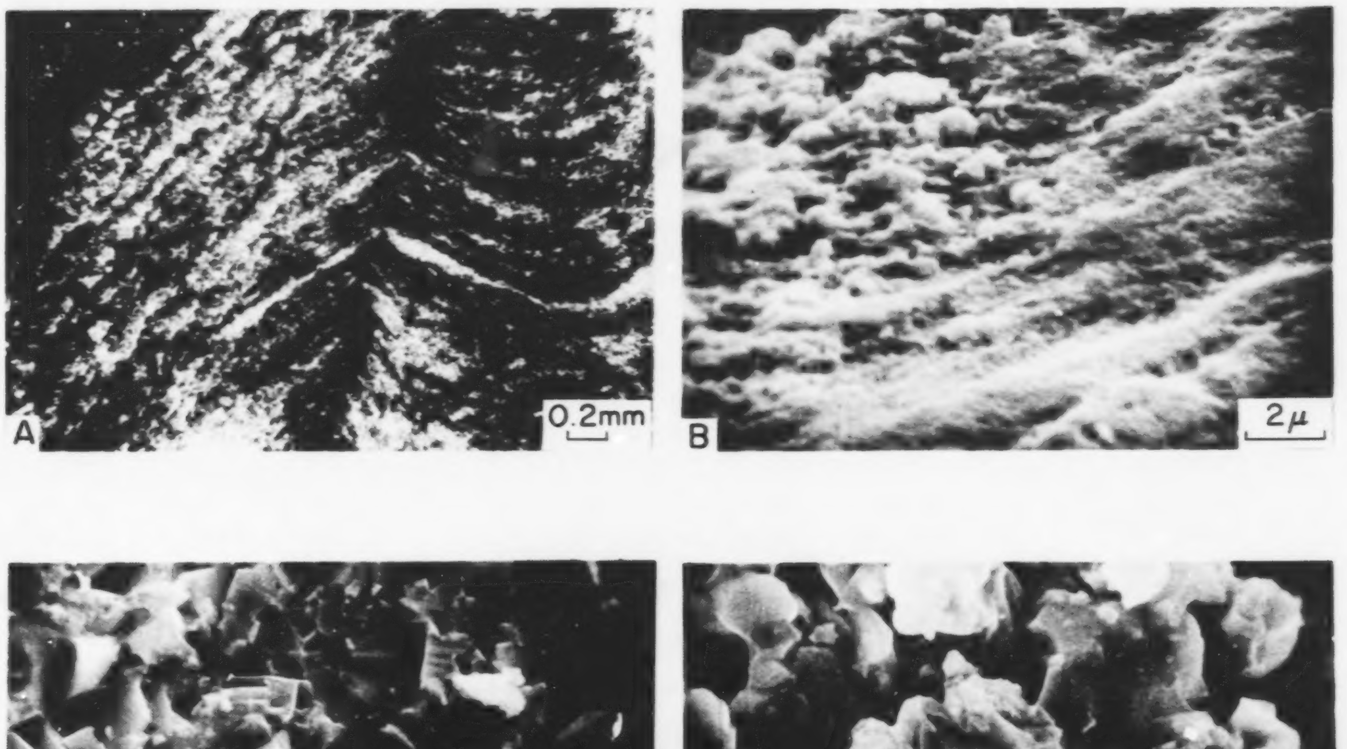
A
0.2mm
B
2μ
C
2μ.
D
2μ
E
2μ
F
2μ

NOT REPRODUCIBLE

Fig. 73 - Micrographs showing the nature of boiler deposits collected June 1970.

Broken surfaces of the buff material (outer layer) consist of well crystallized and tightly interlocking anhydrite grains (fig. 73C and D). The grain size of the anhydrite, where distinct grains could be recognized, ranges from about 1 to 10 μ. From the electron microscope observations, the porosity appears to vary considerably from point to point in any given specimen. One specimen thought to represent zone II of the inner layer showed patches of brown, glassy material surrounded by the soft, brown anhydrite. At high magnification, these glassy areas are very smooth, as illustrated in the background of figure 73E and F. Bladed crystals of anhydrite were observed on broken surfaces of the glassy areas (fig. 73E).

## Concluding Remarks on Boiler Deposits

The fire side boiler deposits observed September 14, 1970, in the reheat section of Unit 10 of the Shawnee Steam Plant were not large enough to significantly deter the passage of flue gases. The deposits that were present had distinct inner and outer layers. The inner layer contains two types of materials, a reddish brown, iron-rich material and a light gray to white, soft, granular material. The iron material occurs in an arcuate zone on both sides of the pipes and near the thin edges of the deposit. Two forms of iron occur, (1) small reddish brown blebs of platy hematite embedded in white, fine granular anhydrite, and (2) a thin scale. The light gray to white material is the most abundant constituent in the inner layer, occurs on the front side of the pipe, and is composed mainly of 1 μ granular anhydrite particles mixed with siliceous spherulites, which are common in normal fly ash. The range of chemical and mineralogical data of the gray to white inner layer overlaps that of the buff outer layer. The iron oxide content of the white inner layer is about the same as that in the outer buff layer. The mean concentration of $K_2O$ of the inner zone I (0.83 percent) is higher than in the outer layer (0.39 percent), and a similar relation holds for the $Na_2O$ values. However, these oxides are most abundant in samples containing the most normal fly ash constituents—quartz, hematite, and magnetite (samples 6 and 8A). Anderson and Diehl (1955) observed much higher enrichments of sodium and potassium in the inner layer in their studies than those reported here.

The apparent porosity and grain shapes of the September anhydrite samples (fig. 72D and E) are quite different from those observed (fig. 73C and D) in the June samples. The outer layer in the June samples contained well crystallized and tightly interlocking grains of anhydrite, indicative of considerable sintering and grain growth.

The observed enrichment of iron oxide in zone II of the inner layer appears to be unique in these deposits. Furthermore, the iron-rich blebs are definitely associated with a well developed white to light gray inner layer, whereas the iron-rich scale occurred in no samples containing a distinct white inner layer. Anderson and Diehl noted significant amounts of iron oxide in the inner layer on several fire side deposits. Basing their conclusions on the weight gained in laboratory experiments designed to simulate the boiler conditions, Anderson and Diehl concluded that sodium-potassium-iron sulfates had formed in fly ash and flue gas mixtures at temperatures ranging from 1000 to 1200° F. Like them, we detected no iron sulfates by X-ray diffraction. Calculation of the $CaSO_4$ content from the chemical analyses of the inner layer samples (table 21) shows excess CaO in all samples except 3A-1. In that sample a deficiency was found, leaving 0.9 percent $SO_3$ that may be combined with iron. In contrast, the other two iron-rich samples from the inner layer (samples 8B and 5A-1) yield excess CaO with respect to $SO_3$. The interlocking granular texture of the iron-rich specimens from the inner layer (fig. 12B and C) supports the conclusion that hematite is the predominant form of iron; however, the possibility that small amounts of very poorly crystalline or glassy masses of iron sulfates occur in the samples is not ruled out.

## SUMMARY AND CONCLUSIONS

### Petrography and Reactivity

Petrographic properties of the various carbonate rocks observed in this study reveal correlations with the $SO_2$ sorption capacity (3½ hr. reaction period).

The pore volume of carbonate rocks appears to be an important index property to the sorption capacity of a rock. The greater the total pore volume of the carbonate rock, especially when pores are between 2 and 16 μ in diameter, the greater its capacity for reacting with $SO_2$ in the fixed-bed tests. In support of this conclusion, the data on two porous dolomite samples show that they had high $SO_2$ reactivity in spite of moderate amounts of inert clay and quartz impurities. Six high-purity dolomites, each consisting for the most part of tightly interlocking rhombic to anhedral grains of dolomite containing many intergranular voids, had an average $SO_2$ sorption capacity of 10.3 grams per 20 grams of calcine, whereas two dolomites containing 10 to 15 percent clay and quartz had an average reactivity of 14.3 g/20 g of calcine. The pore structure of these samples appears to be more influential in their $SO_2$ behavior than does their degree of mineral or chemical purity.

Of the limestones tested, those containing crinoidal fossil fragments had the highest $SO_2$ sorption capacity. The positive influence of the crinoidal grains is probably due to the presence of voids within the grains that make the calcine more porous. These voids probably also contain most of the sodium-bearing soluble salts.

Comparison between the crystallographically "perfect" Iceland spar calcite (type 1) and the calcite spar sample, which contains abundant intracrystalline voids and twin lamellae (type 2), also supports the positive influence of voids on sorptive capacity, type 2 having more than twice the capacity for $SO_2$ sorption of type 1. The pores in carbonate rocks are believed to remain as pores through the early, and possibly the middle, stages of calcination.

Two samples of marl, a chalk, and the aragonite proved to be exceptions to the pore volume-capacity rule. However, the pore volume measurements in these high-capacity samples are probably erroneously low, for 20 other samples of carbonate rocks conform to this rule.

The grain size of carbonate rocks is also a useful index of $SO_2$ sorption capacity. In general, the finer the grain size the higher the $SO_2$ capacity.

The coarsest grained samples—Iceland spar, calcite spar, and marble—had an average capacity of 8.2 g/20 g calcine, whereas the very fine-grained marls, chalks, and oolitic aragonite have an average capacity of 15 g/20 g. However, the limestones are an example of an opposite but explainable trend related to the occurrence of void inclusions in crinoid fragments present in the limestones.

Of particular importance is the observed tendency of the samples with high sodium content to have high sorption capacities. Minor to trace amounts of sodium, frequently present in carbonate rocks as soluble salts and located along grain boundaries and in fluid inclusions within grains (Lamar and Schrode, 1953), may act as a catalytic or fluxing agent to produce a more porous calcine.

Petrographic interpretations of the differential reactivities (120-second reaction period) are not clear. Of the five high-purity dolomites that are nearly identical petrographically, four have differential reactivities ranging from 6.3 to 9.3 mg $SO_3$/30 mg calcine. The fifth (type 5) has a reactivity of 17.0 mg $SO_3$/30 mg calcine. In addition, although the very fine-grained and dense limestone (type 4) is completely different from the coarse crinoidal limestone (type 3) in texture, their $SO_2$ differential reactivities are nearly identical. Differential reactivities are thought to result from slight differences in pore structure of the calcines that result in changes in rate of reaction during the first few tens of seconds of exposure to $SO_2$. These changes give rise to notable differences in the degree of sulfation after a reaction period of 120 seconds. Evaluation of reacted calcines at a constant degree of sulfate loading enabled Borgwardt (1970b) to correlate the differential reactivity with the surface area measurements of the calcines.

The product of the reaction of calcines of carbonate rocks with $SO_2$ in laboratory tests conducted at 1800° F was found to be anhydrite ($CaSO_4$). Two types of reactions were observed by a scanning electron microscope equipped with an X-ray spectrum analyzer. The calcines of the nonporous Iceland spar calcite (type 1) absorbed sulfur only on the outer surface of the particles, while the calcines of a porous limestone (type 3) absorbed sulfur throughout the particles. This supports the conclusion that the pore structure of the rock is maintained through the reactive stage of the calcine.

## Fly Ash and Boiler Deposits

Anhydrite was the only sulfur-bearing compound positively detected in the fly ash samples that is believed to have been formed by reaction of $SO_2$ in the flue gas with CaO derived from the limestone that was injected into the boiler. Some evidence also suggests the presence of trace amounts of $CaSO_3$ in the coarse particles in plane CC in the boiler; no evidence for $CaSO_3$ in plane AA was observed. The size of the anhydrite particles is submicron to about 2 microns in diameter. However, X-ray data show notable percentages of anhydrite in the coarse sieve sizes owing to sintering of crystallites of anhydrite on surfaces of large lime particles. The crystal structure of the anhydrite, as evidenced by X-ray diffraction patterns, is essentially identical to that of the naturally occurring mineral.

The character of limestone-derived and normal fly ash particles in limestone-modified fly ash samples was documented by scanning electron microscope methods. Little development of crystal faces was observed on the anhydrite grains. Sintered textures formed by grain growth on the exterior surfaces of a small number of ash particles are similar to the texture of laboratory-reacted specimens (compare figs. 66A and 60). Several epitaxial growth structures on ash particles were observed, but their significance is not known. Samples from mechanical hoppers proved better than those from the electrostatic hoppers for the recognition and study of lime and anhydrite with microscope techniques. Attempts to concentrate the lime-anhydrite particles in fly ash samples from the mechanical hoppers by magnetic separation to facilitate their study were successful.

Studies of boiler deposits that formed in the reheat section were revealed to have inner and outer layers that could easily be observed with the naked eye. Detailed chemical and mineral analyses showed minor differences between the white inner layer and the buff to brown outer layer. Both layers consist largely of anhydrite mixed with less abundant normal fly ash particles. Sintering and interlocking growth textures of anhydrite grains were observed in the largest and hardest deposits. Iron oxide present in the inner layer is concentrated in blebs and scales on both sides of the steam pipes. The scale deposit was not observed where the white inner zone was well developed, but the blebs, composed of platy hematite, occurred with the white inner zone material. The data suggest $K_2O$ and $Na_2O$ are concentrated to a minor extent in the inner zone, adjacent to the steam pipe. Poorly crystalline or glassy masses of iron sulfates, reported in the fire side boiler deposits by other workers, were not observed in the samples studied but may exist in small amounts.

## Acknowledgments

Melvin C. Stinson of the California Division of Mines and Geology, Marshall T. Hunting of the Washington Division of Mines and Geology, and Edward P. Pearson of Basin Chemicals Incorporated, Cleveland, Ohio, kindly supplied samples of magnesite for this study. Ocean Industries Incorporated provided the sample of oolitic aragonite.

The analytical chemical data reported herein were determined by personnel of the Analytical Chemistry Section of the Illinois State Geological Survey.

The scanning electron microscope used in this study is located in the Center for Electron Microscopy, University of Illinois, Urbana. This instrument was obtained by a grant from the Geology Division of the National Science Foundation. The opportunity to use the scanning electron microscope and other equipment in the Center is gratefully acknowledged.

BLANK PAGE

**Preceding page blank**

## REFERENCES

Anderson, C. H., and E. K. Diehl, 1955, Banded fireside deposits in coal-fired boilers, in Studies relative to ash fouling when burning central Illinois coals: The Babcock and Wilcox Co., Alliance, Ohio, 23 p.

Bishop, R. J., 1968, The formation of alkali-rich deposits by a high-chlorine coal: Jour. Inst. Fuel, v. 51, Feb., p. 51-65.

Borgwardt, R. H., 1970a, Kinetics of the reaction of $SO_2$ with calcined limestone: Environmental Science & Technology, v. 4, no. 1, p. 59-63.

Borgwardt, R. H., 1970b, Isothermal reactivity of selected calcined limestones with $SO_2$: NAPCA Limestone Injection Process Symposium Proc., Gilbertsville, Kentucky, June 22-26.

Chayes, Felix, 1956, Petrographic modal analyses: John Wiley & Sons, New York, 109 p.

Dever, G. R., Jr., and Preston McGrain, 1969, High-calcium and low-magnesium limestone resources in the region of the lower Cumberland, Tennessee and Ohio Valleys, western Kentucky: Kentucky Geol. Survey Bull. 5, 192 p.

Fisher, C., and L. J. Nazareth, 1968, Classified treatments for the application of the Quantimet to stereological problems: The Microscope, v. 16, 2nd quarter, p. 95-104.

Folk, R. L., and W. C. Ward, 1957, Brazos River bar: A study in the significance of grain-size parameters: Jour. Sed. Petrology, v. 27, p. 3-26.

Gillson, J. L., 1960, The carbonate rocks, in J. L. Gillson [ed.], Industrial minerals and rocks: Am. Inst. Mining & Metall. Engrs., New York, p. 123-201.

Keroher, G. C., and others, 1966, Lexicon of geologic names of the United States for 1936-1960: U. S. Geol. Survey Bull. 1200, pt. 1, p. 1424.

Krumbein, W. C., and F. J. Pettijohn, 1938, Manual of sedimentary petrography: D. Appleton - Century Co., New York, p. 240.

Lamar, J. E., and R. S. Shrode, 1953, Water soluble salts in limestones and dolomites: Econ. Geology, v. 48, no. 2, p. 97-112.

Murray, J. A., 1956, Summary of fundamental research on lime: National Lime Assoc., Washington, D. C.

Pettijohn, F. J., 1957, Sedimentary rocks: 2nd ed., Harper & Brothers, New York, p. 368-369, 400, 410-411.

Potter, A. E., 1969, Sulfur oxide capacity of limestones: Am. Ceramic Soc. Bull., v. 48, no. 9, p. 855-858.

Rose, H. E., 1968, The determination of the grain-size distribution of a spherical granular material in a matrix: Sedimentology, v. 10, p. 293-309.

Rosiwal, A., 1898, Ueber geometrische Gesteinsanalysen u.s.w.: Verhandl. der k.-k. Geolog. Reichsanstalt Wien, p. 143-175.

Snedecor, G. W., 1946, Statistical methods: 4th ed., Iowa State College Press, Ames, Iowa, 485 p.

Sorby, H. C., 1856, On slaty cleavage as exhibited in the Devonian limestones of Devonshire: Philos. Mag., v. 11, p. 20-37.

Thomason, E., 1930, Quantitative microscopic analysis: Jour. Geology, v. 38, no. 3, p. 193-222.

Womble, T. D., Jr., and J. T. Reese, 1970, The dry limestone injection process for $SO_2$ control, unit full-scale evaluation: NAPCA Limestone Injection Process Symposium Proc., Gilbertsville, Kentucky, June 22-26.

# GLOSSARY

### *Algae*

Seaweeds and related primitive (aquatic) plants. Some species secrete laminated crusts of calcium carbonate, forming spherical or irregularly shaped fossils composed of very fine-grained calcite.

### *Anhedral*

A term applied to mineral grains that are not bounded by any characteristic crystal face. Contrasted in this paper with rhombic and subrhombic grains.

### *Anisotropic*

A term applied to describe an optical property of nonopaque mineral grains or crystals that transmit light at different velocities along different crystallographic directions. Such grains show double refraction. Contrasts with "isotropic."

### *Brachiopods*

Marine animals with two unequal shells, each of which is bilaterally symmetrical. The shells are common as fossils. Most are composed of fine, interlaminated grains of calcite.

### *Bryozoans*

Colonial marine invertebrates that secrete a calcareous, horny or membranous covering. The calcareous bryozoans have a variety of shapes and are common as fossils. Many are branching or lacelike, some are encrusting, and others form massive growths.

### *Chert*

A very fine-grained variety of silica ($SiO_2$), typically composed of quartz in grains less than 10 microns in diameter.

### *Crinoids*

Marine invertebrates characterized by a radially symmetrical calyx attached to a segmented stem. Most fossils are fragmented calyx plates and stem discs. They consist of relatively coarse-grained calcite.

### *Echinoids*

Sea urchins and closely related marine invertebrates (echinoderms). The shell is composed of a number of small, calcareous plates and is covered by numerous movable spines.

### *Equigranular texture*

A descriptive term applied to rocks that have a granular (as opposed to glassy or amorphous) texture and mineral grains that are all of one order of size.

### *Foraminifera*

Single-celled animals, usually minute, characterized by a perforated shell commonly composed of very fine-grained calcite.

### *Gastropods*

Gastropods, or snails, have a single spirally coiled or cap-shaped shell. A

### *Gastropods* (Continued)

few have no shell at all. They live in shallow marine waters, in fresh water, and on dry land. The mineral content of the shell is aragonite, which alters to calcite on fossilization.

### *Grain*

An individual crystalline unit bounded by an optical discontinuity in rocks.

### *Granularity*

The degree of uniformity of grain size of rock specimens as observed with a petrographic microscope. A relative term useful for describing carbonate rocks.

### *Illite*

A clay mineral commonly occurring in sedimentary rocks (such as limestones) that is composed of a complex hydrous silicate of potassium and aluminum in a layered structure; similar to muscovite mica.

### *Intraclast*

A fragment of consolidated carbonate sediment that has been reworked and redeposited within a sedimentary environment to form a part of a new sediment within the same formation.

### *Isotropic*

An optical property of nonopaque crystals or grains that belong to the isometric crystal system and amorphous substances. Light passes through these materials at the same velocity in all directions, and they have one characteristic index of refraction. Contrasts with "anisotropic."

### *Kaolinite*

A clay mineral that occurs in sedimentary rocks, such as limestones. A hydrous aluminum silicate in a layered structure.

### *Micritic calcite*

Calcite ($CaCO_3$) that is less than 10 microns in grain size, generally 1 to 4 microns; subtranslucent with a faint brownish cast in thin section.

### *Ostracodes*

Minute bivalve crustaceans, mostly marine, abundant as fossils. The shells are generally somewhat bean-shaped. In many species the surface of the shell has a characteristic ornamentation.

### *Pelletoidal*

Refers to pellet-shaped particles in some limestones. The pellets are spherical or ellipsoidal in shape and consist mainly of fine-grained calcite with traces of clay and organic matter.

### *Reef dolomite*

A type of dolomite rock found in reefs (large mounds or ridges) built by marine organisms and characterized by abundant fossils and lack of bedding. Reef dolomites are frequently high-purity dolomite, very porous but of low permeability. The dolomite is generally of secondary origin, formed by replacement of calcite in a former limestone reef.

### *Rhombic*

A term applied to carbonate (usually dolomite) mineral grains that have two or more sides with characteristic rhombic crystal faces.

### *Sparry calcite*

Calcite ($CaCO_3$) that is translucent (sometimes transparent) and more than 16 microns in grain size. Frequently in grains larger than 50 microns. In thin section, sparry calcite is distinctly clear, compared to micritic calcite.

### *Subrhombic*

A term applied to carbonate mineral grains that have one side of the characteristic rhombic outline present as a grain boundary.

### *Thin section*

A fragment of rock ground to a thickness of approximately 30 microns for examination with a petrographic microscope in transmitted and polarized light.

### *Twin lamellae*

Parallel lines on the surface or cross section of a grain (or crystal) that has multiple twinning along parallel planes through the grain.

### *Twinned crystal*

Composite crystals of a single substance, in which the individual parts are related to one another in a definite crystallographic manner—usually a plane through the crystal or grain. The plane represents a discontinuity in the crystallographic structure of the material.